Australian Government
Geoscience Australia

Professional Opinion

No. 2009/11

A Probabilistic Tsunami Hazard Assessment of the Indian Ocean Nations

D.R. Burbidge, P.R. Cummins, R. Mleczko, H. Latief, M. Mokhtari, D. Natawidjaja, C.P. Rajendran, C. Thomas.

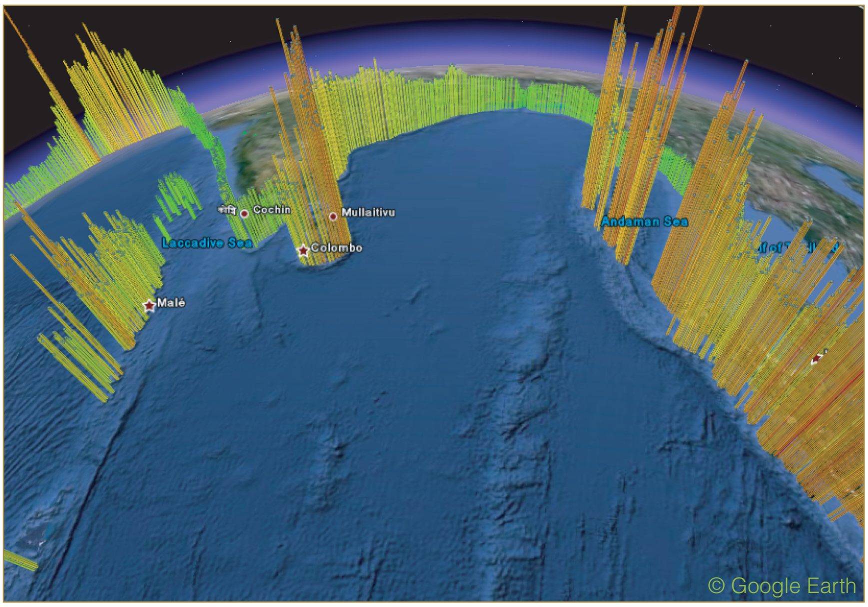

APPLYING GEOSCIENCE TO AUSTRALIA'S MOST IMPORTANT CHALLENGES

Geoscience Australia
Professional Opinion No. 2009/11

A Probabilistic Tsunami Hazard Assessment of the Indian Ocean Nations

D.R. Burbidge[1], P.R. Cummins[1], H. Latief[2], R. Mleczko[1], M. Mokhtari[4], D. Natawidjaja[2], C.P. Rajendran[3], & C. Thomas[1†]

[1]Risk and Impact Analysis Group, Geoscience Australia
[2]Research Center for Geotechnology, Indonesian Institute of Sciences
[3]Centre for Earth Sciences, Indian Institute of Science
[4]International Institute of Earthquake Engineering and Seismology, Iran

September 29, 2009

Australian Government
AusAID

An Australian Government, AusAID initiative

[†]Authors listed in alphabetical order

Department of Resources, Energy and Tourism
Minister for Resources, Energy and Tourism: The Hon. Martin Ferguson, MP
Secretary: Mr John Pierce

Geoscience Australia
Chief Executive Officer: Dr Neil Williams

©Commonwealth of Australia 2009.This material is released under the Creative Commons Attribution 2.5 Australia Licence (http://creativecommons.org/licenses/by/2.5/au/).

Disclaimer

The views expressed in this publication are those of the authors and not necessarily those of the Australian Agency for International Development (AusAID). Geoscience Australia has tried to make the information in the product as accurate as possible. However, it does not guarantee that the information is totally accurate or complete. Therefore, you should not solely rely on this information when making a commercial decision.

GeoCat No. 68717

Bibliographic reference: D.R. Burbidge, P.R. Cummins, H. Latief, R. Mleczko, M. Mohtari, D. Natawidjaja, C.P. Rajendran, C. Thomas, 2009. A Probabilistic Tsunami Hazard Assessment of Indian Ocean Nations *Geoscience Australia Professional Opinion. No.2009/11*

Contents

1 Executive Summary

This report is a result of collaboration by a team of earth scientists from Indian Ocean countries to characterize the tsunami threat to the Indian Ocean region. The project was funded by the Australian Agency for International Development (AusAID), and was carried out under the auspices of Working Group 3 (Risk Assessment) of UNESCO's Intergovernmental Coordination Group for the Indian Ocean Tsunami Warning System (ICG/IOTWS), both of which recognized the need for a broad-brush tsunami hazard assessment that could guide Indian Ocean tsunami mitigation activities.

The project commenced with the UNESCO-IOC Workshop on Methodologies for Indian Ocean Hazard Assessment, convened in Bandung, Indonesia, 17-18 July 2007, and attended by experts in the geology, tectonics and earthquake activity nominated by IOC member states in the Indian Ocean region. The focus of the workshop was on assessing what information exists to constrain the probabilities and magnitudes of tsunamigenic earthquakes, and whether this information was sufficient for developing a useful tsunami hazard assessment. While the discussions recognized the important limitations of a broad-brush hazard assessment, it was recognized that a such an assessment would be an important step towards further work. The 2007 Bandung workshop resulted in the selection of a panel of scientists, each of whom visited Geoscience Australia to provide input into the probabilistic tusnami hazard assessment for the Indian Ocean presented here.

Two views quickly emerged in discussions among the panel of developers. The hazard assessment should, on the one hand, avoid over-estimating the hazard by considering only those sources for which there is solid evidence for generation of large tsunami. On the other hand, the assessment should be careful not to miss source zones that may generate large tsunami even if they have not done so historically - as was the case for the 2004 Indian Ocean Tsunami (IOT). The panel decided these two views could best be accommodated by developing two assessments, referred to here as low-hazard and high-hazard end member assessments. This affords a clear expression of uncertainty in the hazard as the difference between the two end members, while it was hoped that any additional confusion created in application of the two assessments to mitigation would be managable. The geographical pattern of the low-hazard assessment is broadly reflective of the impact of the IOT. The high-hazard assessment, on the other hand, highlights areas potentially threatened by local tsunami, such as the western Makran and southern Java coasts, which are at the same time the areas of highest uncertainty in the hazard assessment.

This broad-brush tsunami hazard assessment is intended to inform tsunami mitigation strategies at the regional scale, and it is hoped that it will provide a foundation for more localized tsunami risk assessments to be undertaken in a systematic and consistent fashion across the Indian Ocean. Also, the uncertainty in the hazard assessment can serve as a guide to where further work is required to address the lack of data on historic and prehistoric tsunami. It should be appreciated, however, that the approach taken in this broad-brush assessment is not sufficient for understanding the tsunami threat at a community level, because the modelling is too coarse to accurately represent the tsunami heights on land that are needed to assess impact. While the assessment presented here can be used to determine what source zones contribute most to the hazard at a given coastal location, a proper assessment of the tsunami threat to a coastal community would require detailed inundation modelling for a range of scenarios to cover the most important source zones. Such modeling should be considered where this assessment suggests high hazard offshore a potentially vulnerable community, but the computational and data requirements for such modelling were well beyond the scope of this project.

2 Introduction

The Indian Ocean tsunami of December 26, 2004 was the first in a series of large tsunamigenic earthquakes that have increased awareness among emergency management authorities, governments and the general public throughout the Indian Ocean nations of the need for more information regarding the hazard faced by those nations from tsunami. Over the last few years the Australian Government has undertaken an effort to support regional and national efforts in the Indian Ocean to build capacity to respond to seismic and tsunami information. As part of this effort, Geoscience Australia has received support from the Australian Agency for International Development (AusAID) to assist Indian Ocean countries in assessing the tsunami hazard faced by them.

The tsunami threat faced by Indian Ocean countries consists of a mix of tsunami from local, regional and distant sources, whose effects at any particular location in the Indian Ocean are highly dependent on variations in seafloor shape between the source and the affected area. These factors make the design of an effective warning system for the Indian Ocean problematic, because so many scenarios are possible and each scenario's impact on different nations is potentially quite varied. In order to provide national governments in the Indian Ocean with the information they need to make informed decisions about tsunami mitigation measures, including development of a warning system, a comprehensive hazard and risk assessment is needed.

The aim of the report is to provide a *probabilistic tsunami hazard assessment* (PTHA) that will quantify the expected hazard for Indian Ocean nations. In this report, the hazard will be reported in terms of:

- tsunami amplitudes[1] at locations offshore the nations included in this study, and
- the probabilities of experiencing these amplitudes.

It is envisioned that this broad-brush PTHA will serve as a first step towards a systematic and comprehensive assessment of tsunami risk for Indian Ocean nations. Such a risk assessment should take into account:

- Actual run-up of tsunamis onshore as well as its impact on coastal communities,
- For Indonesia, a more complete assessment of tsunami sources including those in eastern Indonesia that may affect coastlines of shallow mariginal seas not considered in this study (e.g., Timor, Arufura, Banda and Flores Seas), and
- Non-earthquake sources of tsunami, as well as a more detailed consideration of historical and geological data as described in section 7 on Future Work.

These were beyond the scope of the present study. The offshore tsunami hazard reported here can, however, serve as a guide for prioritizing this more detailed and comprehensive work at national and local levels.

[1] Throughout this report the term *amplitude* is used to denote the wave height from mean sea level to crest.

2.1 Report Structure

This report is broken up into six sections and an appendix.

This first section is designed to be a general overview of the scope and main results of this assessment. It is designed to be high level and does not go into any of the technical details of how the assesment was carried out.

The second section is a general introduction to tsunami in the Indian Ocean. It is written for an audience with a general understanding of the science of tsunami and earthquakes, but who may not have any detailed knowledge of the earthquakes and tsunami in the Indian Ocean specifically. It also includes a detailed summary of the reasoning used to characterize source zones for the low and high hazard assessments.

Section 4 outlines, in general terms, the method used here to calculate the probabilistic tsunami hazard assessments maps. Its main purpose is to explain what the maps and figures in the following sections are meant to represent. The technical details of this particular assessment are described in Appendix A.

Section 5 is the largest section of the report and shows several hazard maps for every country in the Indian Ocean region except Australia. For assistence in interpreting these figures, please consult Section 4.1.

Finally, Section 6 summaries the results and major conclusions from this assessment and Section 7 lists some possible future work that could be done to improve the hazard maps given here.

2.2 Scope

The nations for which tsunami hazard was considered in this study are indicated in Figure 1. The study focused on tsunami caused by earthquakes and, more particularly, earthquakes occurring in subduction zones. While tsunami can be caused by other sources such as asteroid impacts, landslides and volcanic collapses and eruptions, earthquakes in subduction zones are by far the most frequent source of large tsunami, and are therefore the only events considered here. The subduction zones included in this study are limited to those that could credibly generate a large tsunami in the Indian Ocean (i.e. all those around the Indian Ocean Rim, the South Sandwich subduction zone in the southern Atlantic and the Puysegur subduction to the south of New Zealand). Note, however, that Indonesia has only been included as far east as 120° longitude; this was done in part because sources east of 120° longitude are less likely to affect the Indian Ocean beyond the Timor Sea, but also because of the increasingly complex tectonics east of Java. A tsunami hazard assessment encompassing all of Indonesia, including coastlines and sources in the Banda and Flores Seas, would have required resources beyond those available for this project.

Tsunami hazard in this report is expressed as the *annual exceedence probability* of a tsunami exceeding a given amplitude at a given offshore depth. An alternative way of expressing the annual probability is as a *return period*. The return period is the average length of time expected between events exceeding a given amplitude at a given offshore depth. The offshore depth in this assessment was chosen to be 100m. The main reason for choosing this depth was because modelling amplitudes to shallow water depths is a more computationally intensive task that requires higher resolution bathymetric data which do not exist for all regions considered in this study.

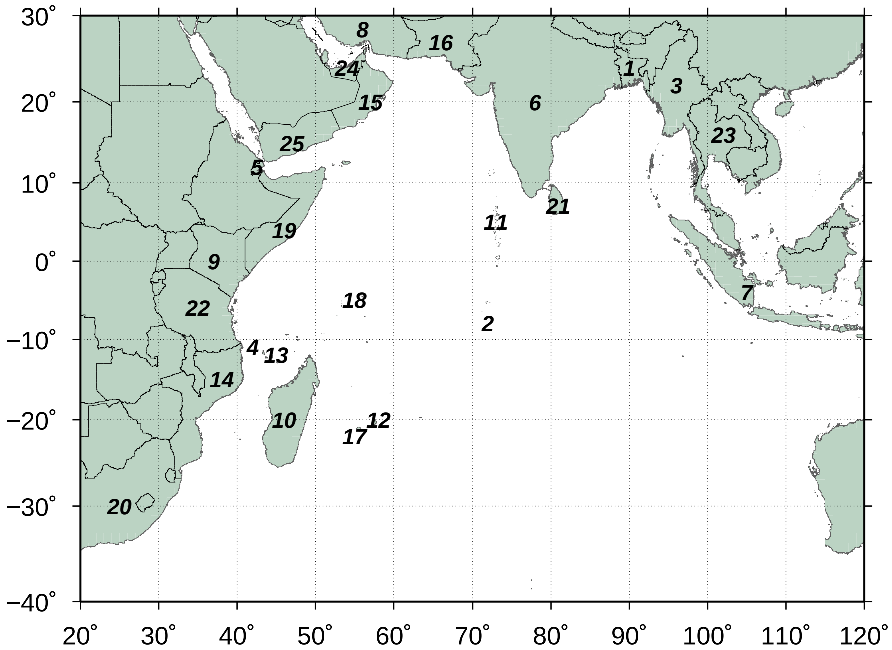

Figure 1: Indian Ocean nations included in the study. The countries are numbered as follows: Bangladesh (1); British Ocean Territory (2); Burma (3); Comoros (4); Djibouti (5); India (6); Indonesia (7); Iran (8); Kenya (9); Madagascar (10); Maldives (11); Mauritius (12); Mayotte (13); Mozambique (14); Oman (15); Pakistan (16); Reunion (17); Seychelles (18); Somalia (19); South Africa (20); Sri Lanka (21); Tanzania (22); Thailand (23); United Arab Emerates (24); Yemen (25).

The quality and resolution of the bathymetric dataset used is one of the factors that limits the accuracy of modelled tsunami amplitudes. While the resolution used in this study (two arc minutes or approximately 3.7km depending on latitude) is considered sufficient for the modelling of tsunami in deep water in the open ocean, in regions of very complex bathymetry close to shore, the results must be interpreted with caution. This highlights the need for more detailed studies in some regions using higher resolution bathymetric data. Another consequence of the resolution of the bathymetry data used is that there may be some very small inhabited islands in the study region that are not represented as islands by the bathymetry, and therefore may not be represented in the study.

It is important to emphasise that the results of this investigation cannot be used directly to infer onshore inundation, run-ups or damage. Such phenomena are strongly dependent not only on the offshore tsunami height, but also on factors such as shallow bathymetry and onshore topography. A study of inundation therefore requires detailed bathymetric and topographic data and involves even more intensive numerical computations than those required for this study. The object of this assessment is to answer the broader question: which Indian Ocean nations might experience offshore amplitudes large enough to potentially result in hazardous inundation, what are the probabilities of experiencing these amplitudes, and from which subduction zones might these tsunami originate? This information can be used to inform further, more detailed, inundation studies, but is not in itself sufficient to characterize impact at the community level.

2.3 Summary of Results

The results for individual countries are discussed in Section 5, and are presented in detail graphically in the KML files on the accompanying DVD. Here we give an overview of the results for the whole region.

For each country, two maps were developed: the "high" hazard and the "low" hazard. The main difference between the two maps is the size of the maximum earthquake that we assumed can occur on each zone. With the low hazard map, we assume that the largest earthquake that can possibly occur for that zone is equal to the largest earthquake known to have occured historically. For example, the maximum earthquake magnitude for the Andaman section of the Sunda Arc subduction zone is assumed to be Mw9.2 in the low hazard map; the same as the USGS magnitude for the earthquake that caused the 2004 Andaman-Sumatra earthquake. By contrast, the maximum magnitude for the Java section of the same zone in the low hazard map is only Mw7.8, since this is the largest earthquake known to have occured there.

In the high hazard map, we assume the maximum magnitude on every zone considered here is the same as the largest earthquake that has occurred on *any* zone in the world, Mw9.5 (the 1960 South Chile earthquake). The difference between the high and low hazard maps is much larger for countries which are mostly affected by nearby zones for which we have no definitive proof that a large magnitude earthquake has ever occurred there. One could thus view the hazard estimates for these countries as much more uncertain. The true hazard is likely to be between the two extremes of the low and high hazard maps.

An alternative approach to the uncertainty in tsunami hazard would have been to combine the low and high hazard source zones using a logic tree approach (see Burbidge *et al.*, 2008, and Parsons and Geist, 2008). This would allow different weights to be assigned to the high and low hazard maps in different source zones depending on the degree of confidence in each hazard map. For example, in central Sumatra lower weight might be assigned to the multiple-segment earthquakes of the high hazard map, since there is no evidence for these in the relatively complete paleotsunami record (Sieh *et al.*, 2009). For the present study however, it was felt that the present state of knowledge of the major earthquake source zones is too incomplete to warrant this approach.

Probabilistic tsunami hazard assessments such as this one create a large amount of data. This data can be mapped or tabulated in a variety of different ways depending on the question to be addressed. Table 1 extracts one measure of the hazard from this assessment, which is the maximum offshore amplitude that has a 1 in 2000 year chance of being exceeded for any point offshore each country considered in this study. The nations shown in red have the highest (greater than 2m maximum tsunami amplitude in the high hazard map) hazard at this return period. The nations shown in green have the lowest (tsunami amplitude is less than 1m in the high hazard map) at the 2000 year return period. The Table also lists which source zones are important for each country for this hazard measure at the 2000 year return period. A 2000 year return period was chosen since this is typically the upper limit used for emergency planning because it is normally associated with a large, but still reasonably probable, event. However, the actual hazard assessment itself was not restricted to this return period or hazard measure. Other hazard measures and return periods are included on the accompanying DVD. Figure 2 shows the maximum amplitudes at the model output points for this hazard measure for the same return period. Also shown are those faults included in the study which lie in the mapped region. It is clear from Figure 2 that most of the nations in the highest category mentioned above (ie shaded red) lie very close to subduction zones. Typically when a nation is close to a subduction zone (the black lines in Figure 2) the bulk of the hazard to that nation naturally comes from that zone. For example, most of the hazard faced by Pakistan comes from the earthquakes along the Makran subduction zone just off its coast. It should also be notedthat large discrepancies in the low and high-hazard assessments (e.g., Iran) reflect where the uncertainty is high due to the poor knowledge of earthquake activity in the corresponding source zones.

(a) (b)

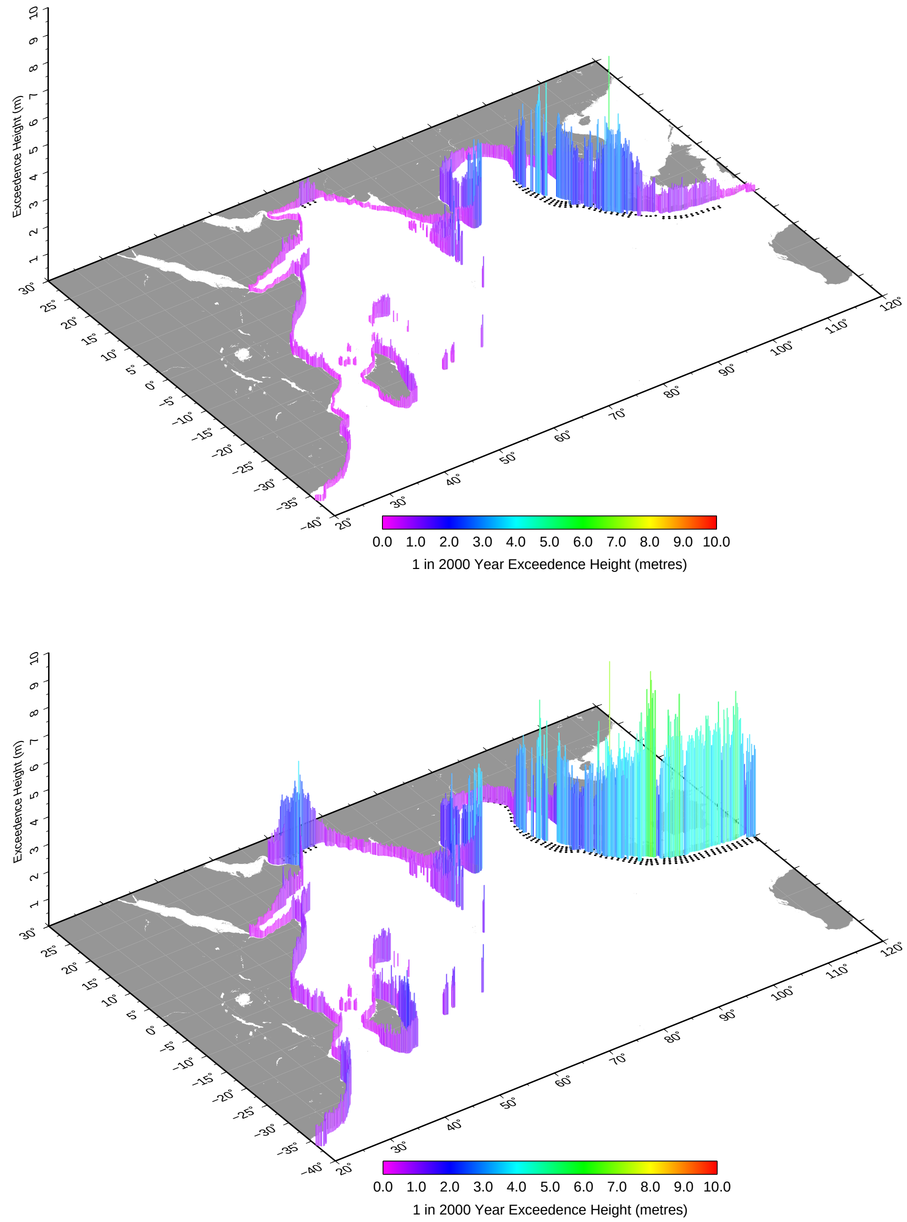

Figure 2: Regional hazard maps at the 2000 year return period for all the nations in the study for (a) the low hazard map and (b) the high hazard map.

The nations in the northeast part of the Indian Ocean (eg Burma, Bangladesh, eastern India, Sri Lanka and northwest Indonesia) are dominated by the hazard from the Andaman-Sumatra segments of the Sunda Arc at the 2000 year return period. Since the largest known earthquake from these zones is quite close to the one used in the high hazard map, the hazard to these countries is similar in both maps. For the Java-Sumba section of the Sunda Arc, on the other hand, the maximum earthquake magnitude is more uncertain, resulting in a much greater difference in the hazard between the low and high maps offshore

Indian Ocean nation	1/2000yr tsunami amplitude (m)		Most Important Subduction Zone Segments
	low	high	
Bangladesh	0.5	0.6	Andaman
British Ocean Territory	1.1	1.7	Andaman, Sumatra
Burma	1.1	1.5	Andaman, Sumatra
Comoros	0.3	0.5	Makran, Andaman, Sumatra
Djibouti	0.2	0.4	Makran
India	1.9	3.1	Makran, Andaman, Sumatra
Indonesia	5.6	7.1	Andaman, Sumatra, Java and Sumba
Iran	0.3	2.7	Makran
Kenya	0.5	0.8	Andaman, Sumatra
Madagascar	1.0	2.2	Andaman, Sumatra, Java, Sth Sandwich
Maldives	2.2	3.0	Andaman, Sumatra, Makran
Mauritius	1.2	1.7	Andaman, Sumatra, Makran
Mayotte	0.3	0.4	Andaman, Sumatra, Makran
Mozambique	0.5	1.4	Andaman, Sumatra, Sth Sandwich
Oman	0.6	3.8	Andaman, Sumatra, Makran
Pakistan	0.9	2.8	Makran
Reunion	0.7	1.4	Andaman, Sumatra, Sth Sandwich
Seychelles	0.8	1.2	Andaman, Sumatra, Makran
Somalia	0.7	1.1	Andaman, Sumatra, Makran
South Africa	0.6	1.6	Andaman, Sumatra, S Sandwich
Sri Lanka	2.9	3.7	Andaman, Sumatra
Tanzania	0.5	0.9	Andaman, Sumatra, Makran
Thailand	1.9	2.6	Andaman, Sumatra
United Arab Emirates	0.1	0.8	Makran
Yemen	0.8	1.3	Makran, Andaman, Sumatra

Table 1: Summary of results for all the nations considered in the study for one particular measure of the offshore tsunami hazard, the name of country is listed in the first column. The second and third columns show the maximum tsunami amplitude with a 1 in 2000 year chance of being exceeded for any point off the Indian Ocean nation shown in the first column for the low hazard and high hazard assessments, respectively. The nations shown in red have the highest (greater than 2m maximum tsunami amplitude in the high hazard map) hazard at this return period. The nations shown in green have the lowest (tsunami amplitude is less than 1m in the high hazard map) at the 2000 year return period. The fourth column lists the subduction zones which make the greatest contribution to the 1 in 2000 year hazard for that particular nation.

Java and the Lesser Sunda islands west of 120° longitude. Overall Indonesia clearly has by far the highest hazard of any nation considered in this study due to its proximity to the Sunda Arc subduction zone. This is true even though the hazard along coastlines of shallow mariginal seas such as the Timor, Arufura, Banda and Flores Seas was not considered in this study.

The 2000 year return period hazard for the nations in the northwest Indian Ocean (eg Djibouti, Pakistan, Iran, United Arab Emirates) is dominated by the hazard from the Makran subduction zone. In a similar way to the Java-Sumba section of the Sunda Arc, the hazard here is quite uncertain primarily because of the lack of evidence for a very large earthquake along the Makran.

For western Indian and the nations in the central Indian Ocean and east Africa, the dominant sources of hazard at 2000 years are both the Andaman-Sumatra segments and Makran. However, because they are much further away from the source of the tsunami these nations usually face a considerably lower overall hazard (this does not necessarily mean the risk to communities is lower, see below).

Finally, the hazard to southwestern Indian Ocean nations (eg South Africa) also originates mainly from Andaman-Sumatra, but in the high hazard map another important zone is the South Sandwich Islands subduction zone in the southern Atlantic. For South Africa and Mozambique the main source of the hazard at the 2000 year return period is the South Sandwich islands, not the Andaman-Sumatra segments of the Sunda Arc.

In summary, the Andaman-Sumatra segments of the Sunda Arc are clearly the most important zones to the bulk of the countries in the Indian Ocean for hazard at the 2000 year return period. The only expectations to this are the countries in the northwest Indian Ocean where the hazard is dominated by the Makran and the nations in the southwest Indian Ocean where the South Sandwich zone may be as important. For a more detailed discussion of every country, see Section 5.

It is also important to emphasise that the *risk* (likelihood of damage or death) from a tsunami depends not only on the hazard, but also on the density of population and infrastructure in low lying areas exposed to tsunami attack, as well as their vulnerability, including the potential to respond to a warning. Some countries, for example low lying Indian Ocean island countries, may be highly vulnerable even to a low level of offshore hazard. Only more detailed modelling and analysis of each specific island could determine whether this is indeed the case.

Other factors to consider are the assumptions in the earthquake recurrence model used in this assessment. The model takes the return periods of smaller magnitude earthquakes that have occurred historically and extrapolates this to longer return periods to estimate the return period of much larger earthquakes that haven't happened historically. Therefore there is much more uncertainity in the hazard estimates at the longer return periods. Additional data, particularly paleotsunami data, is required to reduce the uncertainity in the hazard estimates given here for the longer return periods. This uncertainity is at a maximum for countries whose main source of hazard comes from a zone which has not experienced a very large earthquake in the historic or known pre-historic catalogue. The difference in the 2000 year hazard between the low and high hazard maps is shown in Figure 3.

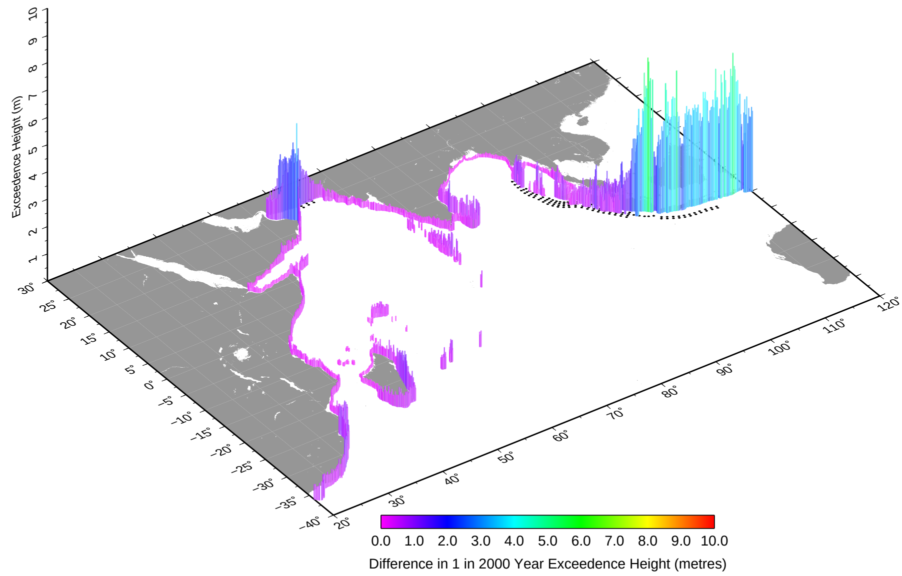

Figure 3: Difference between the "high" (Figure 2a) and "low" (Figure 2b) hazard assessments for all the points considered in this study. The black dots show the centre of the sub-faults contained in both assessment, the red dots were only included in the high hazard assessment. By far the largest difference between the two assessments at the 2000 year return period occurs offshore Java and the Lesser Sunda Islands west of 120° longitude.

2.4 Glossary

Amplitude	Height of the crest of the tsunami wave above mean sea level.
Bathymetry	The measurement of the depth of the ocean floor from the water surface.
Coseismic	At same time as the occurrence of an earthquake.
Hazard	The physical effects of a tsunami that may give rise to risk, such as tsunami amplitude or run-up.
Interseismic	At times between those of repeated earthquake occurrence.
Megathrust	The large fault comprising the boundary between the underthrust and overriding plates in a subduction zone.
Offshore amplitude	The tsunami amplitude at the nearest point to shore at which a water depth exceeds some value, taken as 100m in this study (see Appendix A.3).
Probabilistic Tsunami Hazard Map	A map showing where some measure of hazard (offshore amplitude in this study) has a particular chance of being exceeded per annum.
Return Period	An interval of time long enough to encompass many events, divided by the number of events expected to occur; i.e. ten events in 1000 years would correspond to a return period of 100 years (note that events sometimes occur in rapid succession with long intervals of time in which none occur).
Risk	Loss caused by a tsunami, measured in some combination of "lives, health status, livelihoods, assets and services, which could occur to a particular community or a society" (http://www.unisdr.org)
Run-up height	The maximum water elevation within the limit of inundation. It is usually greater than the wave amplitude at the coast.
Shoaling	"bunching-up" (decreasing wavelength combined with increasing amplitude) of tsunami energy when it enters shallow water, which typically becomes pronounced in water depths of 20 metres or less.
Strain accumulation	Continuous deformation that typically occurs during the time between succesive earthquakes (interseismic), observed using precise geodetic measurements of the earth's surface (e.g., GPS).
Subduction zone	A region of the earth where two tectonic plates converge and one plate is sliding beneath the other. One example is the Sunda Arc that stretches from Timor to Burma.
Teletsunami	A tsunami originating from a distant source, generally more than 1000 km away.
Topography	The measurement of the elevation of the land surface from sea level.
Tsunami	A wave created by a sudden disturbance of water. It is fast moving and has a small amplitude in deep water, but slows and increases in height as it reaches shallow water.
Tsunamigenic	Capable of producing a tsunami.

3 Tsunami in the Indian Ocean

A tsunami is caused when a large mass of water in the ocean is suddenly displaced. Gravity acts to return the displaced water to its equilibrium position and the disturbance propagates as a wave, possibly for a very long distance. They differ from wind generated waves in a number of ways. Firstly, that their wavelengths (distance from peak to peak) are very large, exceeding 100 kilometres in the open ocean. Secondly, they involve movement of the water all the way to the ocean floor, and thirdly they travel very quickly, of the order of 600 to 700 kilometres per hour or more in deep water. Even very significant tsunami will have amplitudes of only a few tens of centimetres in deep water and are likely to pass unnoticed by occupants of a boat. However they carry a great deal of energy and they are able to transport this energy very long distances. When these waves reach shallow water they slow and “bunch up” (their wavelength decreases), and their height increases dramatically, a process known as *shoaling*. The maximum amplitude of the 2004 Indian Ocean Tsunami was estimated to be around 0.6 metres in the open ocean (Song *et al*, 2005) but the tsunami ran up to heights of ten metres along many coasts, even those thousands of kilometres from the earthquake (for example in India, see Narayan *et al*, 2005).

The most common causes of tsunami are large earthquakes occurring under the sea floor, when the sudden movement of large slabs of rock causes the overlying column of water to be displaced. Submarine landslides also cause tsunami, when sediment on steep slopes becomes unstable and fails under gravity, displacing a large volume of water. Less common are tsunami caused by the eruption or collapse of a volcano. Asteroids and comets may also generate tsunami if they fall into the ocean.

3.1 Earthquake Sources

The most common causes of tsunami are earthquakes along oceanic subduction zones. Subduction zones occur where two tectonic plates are converging, and one of the plates is sliding (subducting) beneath the other, the boundary between them forming a large fault known as a *megathrust* (Figure 4). As this happens friction between the two plates may

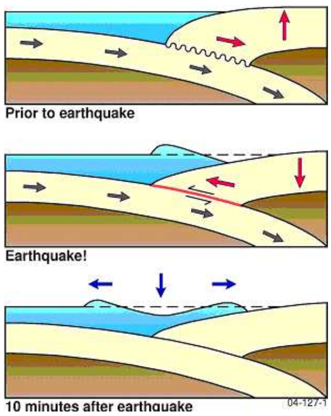

Figure 4: Mechanism for tsunami generation in an oceanic subduction zone.

cause the upper plate to stick to the subducting plate and become distorted by its motion. Eventually the stress associated with this deformation accumulates to such an extent that it can no longer be sustained by the frictional force between the plates, resulting in a sudden movement of the upper plate as it springs back into place. This is known as a subduction zone megathrust earthquake. This movement causes a sudden displacement of the water lying above the plate, producing a tsunami. Not all earthquakes occur in subduction zones, and other types of earthquakes have been responsible for generating tsunami. However, subduction zone megathrust earthquakes are by far the most frequent source of destructive tsunami. For this reason this preliminary assessment of tsunami hazard in the Indian Ocean focuses exclusively on megathrust earthquakes in the oceanic subduction zones that could produce tsunami having significant impact over a wide area. As discussed below, it is recommended that future work on Indian Ocean tsunami hazard consider more carefully other significant sources of tsunami, such as submarine landslides and collapse of volcanic edifices.

3.1.1 Low-hazard vs. High Hazard Assessments

Little is known about maximum earthquake magnitudes, rupture modes and the recurrence times of tsunami events in the Indian Ocean. The 2004 Indian Ocean Tsunami, seemingly unprecedented in the Indian Ocean's written history, showed that the historical record of Indian Ocean earthquakes is insufficient to forewarn of major tsunami. Except on islands off West Sumatra, the studies best suited to improve the record of tsunamigenic earthquake occurrence in the Indian Ocean, geological studies of prehistoric events and geodetic monitoring of strain accumulation, are only beginning to see application (e.g., Jankaew *et al*, 2008, Monecke *et al.*, 2008, and Rajendran *et al*, 2007).

The large gaps in our knowledge of megathrust earthquake occurrence in the subduction zones bordering the Indian Ocean present a dilemma for development of a tsunami hazard map. On the one hand, it is desirable to avoid overestimation of the hazard so that mitigation measures can be appropriately balanced against other demands made on the disaster management community. This argues for consideration of only those sources for which there are clear historical precedents, or some other direct observational evidence of earthquake potential. On the other hand, it could be argued that this approach would ignore important source zones for which the long recurrence intervals of large events may have led to their absence in the historical record. Indeed, such an approach used prior to 2004 would not have identified the threat associated with the Indian Ocean Tsunami.

To resolve this dilemma, it was decided to develop not one but two tsunami hazard maps: a 'low-hazard' one, based on only those earthquake sources of tsunami for which there is definite evidence, and a 'high-hazard' one, based on all potential megathrust earthquake sources, including hypothetical ones for which there is no historical or geological evidence, that may affect Indian Ocean coastlines. The actual hazard lies somewhere between these two, and the difference between the low-hazard and high hazard maps is a simple and effective way to express the uncertainty in the hazard assessment. This uncertainty reflects the lack of knowledge of tsunamigenic earthquake occurrence, and can only be reduced through a better understanding of earthquake and tsunami occurrence in the Indian Ocean.

The probabilistic tsunami hazard assessment presented here considers a wide range of earthquake sources intended to represent all megathrust earthquakes capable of generating a significant tsunami in the Indian Ocean. For the high-hazard end-member assessment, these earthquakes can occur on any of the subduction zones in the Indian Ocean, as well as the South Sandwich Arc in the southern Atlantic Ocean (Fig. 5b; the Puysegur subduction zone south of New Zealand was also considered for the high hazard case, but since it did not significantly contribute to the hazard it is not discussed further). For the high-hazard case, the earthquakes considered can rupture along each subduction zone to a length determined by the lesser of either the length of the subduction zone, or the rupture length associated with a magnitude 9.5 earthquake, which is the maximum used in this study and is equal to that of the largest earthquake ever recorded (the 1960 Chile earthquake). Earthquakes can rupture a "full-width" megathrust, extending from the surface, near the axis of the submarine trench associated with the subduction zone, to the base of a seismogenic zone that is 30-40 km deep and typically about 100 km landward. While massive earthquakes rupturing such wide seismogenic zones and having magnitudes near 9 have historically occurred only in the Sumatra and Andaman Trenches, there is no certainty that such earthquakes cannot occur elsewhere. Therefore, allowing for massive earthquakes along all of the Indian Ocean subduction zones is a reasonable "worst-case" assessment.

The earthquakes considered for the low-hazard hazard assessment form a subset of those considered for the high-hazard case. The earthquakes comprising this subset are limited by the following criteria:

1. **Rupture segmentation.** Megathrust earthquake rupture is confined to subduction zone segments having a contiguous geotectonic character (subducting plate age, megathrust dip, etc.) in which megathrust earthquakes have occurred historically. A further segmentation takes into account segment boundaries where geodetic data indicates there is no interseismic strain accumulation (segments B-E in Fig. 5a).

2. **Maximum magnitude.** The maximum magnitude of megathrust earthquakes in each segment of Fig. 5a is limited to that of the largest historical megathrust earthquake to have occurred there. The Arakan, Sumba, western Makran (segments A, G and H, respectively in Fig. 5a), as well as the South Sandwich and Puysegur zones had a zero maximum magnitude in the low-hazard assessment, since there is no record of any megathrust earthuqake in these generating a destructive tsunami, nor is there any conclusive measurement of interseismic strain accumulation.

3. **Seismogenic zone width.** While the maximum length of earthquake rupture in the direction of the subduction zone axis is limited by the length of the segment on which it occurs, the width is determined by the down-dip width of rupture of historical earthquakes. Thus, earthquake rupture segments are described as either "full-width" or "half-width". For the half-width segments, the down-dip range of the megathrust on which earthquakes can occur is taken to correspond as closely as possible to that on which earthquake rupture has occurred historically.

The purpose of the remainder of this section is to define the earthquake sources used in the low-hazard and high-hazard tsunami hazard maps. The discussion of seismicity in the various subduction zones that may generate tsunami affecting the Indian Ocean presented here will allow us to establish the combinations of source mechanisms and maximum magnitudes to be used in the hazard map. The results of this discussion are summarized in Table 2.

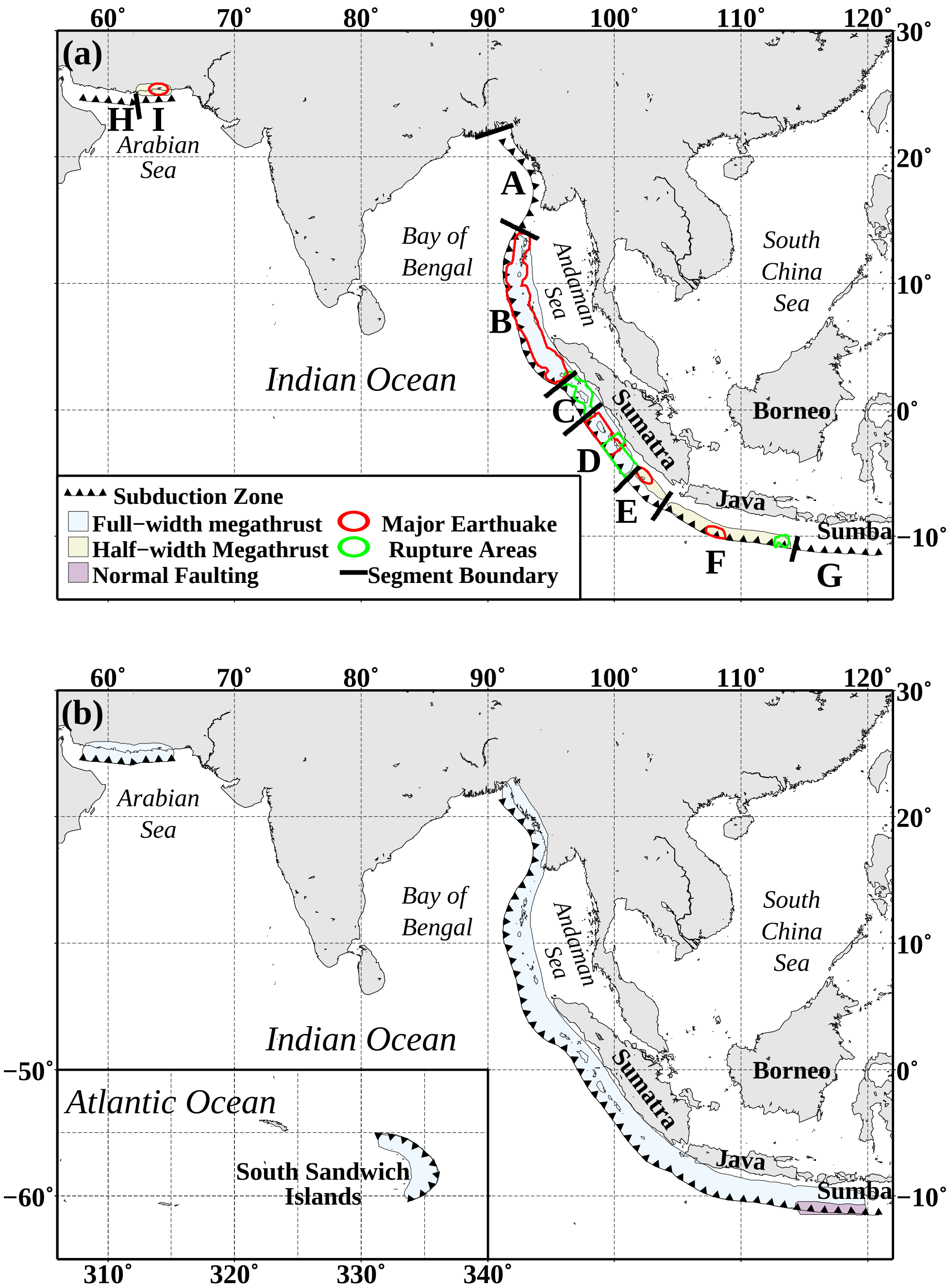

Figure 5: Map of megathrust earthquake sources of tsunami in the Indian Ocean, illustrating the source characterisation used for the low-hazard and the high-hazard maps. (a) The megathrust segmentation for the low hazard map. Also shown are the megathrust seismogenic zones characterized as "full-width" and "half-width". (b) The segmentation for the high-hazard assessment. This figure alsoincludes the South Sandwich Arc, which is a source of tsunami for the high-hazard map but not for the low-hazard one. The Puysegur subduction zone south of New Zealand was included, but made no significant contribution to the hazard along the coastlines coinsidered here. Plate boundaries from Bird (2002).

3.1.2 Andaman-Sunda Arc

The Andaman-Sunda Arc stretches from the Bay of Bengal in the north to the Banda Sea in the east (Fig. 5). It spans several different tectonic environments which are considered here as distinct source zones: the Arakan, Andaman, Sumatra and Java Trenches, where the latter encompasses the source zone offshore the Indonesian island of Sumba. Although tsunami sources east of Sumba (approximately 120° E longitude) may generate tsunami having destructive impact along the coasts of eastern Indonesia and northern Australia, these were considered beyond the scope of this study because they do not direct significant energy into the Indian Ocean.

A review of the seismotectonics of the Sunda Arc and its tsunamigenic potential is given in Burbidge *et al*, (2008). Here we focus on the rationale behind the characterization of sources for the low-hazard and high-hazard earthquake source specifications. For the 'high-hazard' assessment, the entire Sunda Arc is allowed to rupture in earthquakes having magnitudes as large as 9.5, which can occur anywhere along the Sunda Arc (Fig. 5b).

The remainder of this section discusses the choice of sources for the 'low-hazard' assessment. This choice is governed by the principle that earthquake zones will be characterized using only direct evidence for potential earthquake occurrence. Such direct evidence consists of either historical earthquakes or paleoseismic/paleotsunami evidence for prehistoric events. Also, direct evidence for earthquake potential can be inferred from geodetic (including paleogeodetic measurements) of either the presence or lack of crustal strain accumulation that might lead to a large earthquake. These measurements provide the basis for a model of rupture segmentation of the Andaman-Sunda Arc, on the basis that an earthquake rupture is presumed to occur only where the frictional coupling between the subducting and overriding plates is strong, and does not extend beyond segment boundaries where the coupling is weak.

Chlieh *et al*, (2008) give a comprehensive review of coupling along the central Sumatra section of the Sunda megathrust. Their results are based on analysis of coral growth rings and GPS data to study the pattern of coupling on the Sunda megathrust. They concluded that this pattern of coupling is an intrinsic feature of the megathrust that is likely to persist for more than several earthquake cycles. They found that the large megathrust earthquakes of 1797, 1833 and 2005 were confined to the regions of relatively high coupling and did not extend across, nor far into, the regions where coupling is weak. Their modelling suggests coupling of the subducting oceanic plate to the overriding one is heterogeneous and identify several sections in which the coupling is weak:

1. The Simeulue "Saddle", at 2.5°N, at the boundary between the ruptures of the 2004 Sumatra-Andaman and the 2005 Nias earthquake (between segments B and C of Fig. 5a),
2. The Batu islands, where the Investigator Fracture zone intersects the axis of the Sumatra Trench, at the northern limit of rupture of the 1797 Sumatra earthquake (between segments C and D of Fig. 5a), and
3. Enggano Island, at the southern limit of rupture of the 1833 and the 2007 Sumatra earthquakes (between segments D and E of Fig. 5a).

In addition, there are several points along the Andaman-Sunda Arc megathrust where it seems logical, from changes in earthquake activity and tectonic environment, to infer that barriers to earthquake rupture propagtion may exist:

1. The northern limit of rupture associated with the 2004 Sumatra-Andaman earthquake. This is also where the overriding plate in the Andaman-Sunda Arc subduction zone transitions from the Andaman Sea to the continental curst of Myanmar (between segments A and B of Fig. 5a),

2. The Sunda Straight, which marks the gradual transition from oblique subduction of oceanic lithosphere of intermediate age (< 60Ma) beneath Sumatra, to the non-oblique subduction of relatively old oceanic plate (>60 Ma) beneath Java (between segments E and F of Fig. 5a), and

3. The transition in seismicity from shallow thrust off Java, to predominantly normal faulting earthquakes off Sumba (eastern between segments F and G of Fig. 5a).

These six inferred segmentation boundaries divide the Sunda megathrust into the seven regions indicated in Fig. 5a. Maximum magnitudes used for these segments are taken to be the same as the maximum magnitudes of historical earthquakes ocurring in each segment. These are summarized in Table 2. With the exception of segments E and F, all of the historical earthquakes in the Andman and Sumatra segments (B-D) have been large enough to rupture the full width of the megathrust, as indicated by the earthquake rupture areas displayed in Fig. 5a. The largest earthquake occuring in segment E was a Mw7.9 event in 2000, but Abercrombie *et al*'s (2003), analysis of this event showed that only 35% of this earthquake's moment corresponded to megathrust rupture, so the maximum magnitude for megathrust earthquakes in this segment has been taken to be Mw7.6. As with segment F in the Java Trench, only a narrow downdip width of the megathrust has experienced megathrust rupture, so these segments have been taken to have a half-width megathrust seismogenic zone consistent with the rupture areas of the historical events.

While there is historical evidence that segment A has experienced a major earthquake (Cummins, 2007), there is no estimate of its magnitude. It is not clear that it ruptured the megathrust fault specifically, nor that it generated anything more than a local tsunami. The potential for future occurrence of a large tsunamigenic earthquake in this segment is therefore unknown, so for the low-hazard case it is assumed that it has no tsunamigenic potential (i.e., maximum magnitude zero). Segment G was also assumed to have no tsunamigenic potential for the low-hazard case, despite the fact that a major tsunamigenic earthquake occurred there in 1977 (Lynnes and Lay, 1988). This event was a normal faulting, intraslab earthquake that did not rupture along the megathrust fault separating the two plates. Although large normal earthquakes have caused large tsunami in the past (eg the 1977 Sumba earthquake and tsunami), such events are rare and there is no known case of recurrent rupture of such an intraslab, normal fault. Thus, for segment G as well the potential for future occurrence of a large tsunamigenic earthquake is unknown, and the maximum magnitude has been taken as zero for the low hazard case. A more complete assessment of tsunami hazard, especially that takes into account very long return periods, would consider the probability that large, normal faulting earthquakes could occur on any subduction zone.

3.1.3 Makran Subduction Zone

The Makran subduction zone is characterized by the subduction of the oceanic part of the Arabian plate beneath the Eurasian plate, and extends along the Gulf of Oman from the Minab-Zendan Fault system near the Straight of Hormuz in the west, to the Baluchistan volcanic arc in the east (Mokhtari *et al*, 2008). It has one of the largest accretionary prisms

Subduction Zone	Segment	Maximum Magnitude (Mw)		
		Historical	Low Hazard	High Hazard
Andaman-Sunda Arc	A	unknown (1762[1])	0.0	9.5
	B	9.2 (1881[2], 2004[3])	9.2	
	C	8.7 (1861,2005[4])	8.7	
	D	9.1 (1797,1833,2007[5])	9.1	
	E	7.6 (2000[5])	7.6	
	F	7.8 (1994[7],2006[8])	7.8	
	G	none	0.0	
Makran	H	unknown (1483[8])	0.0	9.1
	I	8.1 (1945[9])	8.2	
South Sandwich		none	0.0	9.0

Table 2: Summary of megthrust earthquake tsunami source zones used in the low-hazard and high-hazard maps. The three subduction zones considered are shown, along with the segmentation that was used for the low-hazard maps (see Fig. 5a). The maximum magnitude of the historical earthquakes listed in brackexts is listed in the third column. The maximum magnitudes used to generate the low-hazard and high-hazard assessments are shown in columns four and five. Where the maximum magnitude for historical earthquakes is listed as 'unknown' that indicates that a large (possibly megathrust) earthquake occurred, but its magnitude is unknown. By contrast 'none' indicates that there is no known historical occurrence of a megathrust earthquake large enough to generate a destructive tsunami. The years of historical earthquakes are indicated in parentheses with superscripts to indicate the following references: [1] Cummins (2007), [2] Ortiz and Bilham (2003), [3] Stein and Okal (2005), [4] Briggs *et al* (2005), [5]Natawidjaja *et al* (2006), [6]Abercrombie *et al* (2003), [7] Abercrombie *et al* (2001), [8]Ammon *et al* (2007), [8]Abraseys and Melville (1982), [9]Byrne *et al* (1992). These studies were used to infer the width of the megathrust seismogenic zone used in the low-hazard map, indicated as (full) or (half).

in the world with a wide toe of thick unconsolidated sediments (Byrne, *et al*, 1992), lying above a shallow dipping decollement. The Makran subduction zone appears to be split into two segments; segment H in the west and segment I in the east, as indicated in Fig. 5a, separated by a sinistral fault known as the Sonne Fault.

Major historical earthquakes have been reported for the eastern segment (Ambraseys and Melville, 1982), but the only event that is recent enough to estimate a reliable magnitude is the 1945 earthquake near Pasni (Fig. 5a). This earthquake had source parameters of an megathrust event that ruptured about 100 km, approximately one-tenth the length of the entire subduction zone. According to a dislocation model that fits a single observation of coseismic coastal uplift, the rupture terminated about 30 km offshore, along the shelf edge (Byrne *et al*, 1992), suggesting a relatively narrow megathrust seismogenic zone. The 1945 Makran earthquake generated a tsunami that affected the coasts of Iran, Pakistan, Oman and India (Pendse, 1947; Ambraseys and Melville, 1982; Byrne *et al*, 1992). Because of a disparity between the origin time of the earthquake and the arrival of the tsunami, the latter being delayed by about 30 minutes at locations within the rupture zone (Bilham *et al*, 2007), it has been speculated that a submarine landslide may have been an important contributor to the tsunami excitation (Rajendran *et al*, 2008a and 2008b).

The western segment of the Makran subduction zone may have witnessed the occurrence of a large offshore earthquake in 1483 (Ambraseys and Melville, 1982), although recent work suggests his may have been a moderate event that occurred in the vicinity of Qeshm Island near Hormuz, that may have been incorrectly associated with a separate event in the Zagros region (Musson, 2008). The lack of major earthquakes in the western segment either means the segment has been locked and accumulating strain energy for hundreds of years or it is that this segment is creeping aseismically. The regional GPS estimates indicate a convergence of about 2 cm/year (Bayer *et al*, 2006). However, the existence of Holocene (10000 years) marine terraces (Page *et al*, 1979) indicates that this segment is also active, although the recurrence period of earthquakes (> 8.0) may be much longer (ie thousands of years).

Since there is no certain knowledge of the potential for the western segment (H) of the Makran subduction zone to produce large tsunamigenic earthquakes, it is not included as a source zone in the low-hazard end-member assessment. This assessment allows for a half-width megathrust seismogenic zone on the eastern segment (I), which can produce earthquakes having a maximum magnitude of 8.2, calculated using the Wells & Coppersmith relationship for the area of sement I. This value is also broadly commensurate with the magnitude of 1945 Makran earthquake (around 8.1 to 8.3). For the high-hazard end-member assessment, the entire length of the Makran subduction zone is allowed to rupture over the full width of the megathrust, resulting in a maximum magnitude of Mw9.1 from Wells & Coppersmith's (1994) scaling relation (see Fig. 5b).

3.1.4 Central Indian Ocean

In June 2000 an Mw 7.9 event occurred about 150km to the southeast of the Cocos (Keeling) Islands in the middle of the Indian Ocean. Analysis of the event indicates that the earthquake started as a strike-slip event but then may have triggered a simultaneous earthquake on another fault (a compound rupture). The second fault has variously been argued to be another strike-slip fault or a thrust fault (Abercrombie *et al*, 2003). This earthquake was a typical, if large, example of the earthquakes that occur right across the Indian Ocean. Events in this region tend to be a mix of thrust and strike-slip earthquakes. The central

Indian Ocean is one of the most seismically active ocean basins, however its level of activity is still much less than the Andaman-Sunda Arc.

The central Indian Ocean region is currently thought to be a diffuse plate margin separating the Indian and Australian plates (Bird, 2003). Australia and India are approaching each other by less than 8mm/yr (Bird, 2003). Unlike other oceanic plate margins this convergence is being accommodated over a very large region which is at least 25 degrees in longitude and 15 degrees in latitude. One transect of the region counted as many as 134 active faults over a distance of 2100km (Chamot-Rooke *et al*, 1993). The deformation in this region appears to be accommodated by a complex mix of:

- Strike-slip earthquakes along pre-existing transforms formed at the Australian-Antarctic spreading centre;
- Pre-existing normal faults formed at the spreading centre and reactivated as reverse faults; and
- Recently formed thrust faults scattered throughout the Indian Ocean.

Since the convergence is spread over so many small faults, the individual slip rate on any fault is probably less than 0.1mm/yr. Cumulatively this adds up to the still very small 8mm/yr of relative convergence between the Indian and Australian plates.

There are far too many faults in this area to consider in a probabilistic tsunami hazard assessment using unit sources, as the one described here. One would have to use an areal source, similar to the method used in seismic hazard studies in other intra-plate regions, since there is also no known fault map for the area. The slip rates are probably low, so it is quite likely that the effect on the hazard maps to follow will be very small. However, it is worth acknowledging that there is a small, but non-zero, chance of a major earthquake (up to at least magnitude 8) occurring anywhere in the Indian Ocean. If they are large enough and located close enough to the coast, they may produce a hazardous tsunami. The return periods for a hazardous tsunamigenic events is likely to be very long for any particular fault in this region. For this reason earthquakes in central Indian Ocean are not coinsidered in either the low hazard or high hazard assessments.

3.1.5 South Sandwich Arc

No destructive tsunami are known to have been generated by earthquakes in the South Sandwich Arc, located in the southern Atlantic Ocean, and for this reason it has not been included as a source zone in the low-hazard map. On the other hand, several earthquakes with magntiudes greater than 7 have occurred near this subducton zone, including the largest historical earthquake of magnitude 8.1 (Okal and Hartnady, 2008), which occurred in 1929. While many of these earthquakes appear to be associated with subduction-related faults other than the megathrust, the potential for large megathrust earthquakes to occur on this zone cannot be discounted. Since the potential for the South Sandwich megathrust to produce large tsunamigenic earthquakes cannot be discounted, the high-hazard map includes this as a source zone comprising a full-width megathrust that can produce earthquakes up to a maximum magnitude of 9.0.

3.2 Non-earthquake source of tsunami

Non-earthquake sources of tsunami hazard in the Indian Ocean have not been considered in either of the low hazard or high hazard assessments because they are poorly constrained and probably very rare. However, since they may be considered in future work, we briefly summarize them as follows:

Submarine landslides Submarine landslides near the coast have the potential to produce large, local tsunami. While there is evidence of large, potentially tsunami-generating submarine slope failures off Sumatra and Christmas Island, the sparsity of data in the Indian Ocean precludes any definitive statement about the frequency of submarine slope failures. Our understanding of the tsunamigenic potential of submarine landlides in the Indian Ocean is too poor at present to consider including in this preliminary tsunami hazard assessment for the Indian Ocean. However, it is important to bear in mind that two of the largest submarine accumulations of sediment in the world, the Bengal and Indus Fans, are in the Indian Ocean. These enormous sedimentary fans have formed due to the rapid flux of sediment caused by the uplift of the Himalaya and Karakoram mountain ranges. The presence of these sedminetary fans adjacent to active subduction zones implies that the potential for large, regional or even teletsunami to be generated by submarine landslides should not be discounted (indeed, this may be the dominant component of the 1945 Makran tsunami generation, see Rajendran *et al*, 2008). The importance of landslide-generated tsunami may be more important in the Indian Ocean than elsewhere, and future work on tsunami hazard in the Indian Ocean should consider this possibility.

Volcanic eruptions The 1883 eruption of Krakatau is the only known major volcanic eruption that has triggered a tsunami which has affected most of the Indian Ocean. The Krakatau eruption caused a large (42m local run-up) tsunami which was observed all around the Indian Ocean and the rest of the world. The average recurrence time for major eruptions at Krakatau is thought to be 21,000 years (Beauregard, 2001). The potential for other volcanoes in the region generating a tsunami large enough to contribute to an ocean-wide hazard is unclear. Some potentially hazardous volcanoes in the Indian Ocean include: Barren Island, Piton de la Fournaise on Reunion Island, La Grille on Grand Comore Island and Big Ben on Heard Island.

Asteroid/meteorite impacts The largest tsunami of all are likely to be generated by asteroid/meteorite impacts. It is known that some major extinction events, such as that between the Cretaceous and Tertiary periods 65 million years ago, concided with impacts of comets or asteroids of about ten kilometres in diameter. Such events are almost certainly associated with massive tsunami, with wave amplitudes far exceeding any tsunami in historic times, but are extremely rare. Intermediate-sized objects with diameters in the range 100 metres to one kilometre could affect any coastal community, with estimates of return times of 11,000 and 30,000 years for a (respectively) 2m and a 5m tsunami impacting Perth (Ward & Asphaug, 2000), but there is considerable uncertainty about the generation and propagation of tsunami waves from such impacts. Smaller objects probably do not generate hazardous tsunami (Ward & Asphaug, 2000).

4 Method Outline

The method used in this investigation may be summarised as follows:

- Determine the earthquake source zones to be included in the study (Figure 5 and the discussion in Section A.4 of the Appendix).
- For each source zone, determine the possible characteristics of the earthquakes that could occur in that source zone, and the probability of each such earthquake occurring. Use this to assemble a large catalogue of possible (or synthetic) earthquakes.
- Simulate the tsunami from each synthethic earthquake and estimate the maximum tsunami amplitudes that result from each tsunami at a number of selected locations (called *model output points*) near each Indian Ocean nation.
- Combine these results to calculate the probability a given maximum tsunami amplitudes could be exceeded per year.

The assumed maximum earthquake magnitude assigned to each source zone segment for the low hazard map is listed in Table 2 and for the high hazard map all zones had a maximum magnitude of Mw9.5. Earthquakes with magnitudes ranging from Mw7.0 to the maximum (in increments of 0.1) with various characteristics were simulated. A total of 24,714 simulated (or *synthetic*) earthquakes were included, 5,948 in the low hazard assessment and 18,766 in the high hazard one. Not as many earthquakes were included in the low hazard assessment because there were fewer and smaller zones in that assessment and the maximum magnitude of the earthquakes were considerably smaller. In the high hazard assessment the full width of the Sunda Arc zone from Burma to the Indonesian island of Sumba was included as well as the whole of the Makran, Puysegur and South Sandwich zones. In the low hazard assessment only some sections of the Sunda Arc and Makran were included in that assessment, see Section 3.1.1 for more details.

Probabilities were assigned to each of the synthetic events using the historical record and the available geophysical information. The most important factors controlling the earthquake probability are the rate of covergence across each segment, the overall global rate of earthquake occurence at subduction zones observed historically and the maximum magnitude assumed for each zone. Details of this method are outlined in Appendix A.

Numerical computations were performed to simulate the propagation of tsunami waves from the earthquake source zones to the model output points. The results of these simulations were used to estimate the maximum tsunami amplitude at each model output point due to each synthetic earthquake. The resulting data may be mapped in various ways to give a visual representation of the hazard faced by each of the nations, and the sources of that hazard.

4.1 The Hazard Maps

In this report the results of the study are presented with the aid of the following types of diagrams:

1. **Hazard Curves:** These describe the relationship between the return period and the maximum tsunami amplitude for a particular model output point. The tsunami

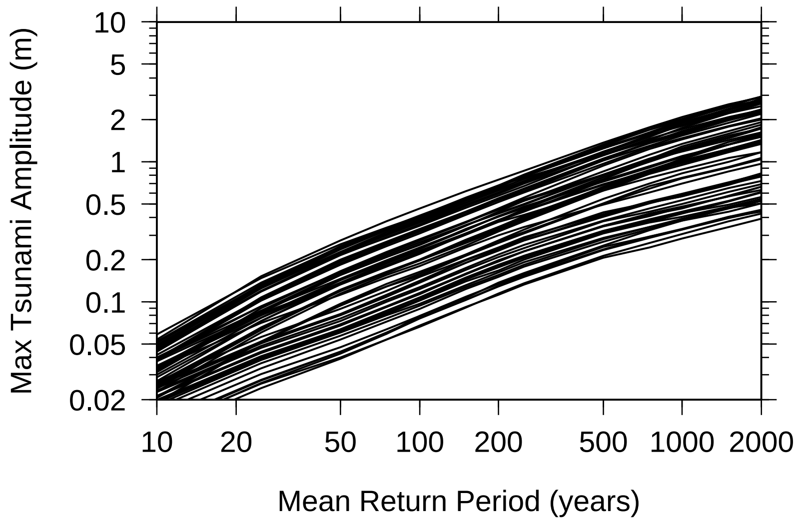

Figure 6: Hazard curves for all points offshore Sri Lanka. This shows the maximum tsunami amplitude for a range of different return periods for all the points in this PTHA assessment. The amplitude of the wave given on the y-axis can be expected to be exceeded at the return periods given by the x-axis.

amplitude given on the y-axis is predicted to be exceeded with the average return period given by the x-axis. In Section 5, which describes the results for each country, hazard curves are shown as part (a) in the figure within each country's section. For example, Figure 6 shows the hazard curves for all the points offshore Sri Lanka in the "low hazard" map.

2. **Maximum Amplitude Maps:** The maximum tsunami amplitude that will be exceeded at a given return period for every model output point in a region. A different map for the region can be drawn for each return period. Figure 7 is an example of this type of map shown in Google Earth^{TM}. In Section 5, these maps form part (c) of each country's respective figure.

3. **Probability of Exceedance Maps:** For a given amplitude, these maps show the annual probability of that amplitude being exceeded at each model output point in a region. A different map can be drawn for each amplitude for that region. KML files on the DVD that can be loaded in to Google Earth to produce these maps are discussed in Section 4.1.1.

4. **Deaggregated Hazard Maps:** These indicate the relative contribution of different source zones to the hazard *at a single location.* A different map will be obtained for every choice of model output point (and for different return periods), and so there are a great many possible deaggregated hazard maps that may be drawn for any given region. Examples of deaggregated hazard maps can be produced using software found on the DVD (see Section 4.1.1).

5. **National Weighted Deaggregated Hazard Maps:** These give an indication of the source of the hazard to a nation or region as a whole, and are are not specific to a particular offshore location. The national weighted deaggregated hazard maps provide a convenient summary of the source of hazard over a region. However, if one is interested in the hazard at a particular location, near a large town for example, then a deaggregated hazard map for a model output point near that particular location would be more useful. Part (b) of the figures shown in Section 5 show examples of this type of hazard map.

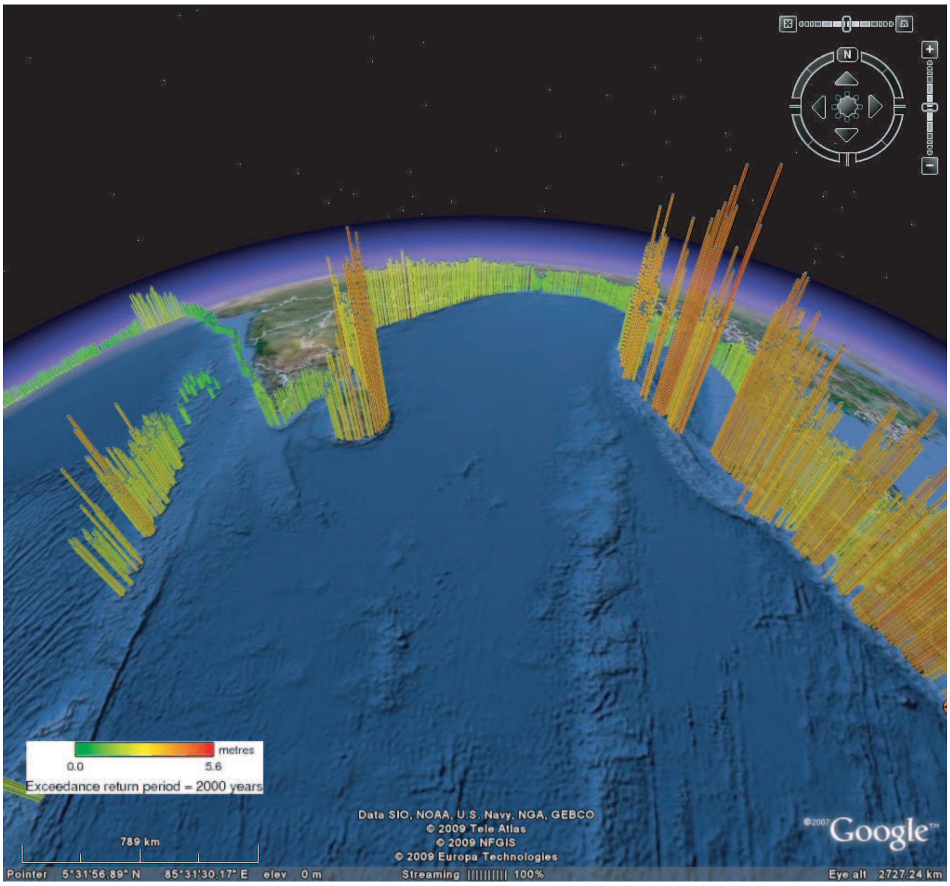

Figure 7: The maximum tsunami amplitude with a 1 in 2000 year chance of being exceeded per annum for points along a selected 100m depth contour. This is a Google Earth™screenshot of one of the KML maps included on the DVD.

More details are given about the method of producing the deaggregated and national weighted deaggregated hazard maps in Section A.7 of Appendix A.

4.1.1 KML Files on the Companion DVD

It is possible to draw many more maps than sensibly can be placed in a report such as this. Moreover, diagrams of types 2 to 5 above are very well suited to being presented using Google Earth™. Accordingly, on the companion DVD there is a directory labelled "hazard_maps", which contains a directory for each of the two end-member hazard assessments considered in this report: "high_hazard" and "low_hazard". Each of these directories contains files of the following two types:

1. Files with names of the form "probability_of_exceedance_x.kml" show estimates of the annual probability of the maximum amplitude of a tsunami exceeding "x" metres at approximately the 100m contour. For example, the file "probability_of_exceedance_1.0.kml" is the annual probability of a tsunami wave exceeding 1.0m at the locations of the bars. This dataset allows the user to determine how often a tsunami could be expected to exceed a specific amplitude of interest (e.g. one metre). If there is a specific amplitude of interest, then these maps can tell the user the probability of that response being needed per annum for that location offshore.

2. KML files with names of the form "wave_amplitude_x.kml" on the DVD show the maximum tsunami amplitude that is estimated to be exceeded every "x" years. For example, "wave_amplitude_1000.kml" is a map showing the maximum wave amplitude with a 1 in 1000 year chance of being exceeded at the locations of the bars. This is an alternative way of plotting the hazard where the probability is fixed and the amplitude is plotted, instead of fixing the amplitude and plotting the annual probability. This functionality allows the user to determine the maximum "1 in x year wave amplitude" for a particular offshore location. Tsunami with an amplitude greater than this number therefore only happen less often than 1 in "x" years.

(It should be remembered that the tsunami amplitudes in these maps refer to the amplitude of the tsunami offshore, in water of 100 m depth, which can be several times smaller than the amplitude of the tsunami at the coast - see Section 2.2.)

In addition, the companion DVD contains a software tool, 'Hazmap Viewer', for generating KML files that, when imported into Google Earth^{TM}(or similar mapping software), give a very good representation of deaggregated hazard maps. Hazmap Viewer should be started automatically after the DVD is inserted into a PC running Windows, but it can also be start by clicking on the 'hazmap.bat' file on the DVD. It allows for selection of coastal points for which deaggregated hazard maps can be displayed, and KML files for these maps to be generated. Each KML file produces a collection of coloured columns showing the relative values of a dataset from the PTHA. The height and colour of the columns reflect the values of the data being represented, and the map can be interrogated by clicking on the top of each column, which will display the value represented by that column.

These deaggregated hazard maps show the percentage of the annual probability of exceedance at a specific return period which results from each sub-fault. This value varies depending on the specific location off the coast chosen for the deaggregation. These maps allow the user to determine which zones are the most important for a given location at a given return period (e.g. which zones can contribute to the 1 in 2000 year wave for a particular section of coast). Generally the smaller wave amplitudes (or equivalently shorter return periods) originate from a wider range of possible sources. Conversely, the larger wave amplitudes (or equivalently longer return periods) originate from a more restricted range of possible sources, usually from a fault that is ideally located to direct large waves to that location. The deaggregation location (x, y) is indicated on the map by a white square with zero height. Google Earth^{TM}will automatically zoom into this square when the dataset is loaded.

5 Results

This section discusses the results as they apply to each Indian Ocean nation included in the study. The diagrams presented in this section have been limited to hazard curves for return periods of between 10 and 2000 years, and maximum amplitude exceedence and national weighted deaggregated hazard maps at 2000 year return periods. For some nations the results have been further divided, either because of geographic spread, or because different regions have significantly different hazard profiles.

In each section there will be one figure containing three hazard maps for that region. Part (a) shows the hazard curves, (b) the national weighted deaggregated hazard map and (c) is the maximum amplitude map for the 2000 year return period. For a more detailed explanation of the maps, please see Section 4.1. For the deaggregated map (Part c) we focus the map on the areas which contribute to the hazard. This means that the Puysegur zone and South Sandwich zones only appear on deaggregated maps where they contribute significantly to the 2000 year hazard.

The diagrams and discussion in this section can only give an overview of the magnitude and source of the hazard faced by each nation. The maximum amplitude maps are restricted to a 2000 year return period, and the national weighted deaggregated hazard maps only give a general idea of the source of the hazard for the region as a whole. The KML files on the accompanying DVD can be used to gain a more detailed picture of the hazard of each nation. For example, if one is interested in the source of the hazard at a particular location one should look on the accompanying DVD for a deaggregated hazard map drawn for a model output point close to that location. Similarly, if one is primarily interested in the hazard at a different return period than 2000 years, please consult the KML files on the DVD.

5.1 Bangladesh (low hazard)

The hazard at the 2000 year return period for Bangladesh comes mainly from the Aceh region of the Sunda Arc subduction zone Figure 8(b). The 2000 year maximum amplitudes are of the order of 0.2 to 0.5 metres (Figure 8(a)) and is higher off eastern Bangladesh than western Bandladesh (Figure 8(c)).

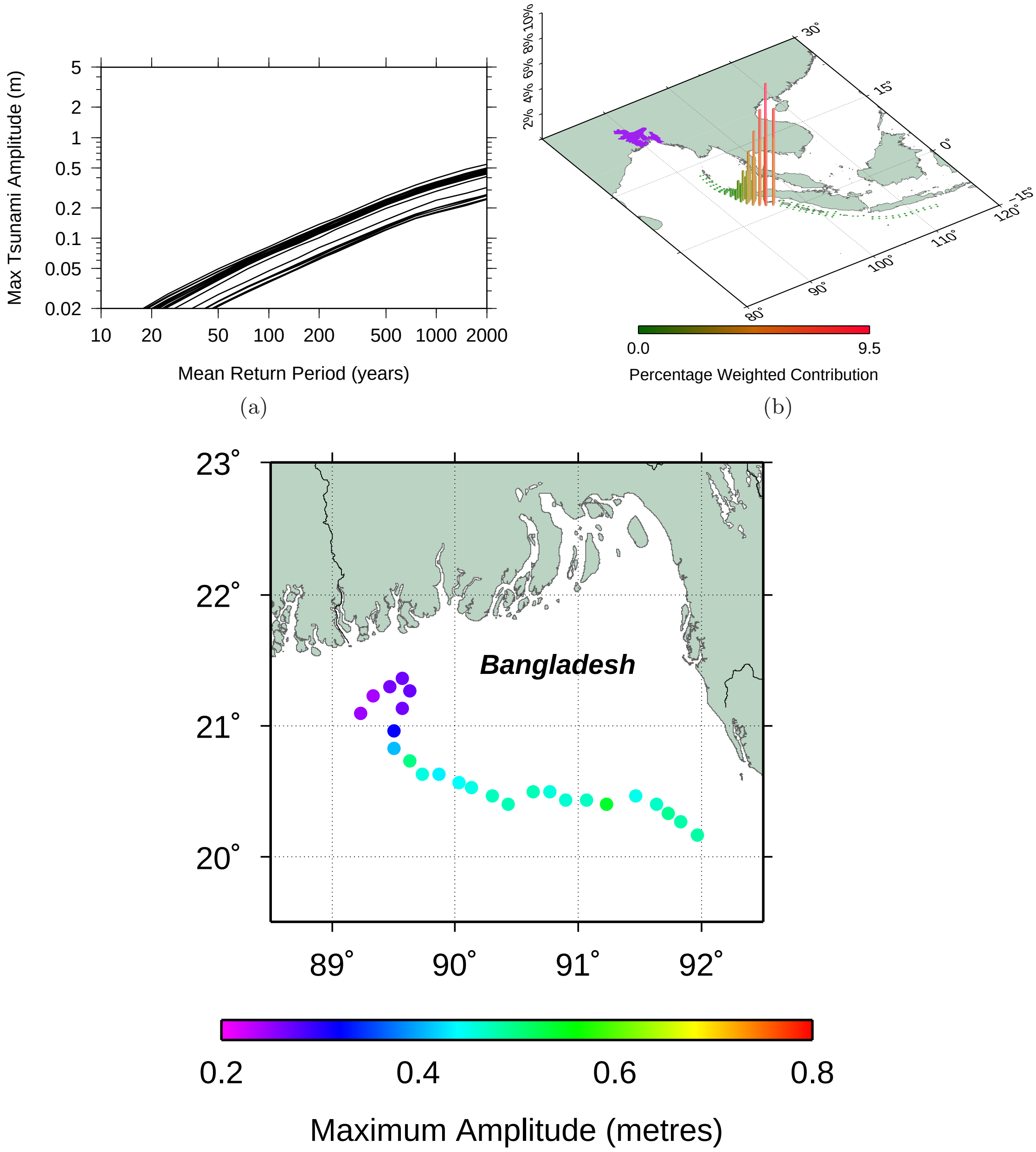

(c)

Figure 8: Bangladesh:- (a) Hazard curves for all model output points. (b) National weighted deaggregated hazard. (c) Maximum amplitude at a 2000 year return period for all model output points.

5.2 Bangladesh (high hazard)

The hazard at the 2000 year return period for Bangladesh in the high hazard map mostly originates from the Arakan extension of the Sunda Arc subduction zone. The 2000 year maximum amplitudes range from over 0.3m to about 0.6m and is again higher in the east (where it is close to the Arakan zone) than the west (Figure 9(a and c)).

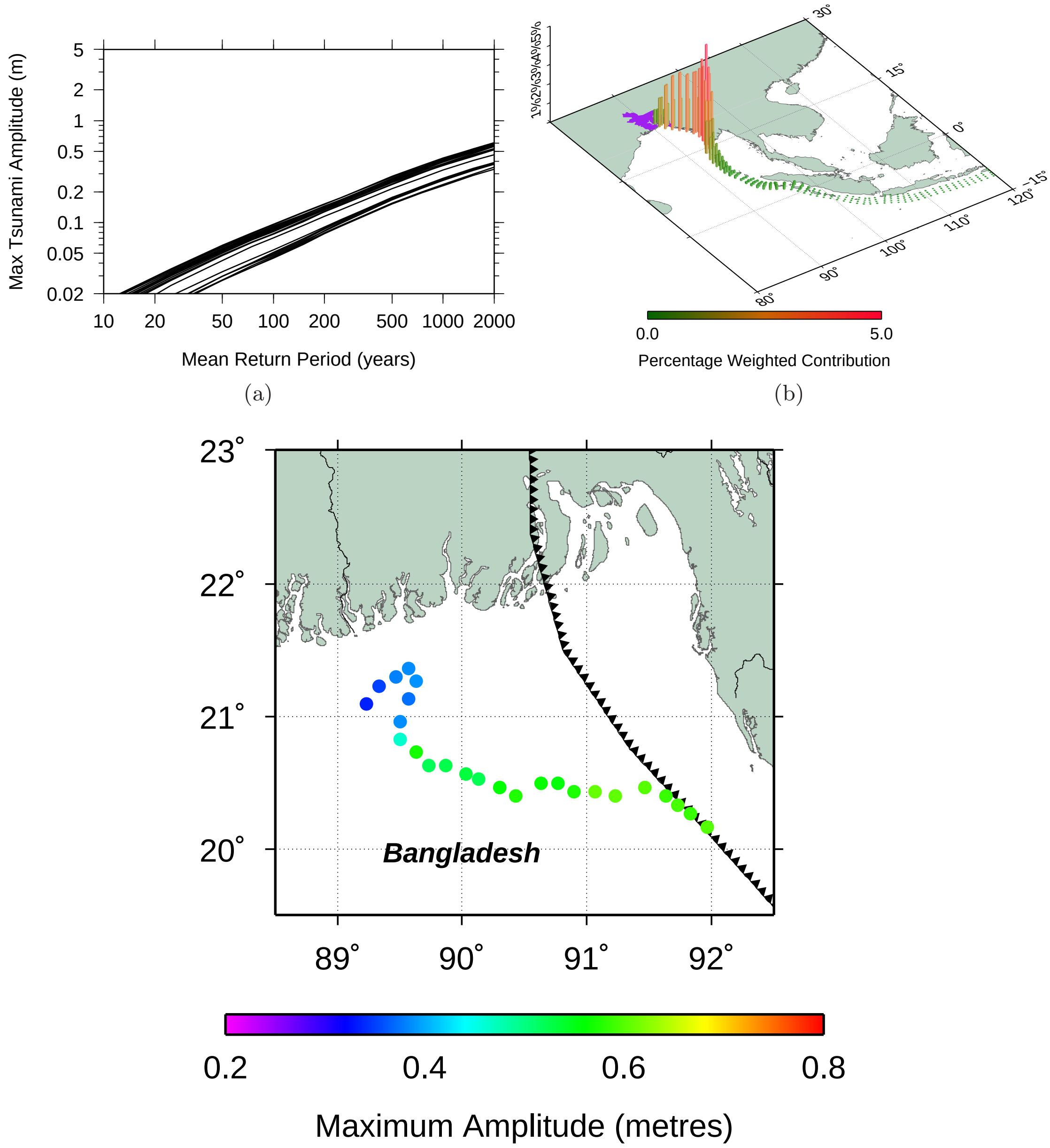

(a) (b) (c)

Figure 9: Bangladesh:- (a) Hazard curves for all model output points. (b) National weighted deaggregated hazard. (c) Maximum amplitude at a 2000 year return period for all model output points.

5.3 British Indian Ocean Territory (low hazard)

The major contribution to the hazard of the British Indian Ocean territiory of Diego Garcia (for the 2000 year return period) comes from the Aceh-Andaman section of the Sunda Arc. Central Sumatra is also somewhat important (Figure 10(b)). Diego Garcia can expect offshore maximum amplitudes at the 2000 year return period of between 0.6 and 1.1m metres (Figure 10(a and c)).

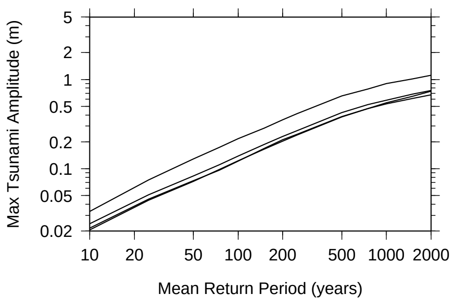

(a)

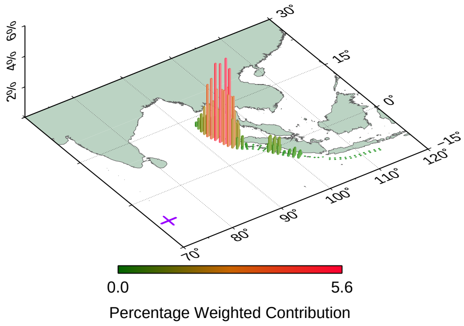

(b)

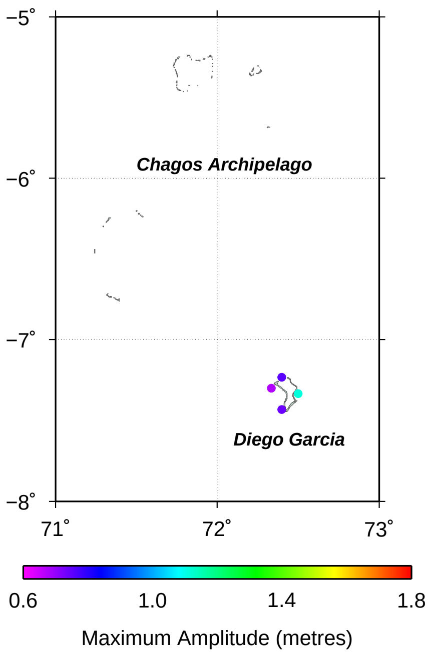

(c)

Figure 10: BIOT:- (a) Hazard curves for all model output points. (b) National weighted deaggregated hazard. (c) Maximum amplitude at a 2000 year return period for all model output points.

5.4 British Indian Ocean Territory (high hazard)

The major contribution to the hazard of Deigo Garcia in the high hazard map also comes from the Arakan-Sumatra section of the Sunda Arc subduction zone but is more uniformly spread along the zone in the high hazard deaggregation map than it was in the low hazard map (Figure 11(b)). Diego Garcia can expect maximum amplitudes at the 2000 year return period of between 1.1 to 1.7 metres (Figure 11(a and c)) according to this assessment.

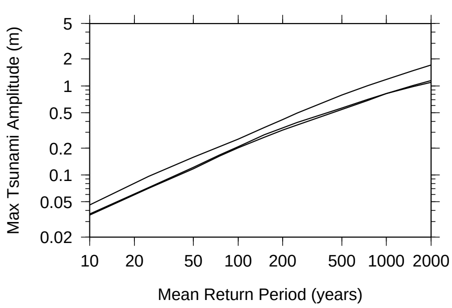

(a)

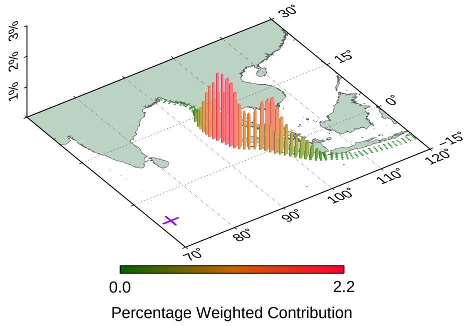

(b)

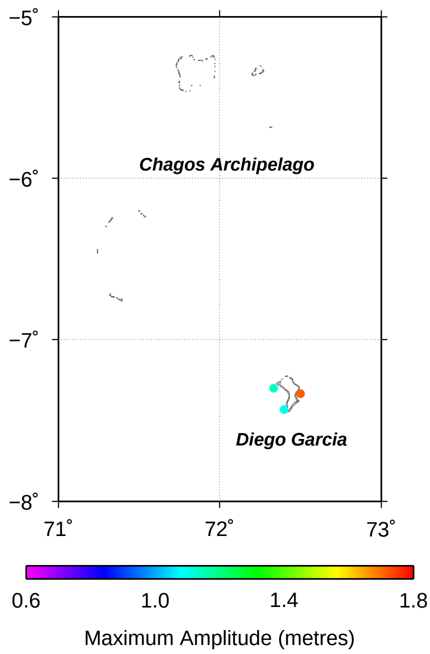

(c)

Figure 11: BIOT:- (a) Hazard curves for all model output points. (b) National weighted deaggregated hazard. (c) Maximum amplitude at a 2000 year return period for all model output points.

5.5 Burma (low hazard)

Figure 12(a) shows that the tsunami amplitudes offshore Burma range between 0.7 and 1.1m, the highest values to the south (Figure 12(a and c)). At the 2000 year return period, the deaggregated hazard mostly originates from the southern Andaman. The islands in the northern Andaman act to protect Burma from tsunamis coming from this section of the Sunda Arc.

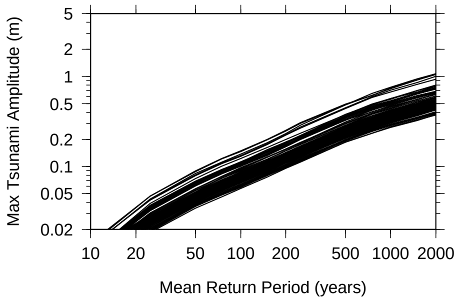

(a)

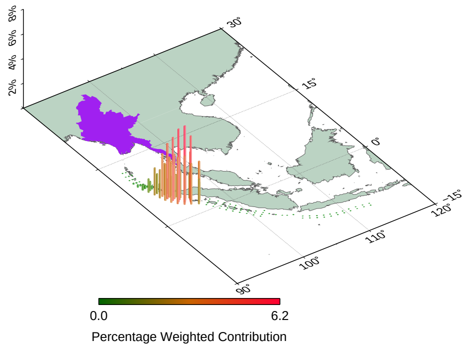

(b)

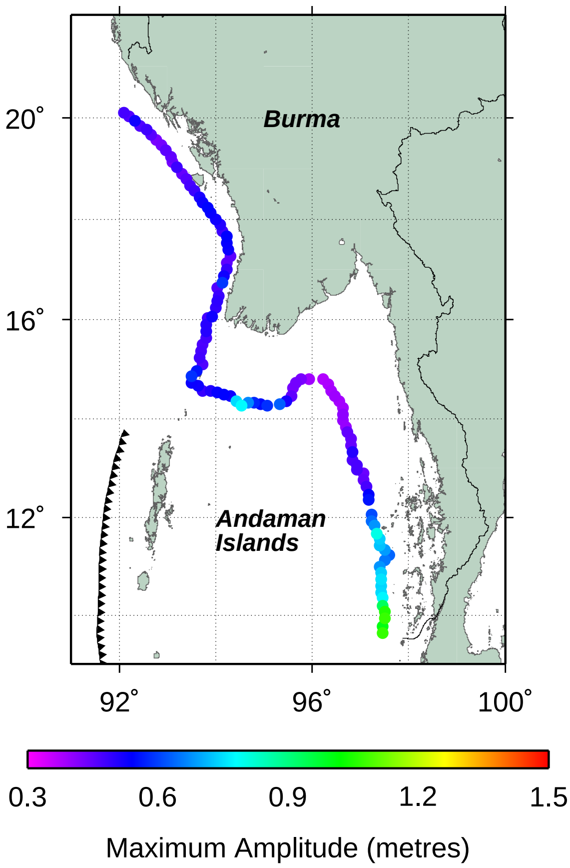

(c)

Figure 12: Myanmar:- (a) Hazard curves for all model output points. (b) National weighted deaggregated hazard. (c) Maximum amplitude at a 2000 year return period for all model output points.

5.6 Burma (high hazard)

Figure 13(a) shows that the maximum amplitudes offshore Burma in the high hazard map range from 1m to 1.7m for the 2000 year return period. Unlike the low hazard map, the hazard offshore northern Burma is much higher than in the south. The hazard is controlled by the Arakan subduction zone. The Andaman is relatively much less important in the high hazard map than it was in the low one (Figure 13(b)).

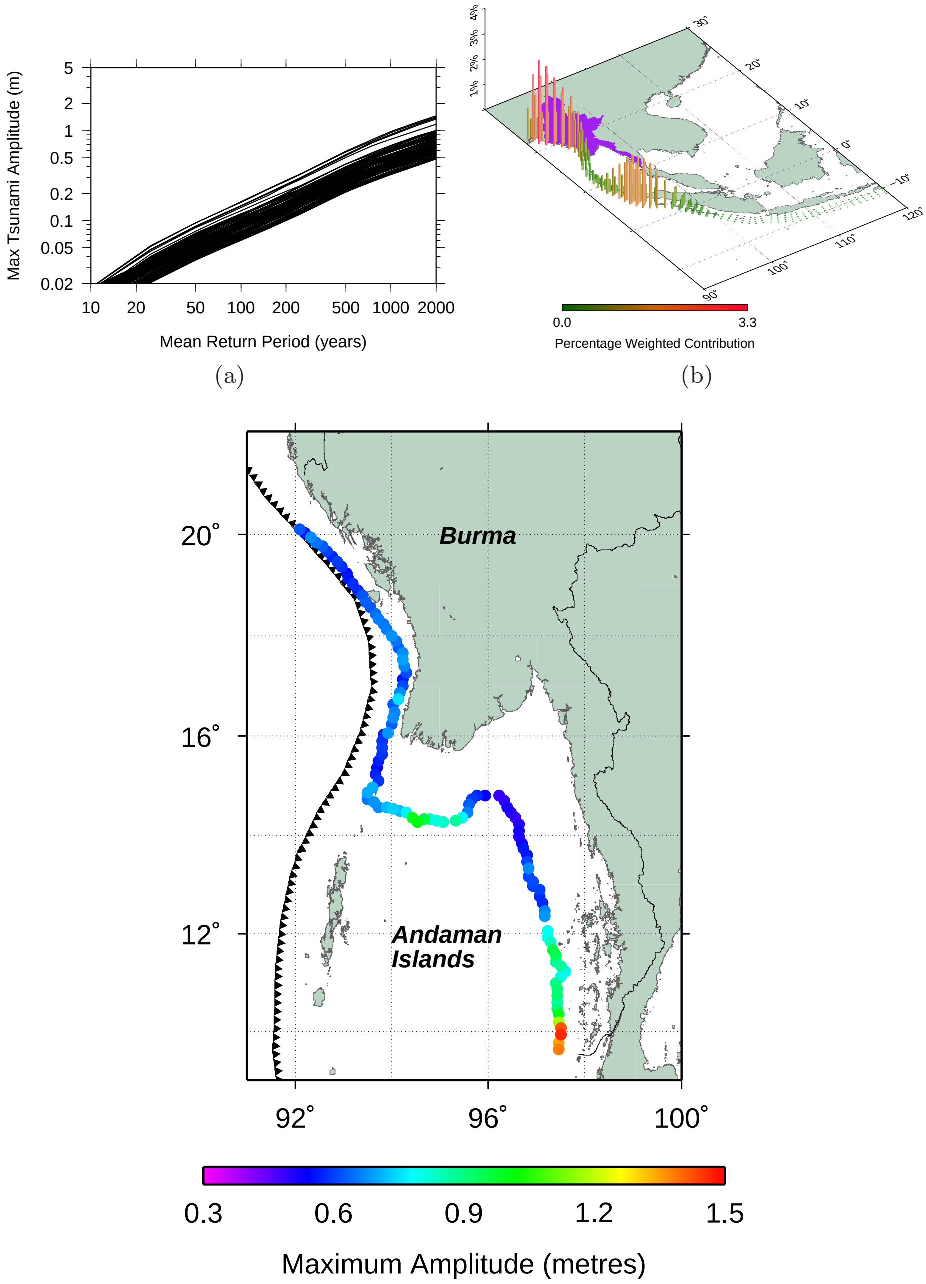

(a) (b) (c)

Figure 13: Myanmar:- (a) Hazard curves for all model output points. (b) National weighted deaggregated hazard. (c) Maximum amplitude at a 2000 year return period for all model output points.

5.7 Comoros (low hazard)

As Figure 14(b) shows, the hazard at the 2000 year return period is dominated by the Andaman zone, with some contribution from the soutern Sumatra section. The maximum amplitudes at the 2000 year return period (Figure 14(c)), range from 0.2 to 0.3m. The amplitudes on the sides of the islands facing the zone is larger than on the sides of the islands facing away from the Sunda Arc.

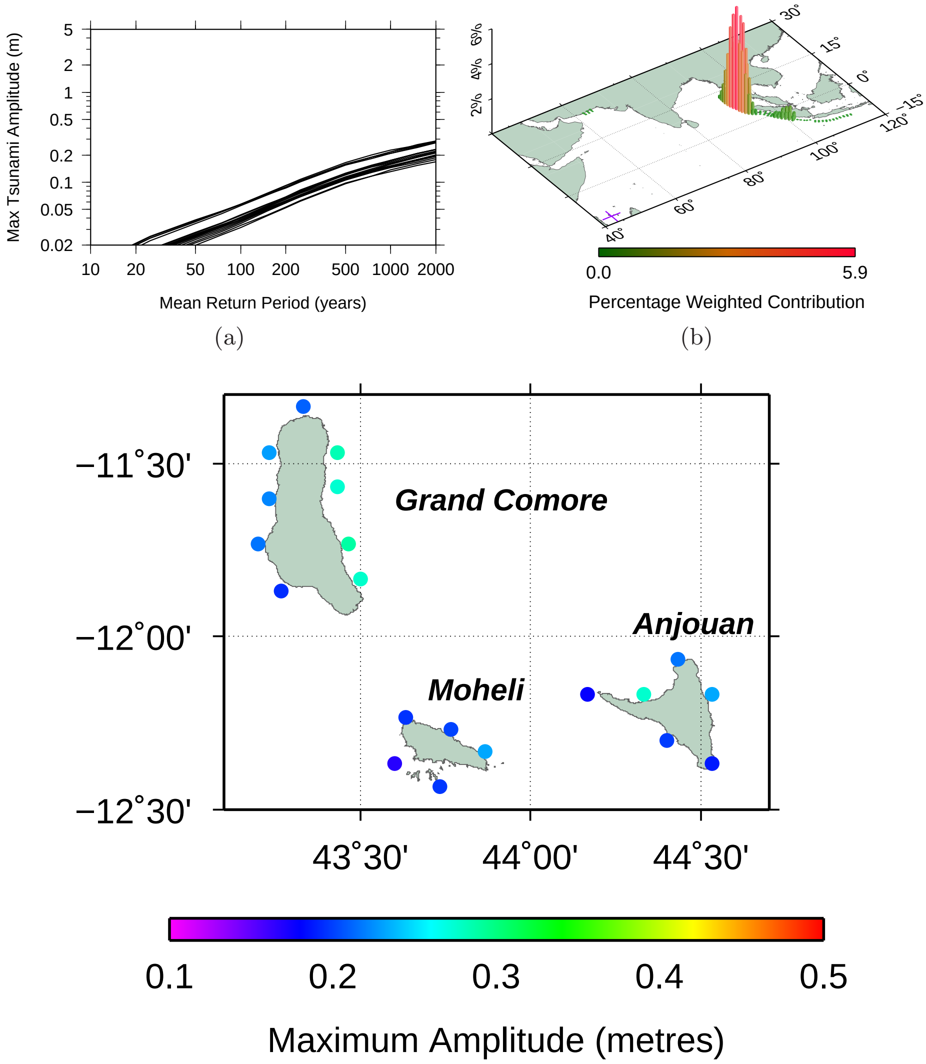

(a) (b)

(c)

Figure 14: Comoros:- (a) Hazard curves for all model output points. (b) National weighted deaggregated hazard. (c) Maximum amplitude at a 2000 year return period for all model output points.

5.8 Comoros (high hazard)

As Figure 15(b) shows, the hazard at the 2000 year return period is dominated by the Andaman zone in this assessment as well. The Sumatran zone is a stronger contributer to the hazard in this map than it was in the low hazard map. The maximum amplitudes at the 2000 year return period (Figure 15(c)) range from 0.3 to 0.5m and again is higher on the eastern and northern sides of the islands.

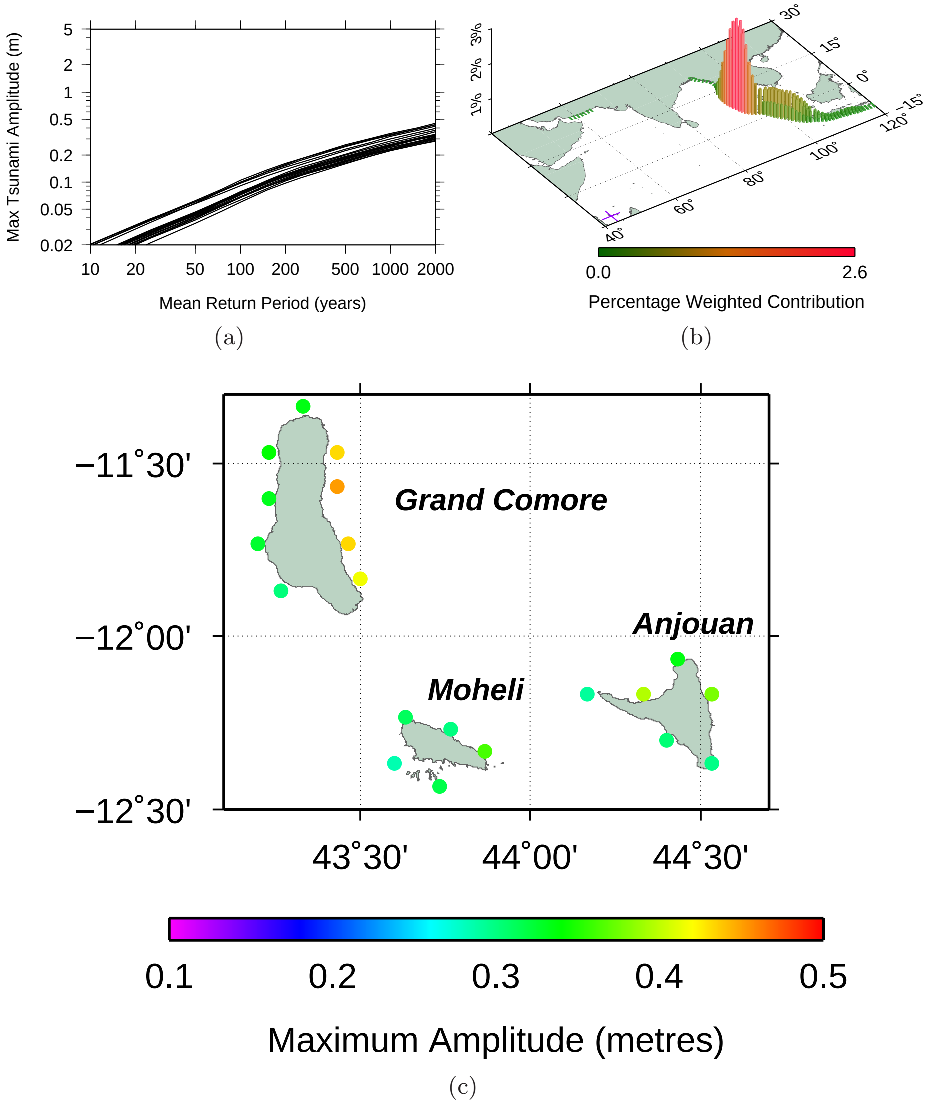

Figure 15: Comoros:- (a) Hazard curves for all model output points. (b) National weighted deaggregated hazard. (c) Maximum amplitude at a 2000 year return period for all model output points.

5.9 Djibouti (low hazard)

Figure 16(a) shows that the maximum amplitudes are relatively uniform for the whole of Djibouti and ranges from 0.2 to 0.3m at the 2000 year return period (Figure 16(c)). At the 2000 year return period the deaggregated hazard mostly comes from central Sumatra, with some contribution from the Andaman as well (Figure 16(b)).

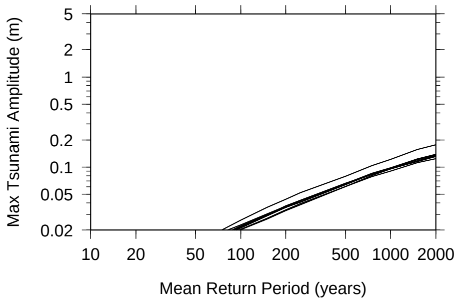

(a)

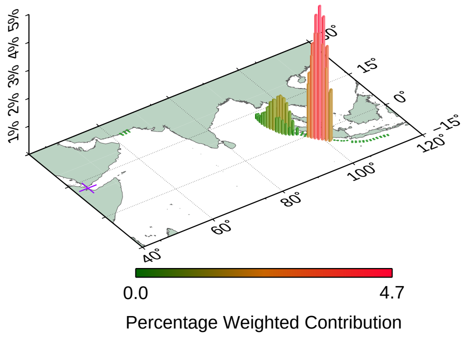

(b)

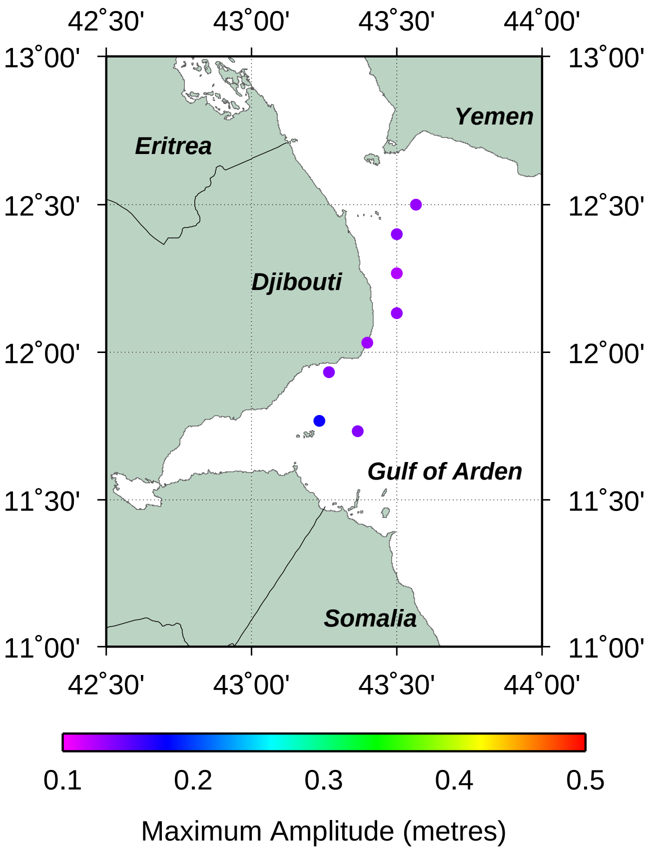

(c)

Figure 16: Djibouti:- (a) Hazard curves for all model output points. (b) National weighted deaggregated hazard. (c) Maximum amplitude at a 2000 year return period for all model output points.

5.10 Djibouti (high hazard)

Figure 17(a) shows that the maximum amplitudes are again relatively uniform over all model output points offshore Djibouti, with maximum amplitudes of 0.3 to 0.4 metres expected at the 2000 year return period (Figure 17(c)). At the 2000 year return period the deaggregated hazard is dominated by the Sumatra section of the Sunda Arc but a significant contribution also comes from the eastern Makran (Figure 17(b)).

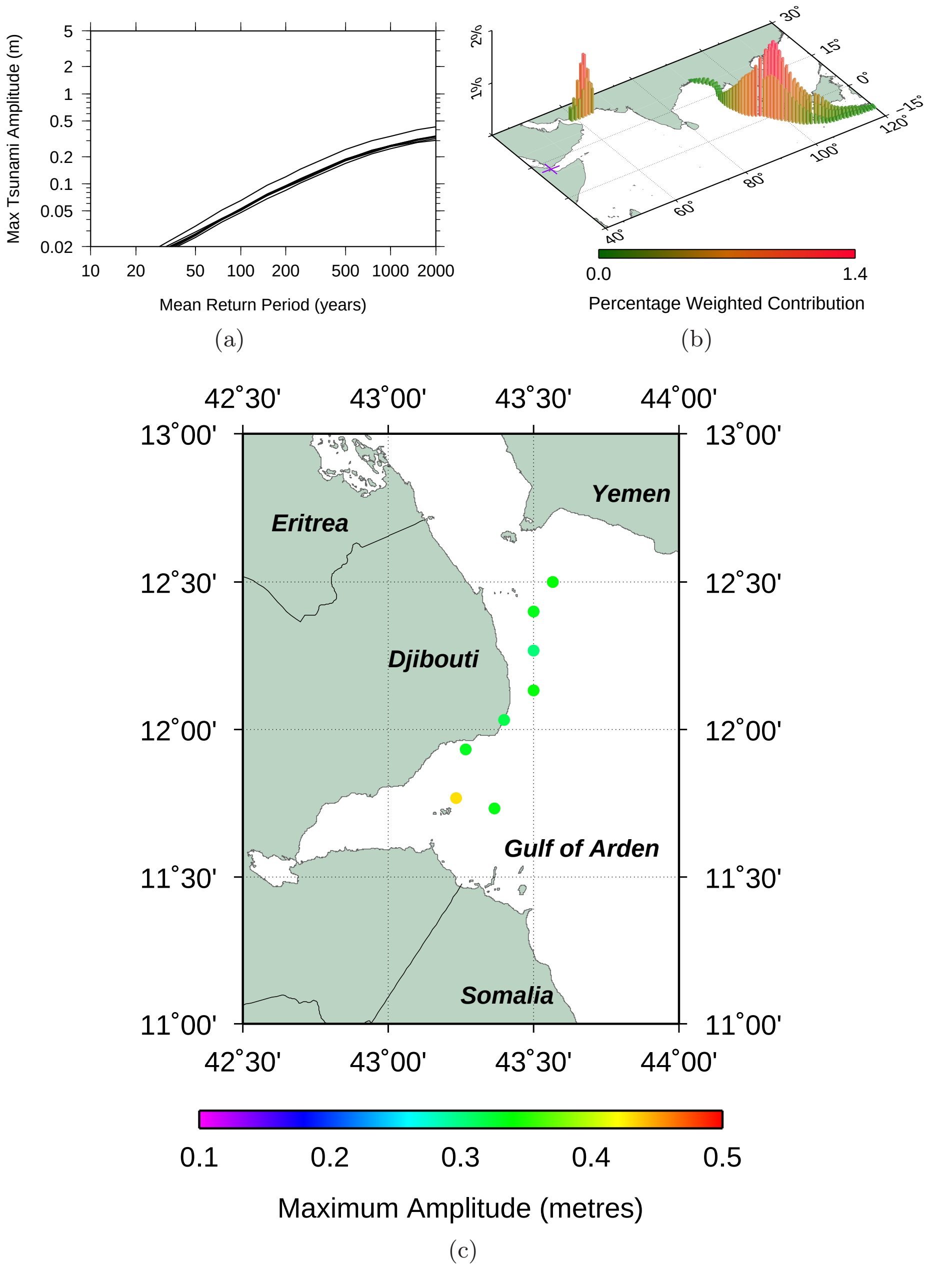

Figure 17: Djibouti:- (a) Hazard curves for all model output points. (b) National weighted deaggregated hazard. (c) Maximum amplitude at a 2000 year return period for all model output points.

5.11 India

5.11.1 Indian Mainland (low hazard)

The large 2000 year maximum amplitude has a very large spread of values for mainland India. It is far higher on the east coast than on the west coast (Figure 18(c)). Values at the 2000 year return period range from 0.1m (west coast) to 1.9m (east coast). The hazard here is dominated by the southern and central Andaman zone (Figure 18(b))

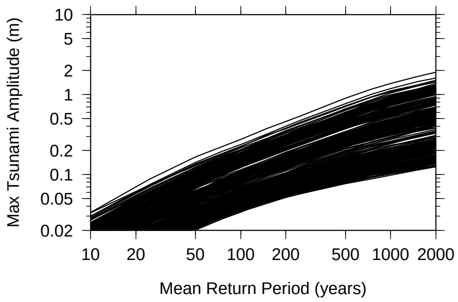

(a)

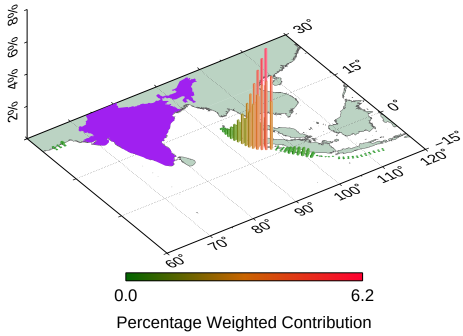

(b)

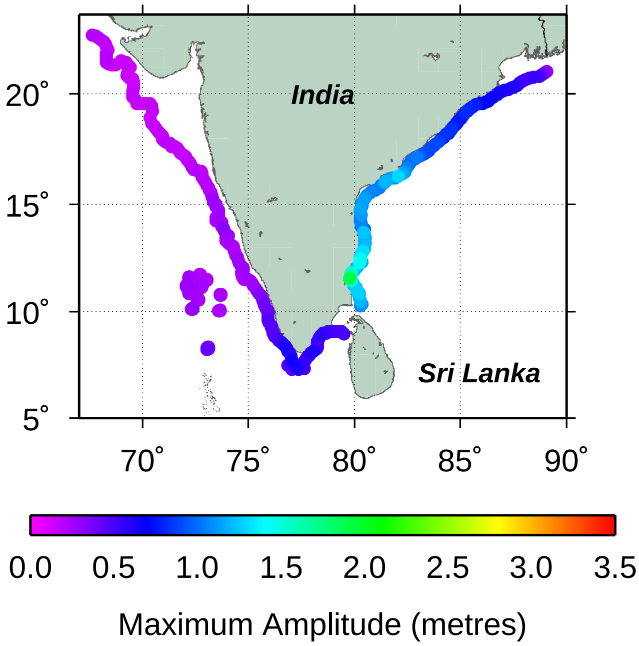

(c)

Figure 18: India:- (a) Hazard curves for all model output points. (b) National weighted deaggregated hazard. (c) Maximum amplitude at a 2000 year return period for all model output points.

5.11.2 Indian Mainland (high hazard)

The large 2000 year maximum amplitude in the high hazard again is much higher on the east coast than the west (Figure 19(c)). The hazard ranges from over 3m (east coast) to 0.3m (west coast). The single high hazard value for the east coast in both the low and high hazard maps should be interpreted with caution as this could be due to a local bathymetric anomaly in the global bathymetry dataset used in this assessment. The deaggregated hazard map (Figure 19(b) shows that the most important zone is the Andaman, but significant contributions also come from the Arakan (east coast) and Makran (west coast).

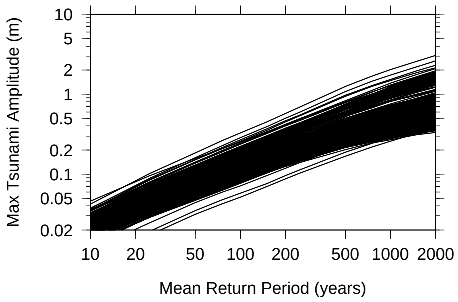

(a)

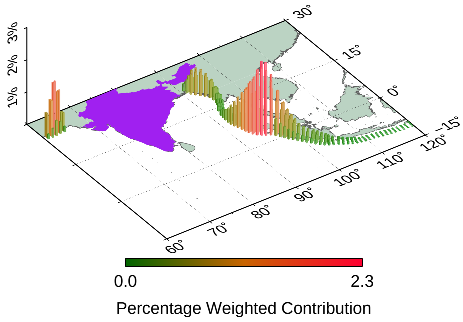

(b)

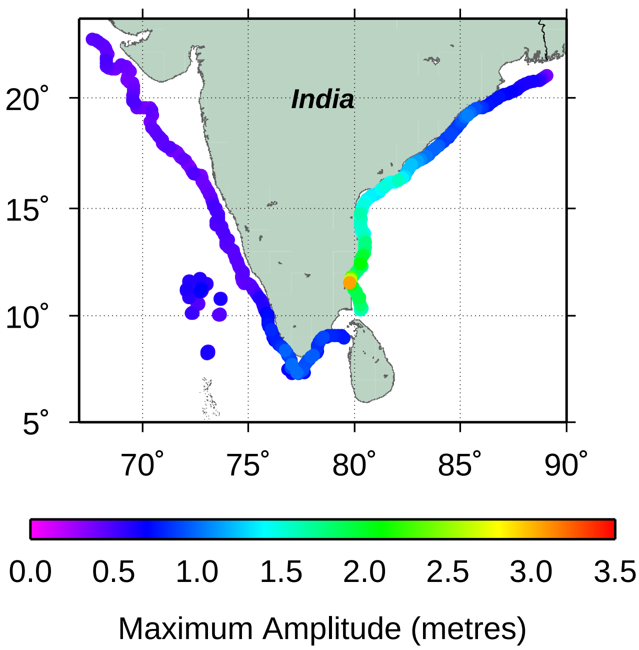

(c)

Figure 19: India:- (a) Hazard curves for all model output points. (b) National weighted deaggregated hazard. (c) Maximum amplitude at a 2000 year return period for all model output points.

5.11.3 Andaman and Nicobar Islands (low hazard)

The 2000 year maximum amplitude ranges from 0.5m to over 4m along the Andaman chain of islands (Figure 20(a)). The hazard naturally mostly comes from the central-southern Andaman zone itself (Figure 20(b)). The hazard is significantly lower offshore the northern Andaman islands which lie to the north of the end of the Andaman zone (Figure 20(c)).

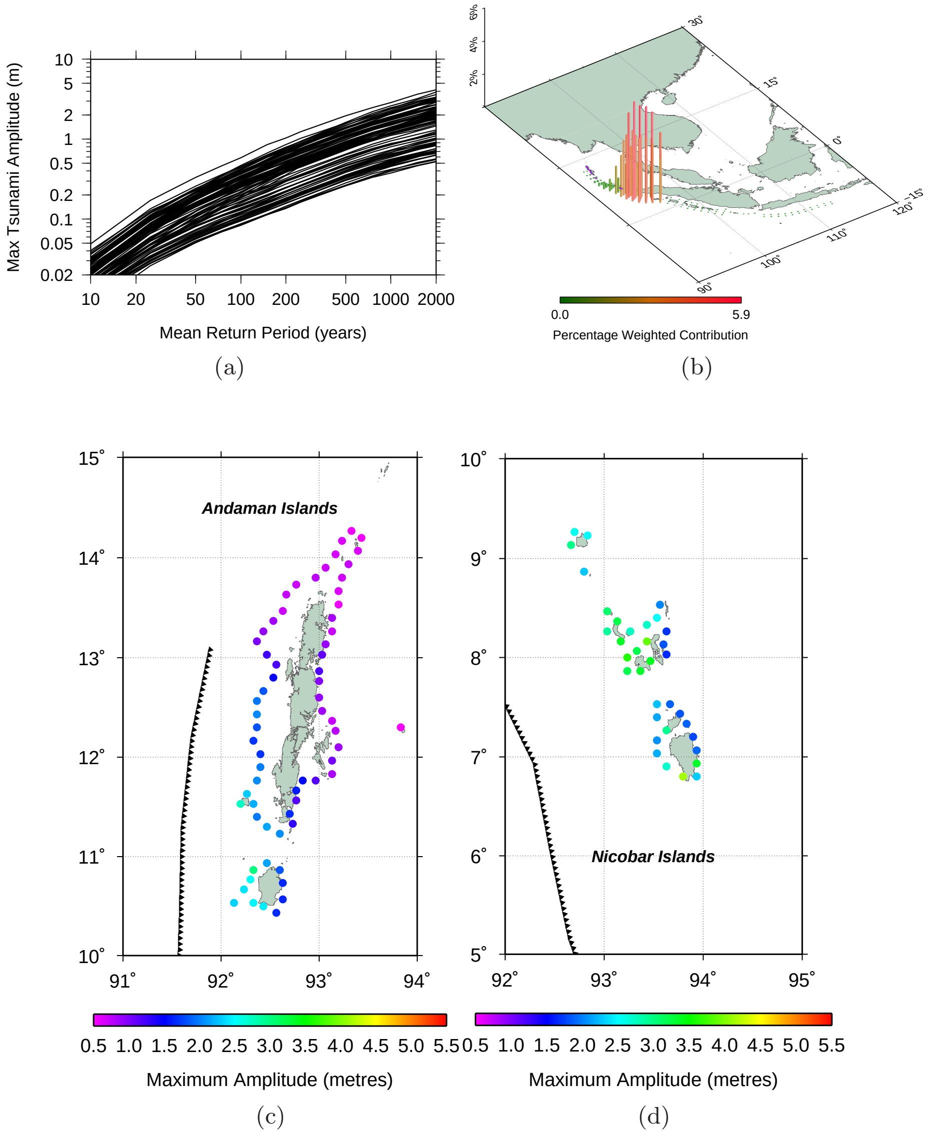

Figure 20: Andaman and Nicobar Island:- (a) Hazard curves for all model output points. (b) National weighted deaggregated hazard. (c) Maximum amplitude at a 2000 year return period for all model output points.

5.11.4 Andaman and Nicobar Islands (high hazard)

The large 2000 year maximum amplitude for the Andaman Islands in the high hazard model ranges from over 0.7m to just over 5m (Figure 21(a)). The hazard again mostly originates from the southern and central Andaman, with only a very small contribution from the Arakan zone (Figure 21(b)). The hazard again is again higher in the north than the south (Figure 21(c))

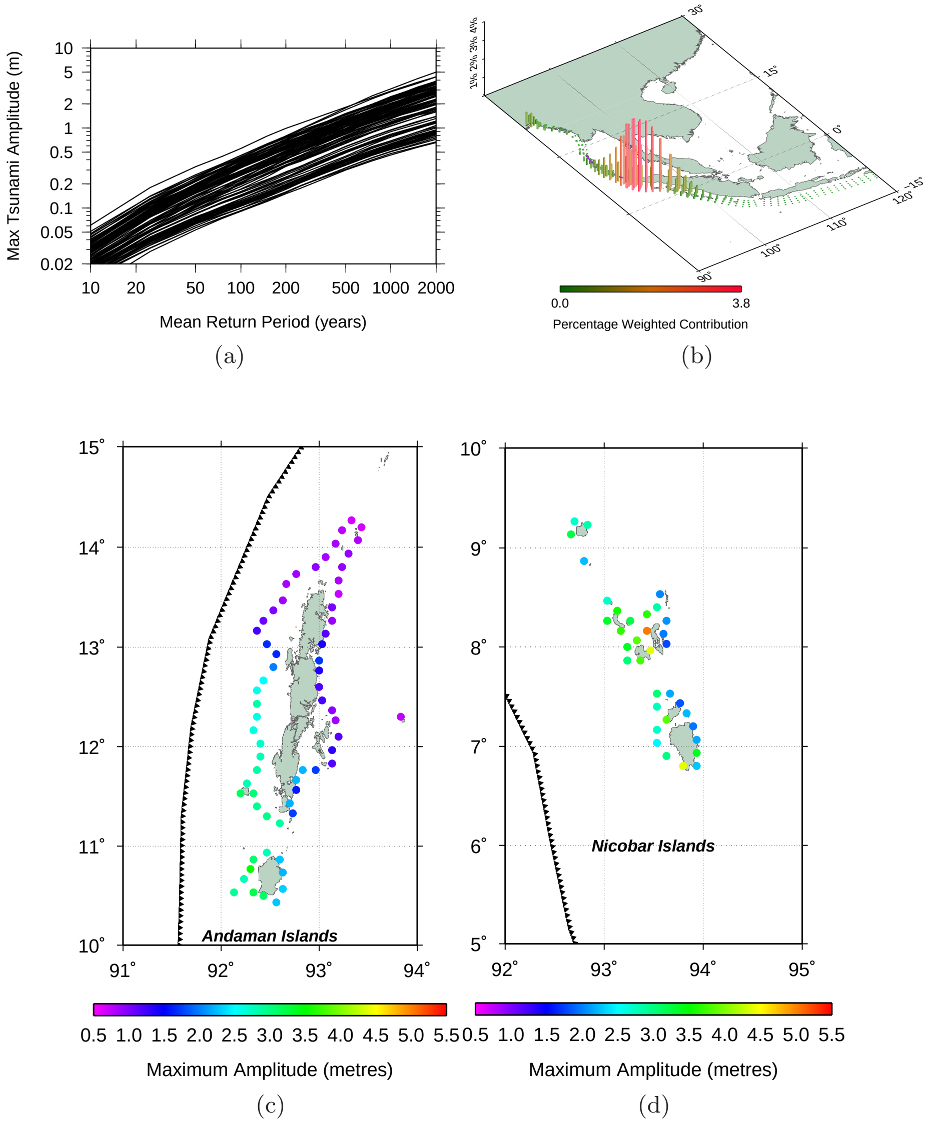

Figure 21: Andaman and Nicobar Island:- (a) Hazard curves for all model output points. (b) National weighted deaggregated hazard. (c) Maximum amplitude at a 2000 year return period for all model output points.

This page was deliberately left blank.

5.12 Indonesia

Note that, as described section 2.2, Indonesia has only been included as far east as 120° longitude. This was done in part because sources east of 120° longitude are less likely to affect the Indian Ocean beyond the Timor Sea, but also because of the increasingly complex tectonics east of Java. Because of this complexity, a tsunami hazard assessment encompassing all of Indonesia, including coastlines and sources in the Banda and Flores Seas, would have required resources beyond those available for this project. Both historical tsunami data and the very active tectonics of Indonesia east of 120° longitude suggest that the hazard there is high, so that any national tsunami hazard assessment for Indonesia should take these into account.

5.12.1 Sumatra (low hazard)

Maximum amplitudes at a 2000 year return period range from 0.7m to over 5.6m for Sumatra (Figure 22(a)). The presence of islands above the subduction zone (like Nias) act to protect the main island of Sumatra. Hazard values are naturally much larger on the western side of such islands than the eastern side (Figure 22(c)). The absence of these islands in southern Sumatra means the hazard there is quite a bit higher than in the north. For this return period of 2000 years the Sumatran and to a lesser extent Andaman zone dominate the hazard (Figure 22(b)).

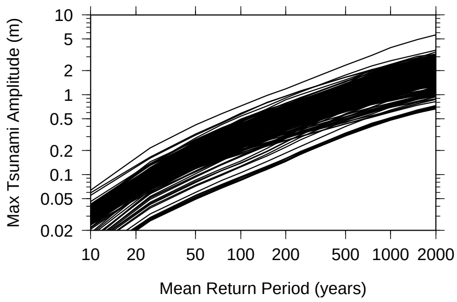

(a)

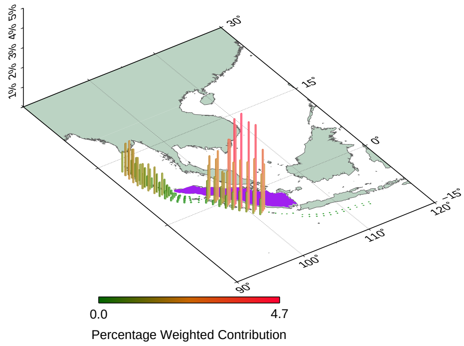

(b)

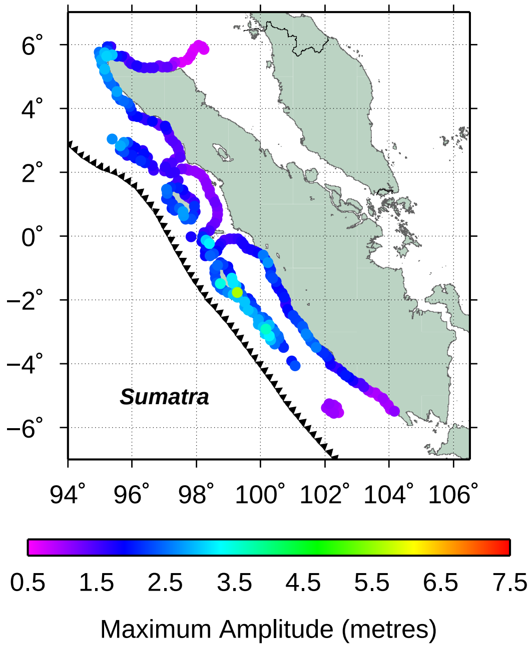

(c)

Figure 22: Sumatra:- (a) Hazard curves for all model output points. (b) National weighted deaggregated hazard. (c) Maximum amplitude at a 2000 year return period for all model output points.

5.12.2 Sumatra (high hazard)

Maximum amplitudes at a 2000 year return period in the high hazard map range from about 0.8m to just over 7.1m in the high hazard map (Figure 23(a)). The deaggregated map again shows that the Sumatran, and to a lesser extent Andaman zones dominate the 2000 year hazard (Figure 23(b)). The hazard is again higher on the islands offshore Sumtra, and on the northern and southern coasts of Sumatra that are not shielded by these islands (Figure 23(c)). Again, the hazard is dominated by the Sumatran and to a lesser extent the Andaman zones. (Figure 23(b)).

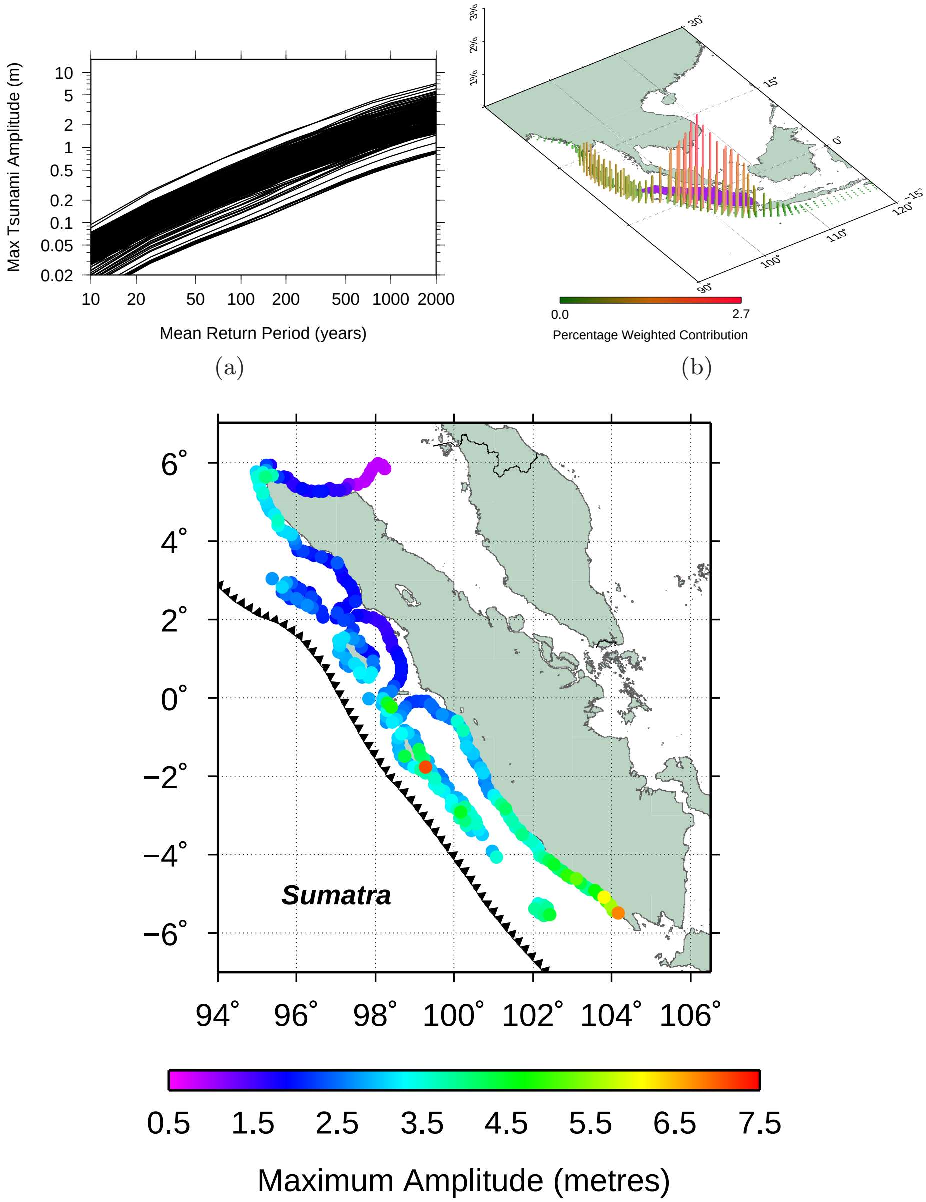

(a) (b)

(c)

Figure 23: Sumatra:- (a) Hazard curves for all model output points. (b) National weighted deaggregated hazard. (c) Maximum amplitude at a 2000 year return period for all model output points.

5.12.3 Java (low hazard)

Maximum amplitudes at a 2000 year return period of range between 0.4m up to just over 1.3m in the low hazard map ((Figure 24(a))). Compared to other countries the hazard doesn't change as much with return periods due to the relatively low maximum magnitude chosen in the low hazard map. The hazard is quite uniform across the whole of Java (Figure 24(c)) and mostly comes from the Java section itself (Figure 24(b)).

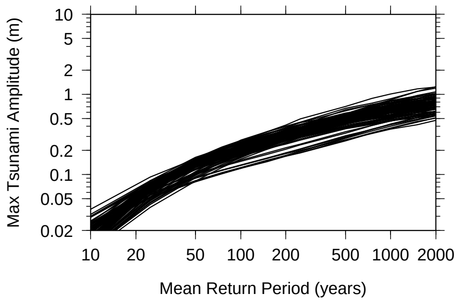

(a)

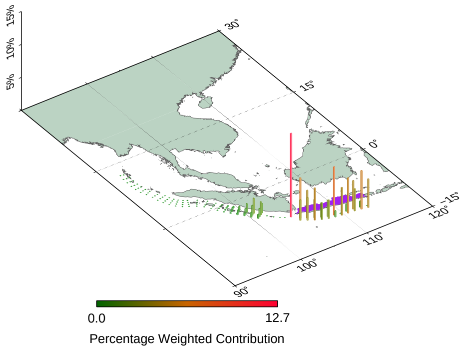

(b)

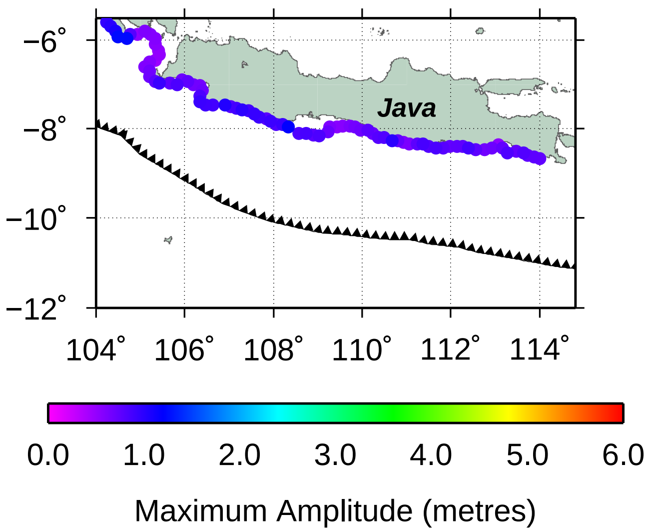

(c)

Figure 24: Java:- (a) Hazard curves for all model output points. (b) National weighted deaggregated hazard. (c) Maximum amplitude at a 2000 year return period for all model output points.

5.12.4 Java (high hazard)

By contrast, the hazard in the "high" hazard assessment for Java is very high, and ranges from 2m to 6.5m at the 2000 year return period (Figure 25(a)). The hazard mostly originates from Java and southern Sumatra sections of the Sunda Arc (Figure 25(b)). Hazard is fairly unform from west to east but has several distinct peaks which approach 9m (Figure 25(c)).

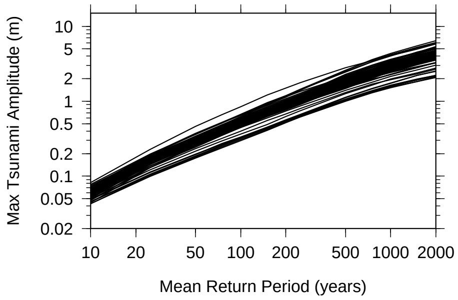

(a)

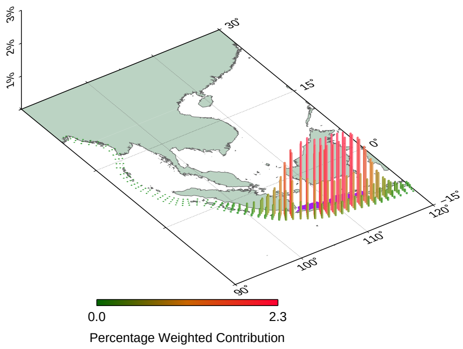

(b)

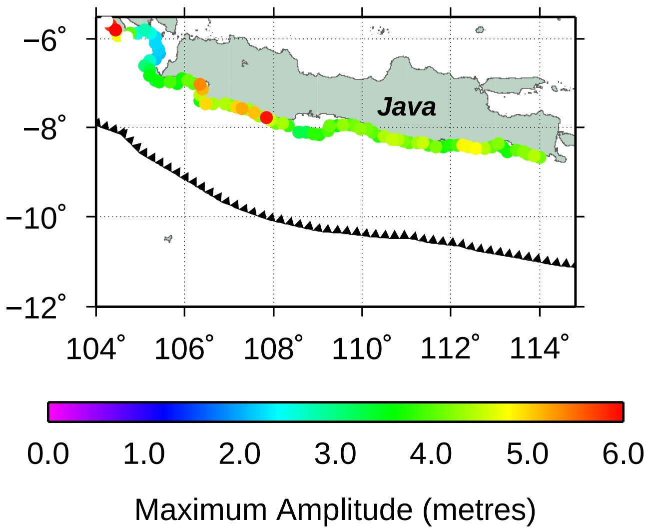

(c)

Figure 25: Java:- (a) Hazard curves for all model output points. (b) National weighted deaggregated hazard. (c) Maximum amplitude at a 2000 year return period for all model output points.

5.12.5 Lesser Sunda Islands West of 120° Longitude(low hazard)

The hazard off the Lesser Sunda Islands west of 120° longitude (Bali, Lombok, Sumbawa, Sumba) is quite low and uniformly distibuted (Figure 26(c)). At the 2000 year return period it ranges from 0.1 to 0.6m and doesn't change significanlty with return period (Figure 26(a)). The hazard all comes from the eastern Java segment of the Sunda Arc (Figure 26(b))

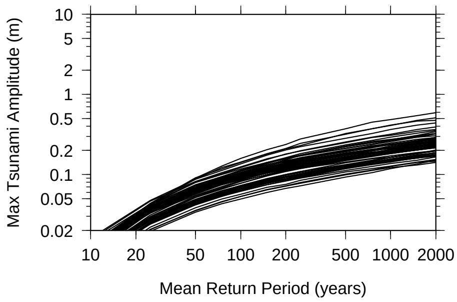

(a)

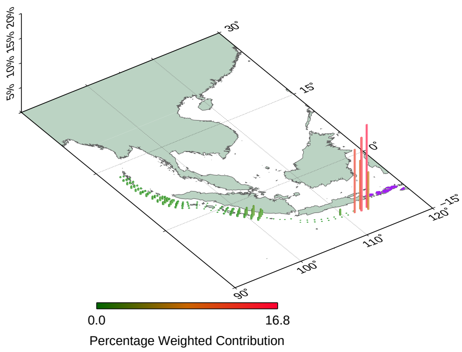

(b)

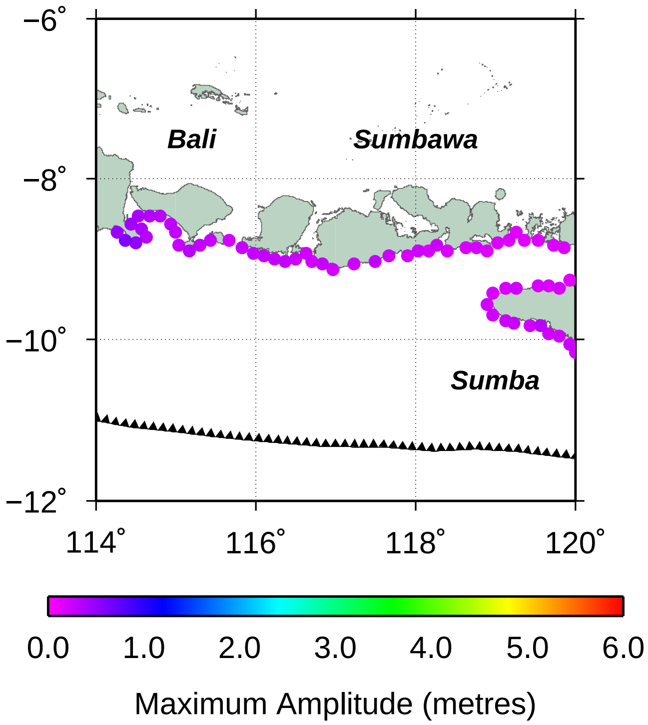

(c)

Figure 26: Lesser Sunda Islands:- (a) Hazard curves for all model output points. (b) National weighted deaggregated hazard. (c) Maximum amplitude at a 2000 year return period for all model output points.

5.12.6 Lesser Sunda Islands West of 120° Logitude (high hazard)

In the high hazard assessment, the hazard off the southern coast of these islands is much higher and ranges from over 1.5m to 5.4m at the 2000 year return period (Figure 27(a)). The hazard at this return periopd all comes from the eastern Sunda Arc (Figure 27(b)) and is slightly higher offshore the western most island than those further to east (Figure 27(c)).

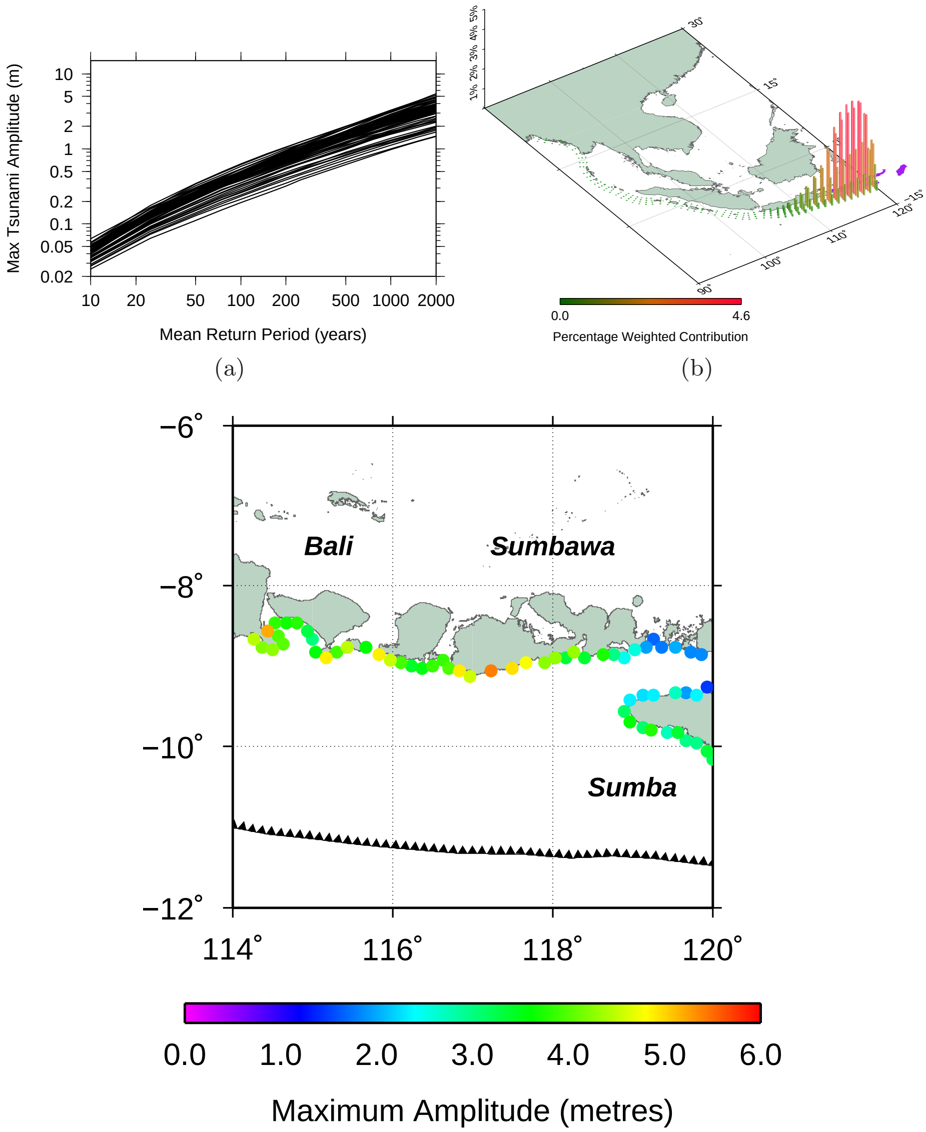

(a) (b)

(c)

Figure 27: Lesser Sunda Islands:- (a) Hazard curves for all model output points. (b) National weighted deaggregated hazard. (c) Maximum amplitude at a 2000 year return period for all model output points.

5.13 Iran (low hazard)

The 2000 year maximum amplitudes offshore Iran are quite uniform, but is slightly higher in the east than the west (Figure 28(c)). At the 2000 year return period they range from 0.1m to 0.3m (Figure 28(a)). The hazard at this return period all comes from the eastern Markan (Figure 28(b)).

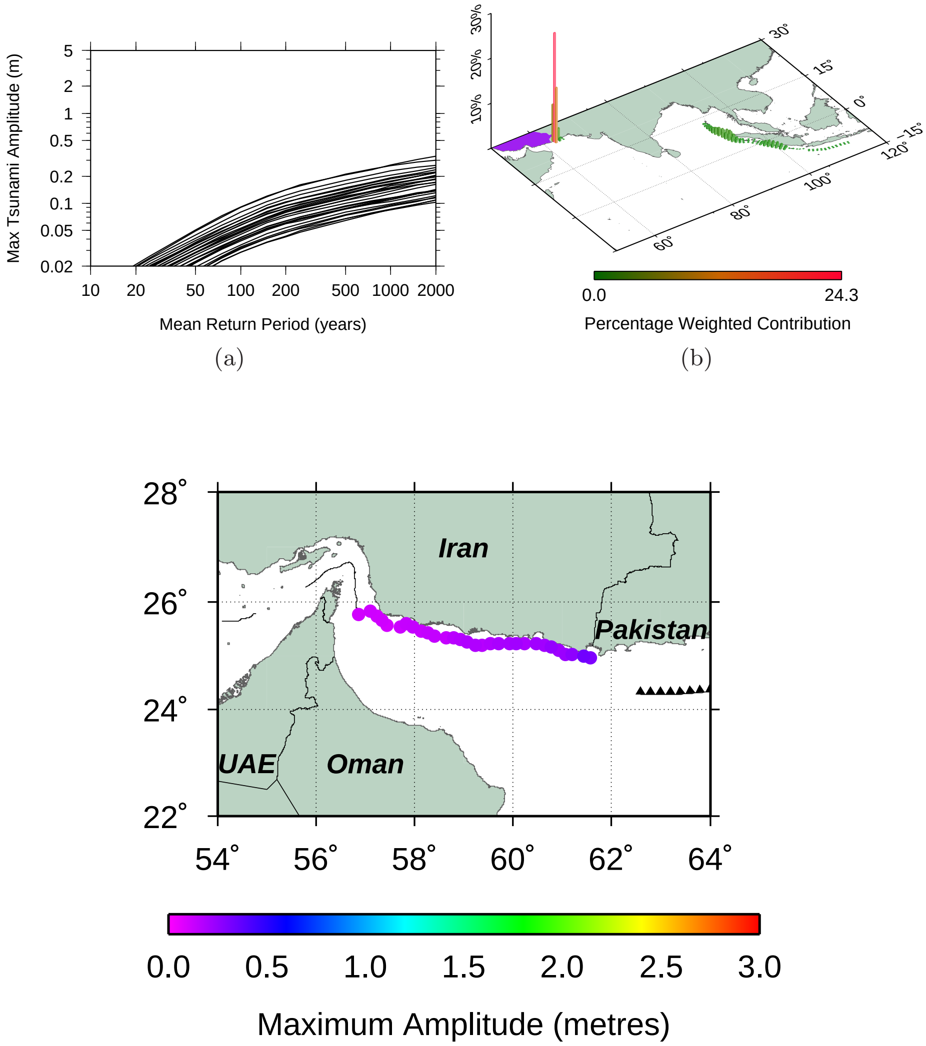

(a) (b)

(c)

Figure 28: Iran:- (a) Hazard curves for all model output points. (b) National weighted deaggregated hazard. (c) Maximum amplitude at a 2000 year return period for all model output points.

5.14 Iran (high hazard)

The 2000 year maximum amplitudes are much higher in the "high" hazard assessment and are much larger in the east than in the west of Iran (Figure 29(c)). At the 2000 year return period the hazard ranges from 0.7m to 2.7m (Figure 29(a)) and comes entirely from the Markan zone (Figure 29(b)).

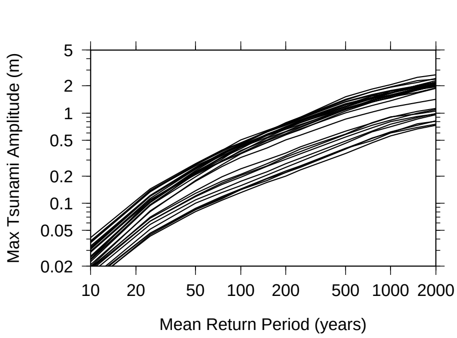

(a)

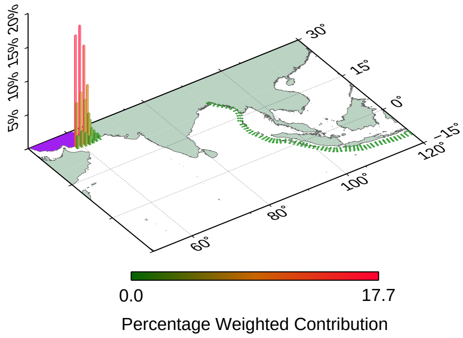

(b)

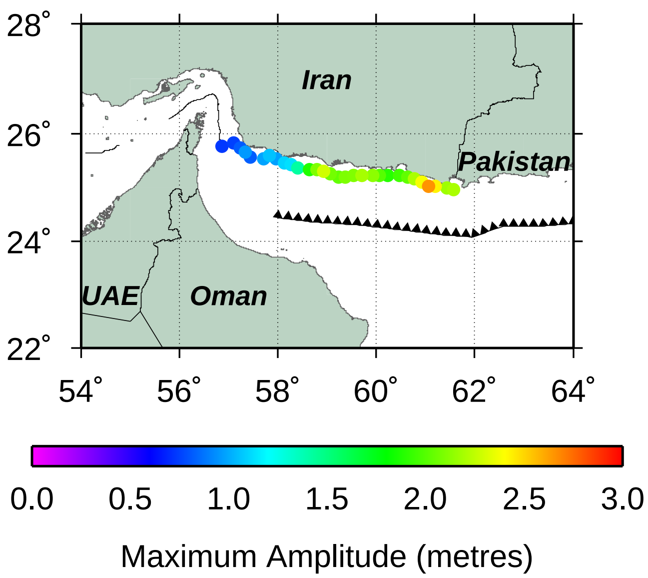

(c)

Figure 29: Iran:- (a) Hazard curves for all model output points. (b) National weighted deaggregated hazard. (c) Maximum amplitude at a 2000 year return period for all model output points.

5.15 Kenya (low hazard)

Maximum amplitudes of the order of 0.3 to 0.5m were computed offshore the Kenya coast in the “low” hazard assessment (Figure 30(a)). The hazard at this return period all comes from the Andaman and southern Sumatran zones (Figure 30(b)) and is fairly uniform along the coast (Figure 30(c)).

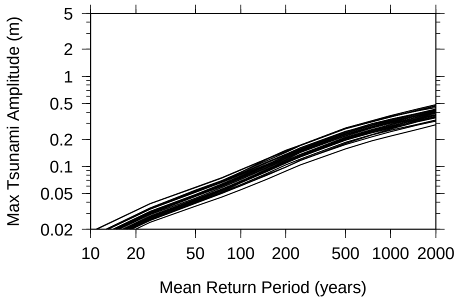

(a)

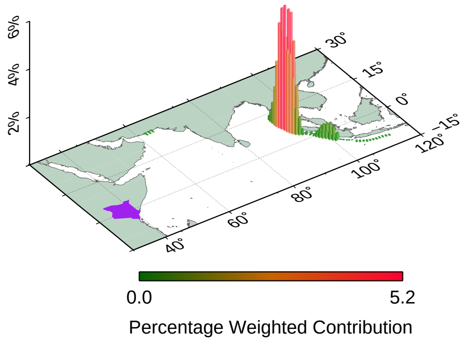

(b)

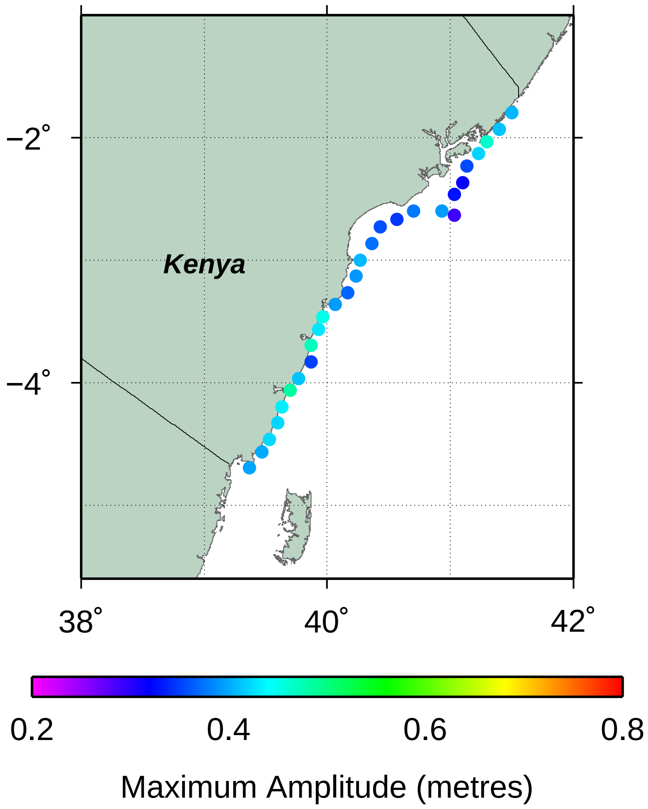

(c)

Figure 30: Kenya:- (a) Hazard curves for all model output points. (b) National weighted deaggregated hazard. (c) Maximum amplitude at a 2000 year return period for all model output points.

5.16 Kenya (high hazard)

Maximum amplitudes of the order of 0.5 to over 0.8m were computed offshore Kenya in the "high" hazard assessment (Figure 31(a)). Hazard was again fairly uniformly distributed (Figure 31(c)) and originates from the Andaman and Sumatran subduction zones (Figure 31(b)).

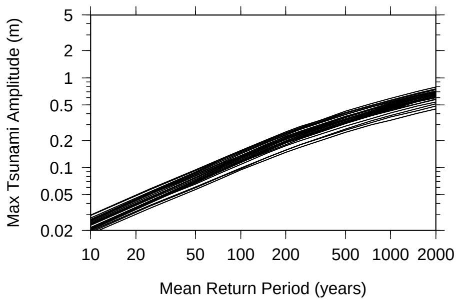

(a)

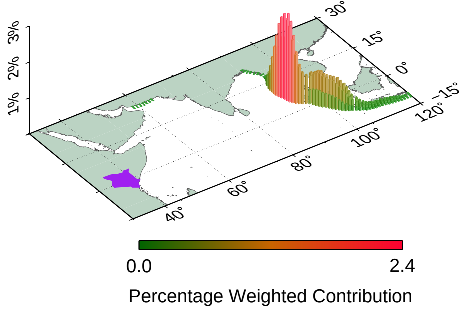

(b)

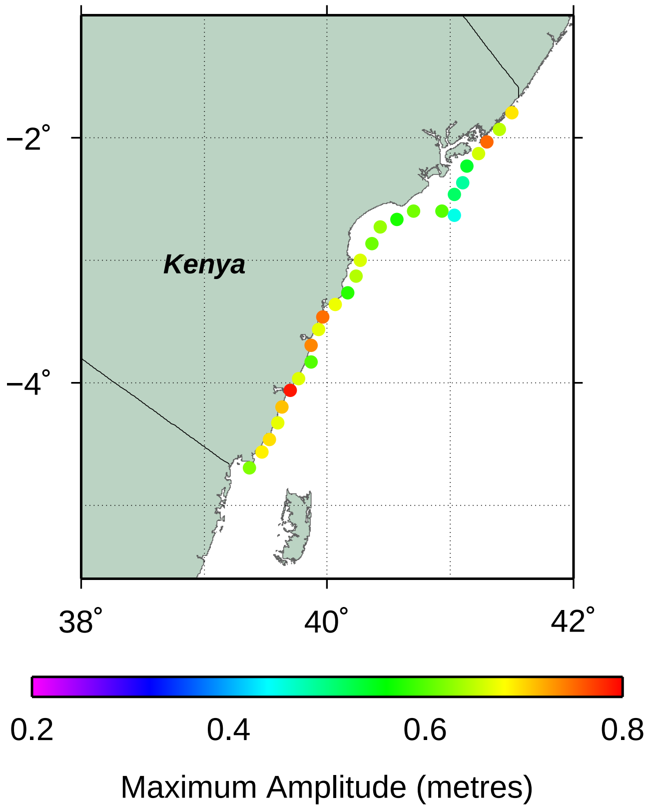

(c)

Figure 31: Kenya:- (a) Hazard curves for all model output points. (b) National weighted deaggregated hazard. (c) Maximum amplitude at a 2000 year return period for all model output points.

5.17 Madagascar (low hazard)

The hazard offshore Madagascar in the low hazard assessment is much higher offshore eastern and south-eastern coasts than the western and north-western coasts (Figure 32(c)). The south-eastern coast has hazard noticably larger than the rest of the east coast. Hazard values at the 2000 year return period range from 0.1m (west coast) to 1m (southeast coast) (Figure 32(a)) and comes from both the Sumatran and Andaman zones (Figure 32(b))

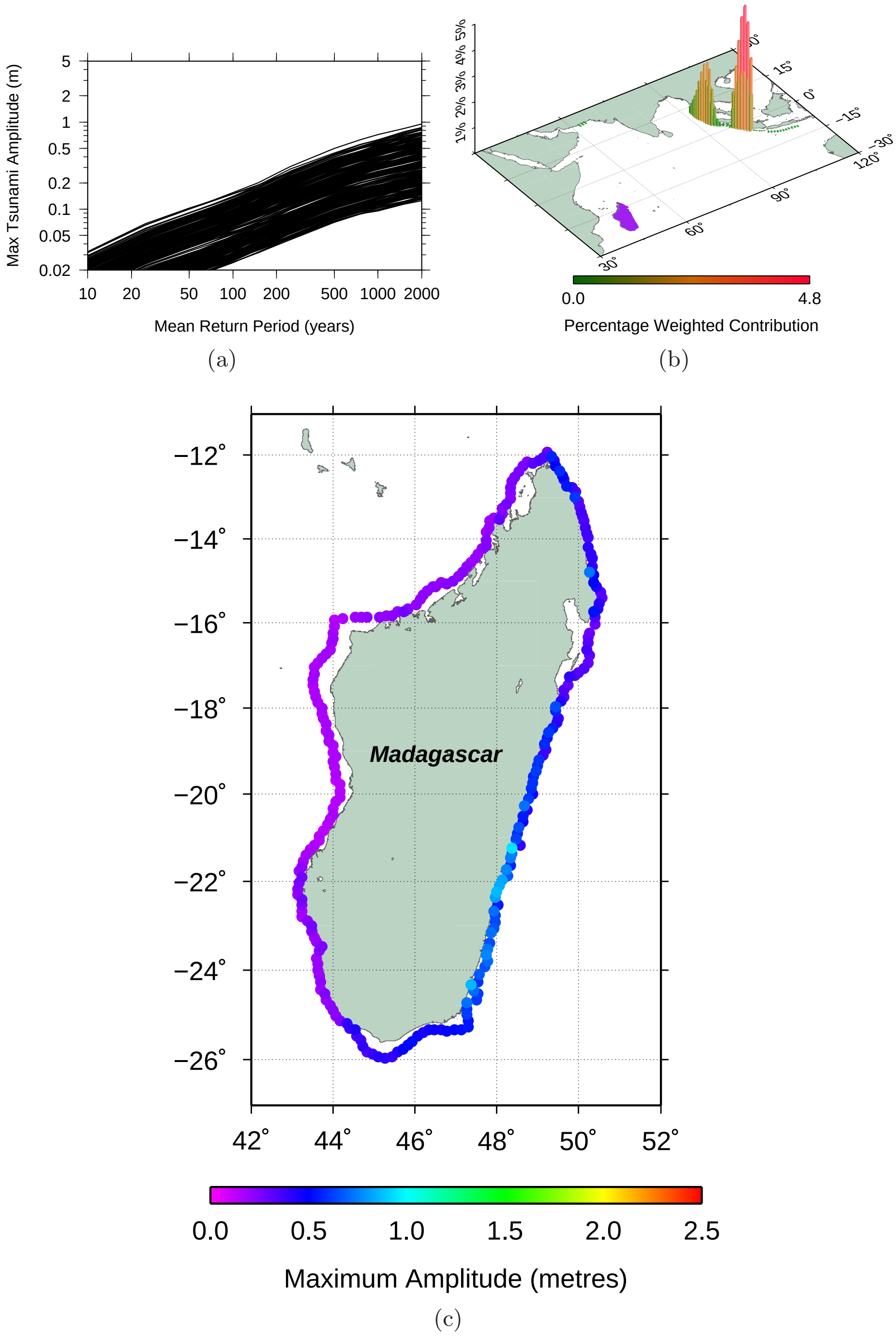

Figure 32: Madagascar:- (a) Hazard curves for all model output points. (b) National weighted deaggregated hazard. (c) Maximum amplitude at a 2000 year return period for all model output points.

5.18 Madagascar (high hazard)

In the high hazard assessment the hazard is again much higher off the west to southwest coasts of Madagascar (Figure 33(c)). The hazard off the south and northeast coast is intermediate and that off the western coast is much smaller. At the 2000 year return period the hazard ranegs from 0.2m to 2.2m (Figure 33(a)). The hazard mostly comes from the Sunda Arc zones, but there is also a significant contribution from the South Sandwich zone (Figure 33(b)).

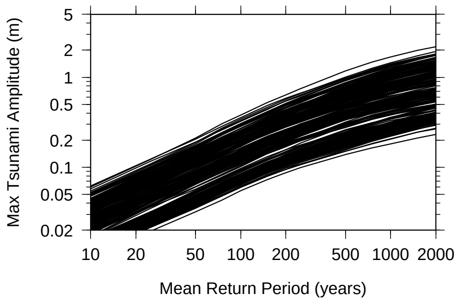

(a)

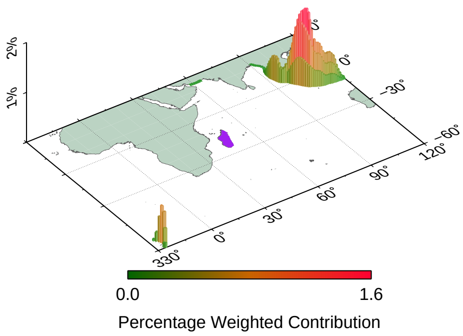

(b)

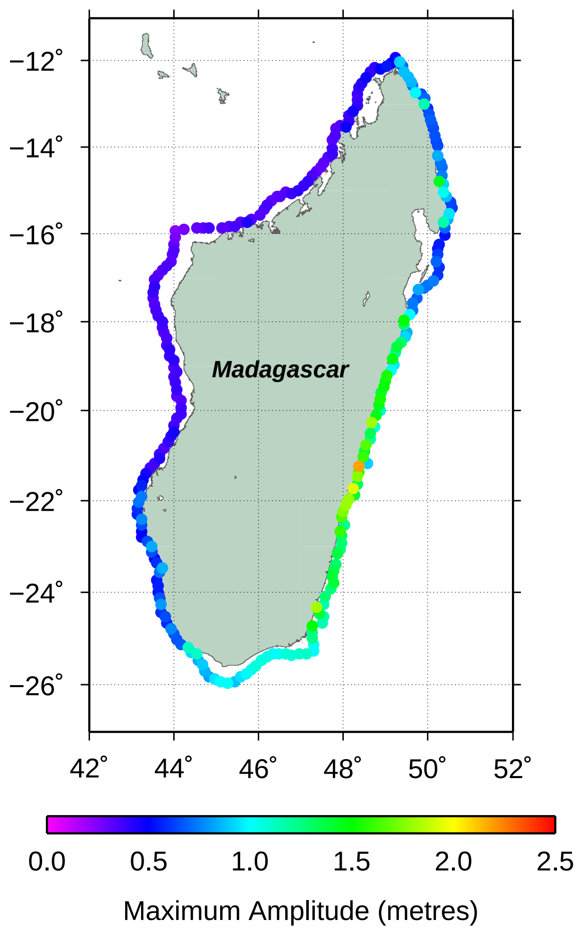

(c)

Figure 33: Madagascar:- (a) Hazard curves for all model output points. (b) National weighted deaggregated hazard. (c) Maximum amplitude at a 2000 year return period for all model output points.

5.19 Maldives (low hazard)

The hazard offshore the Maldives in the low hazard assessment is much higher offshore the eastern coasts than the west and higher in south than the north (Figure 34(c)). The hazard at this return period comes entirely from the Andaman zone (Figure 34(b)) and ranges from 0.3m to 2.2m depending on location (Figure 34(a)).

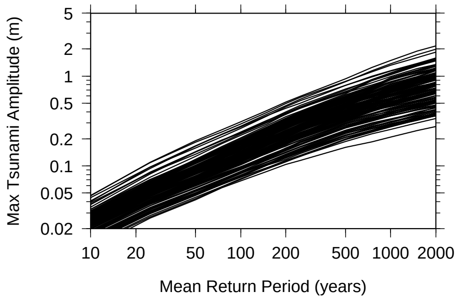

(a)

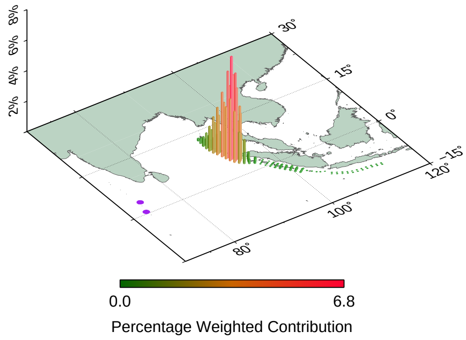

(b)

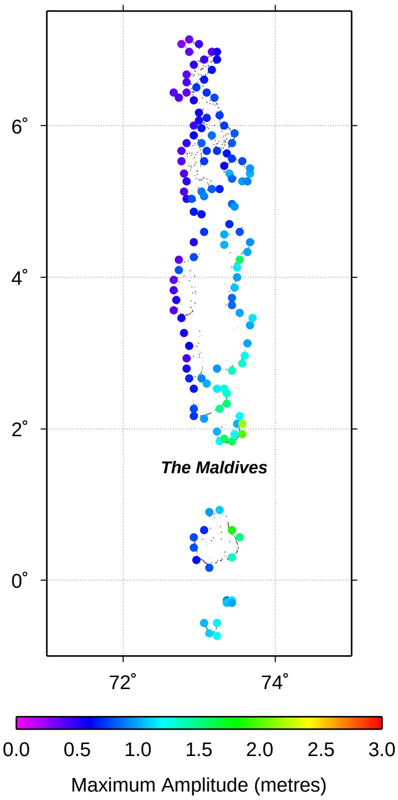

(c)

Figure 34: Maldives:- (a) Hazard curves for all model output points. (b) National weighted deaggregated hazard. (c) Maximum amplitude at a 2000 year return period for all model output points.

5.20 Maldives (high hazard)

The distribution of hazard in the high hazard assessment of the Maldives is similar to the low hazard one (Figure 35(c)). The 2000 year hazard values range from 0.6m to 3.0m depending on which side of the chain the points are located (Figure 35(a)). Hazard again mostly originates from the Andaman zone, with a small contribution from Sumatra as well (Figure 35(b))

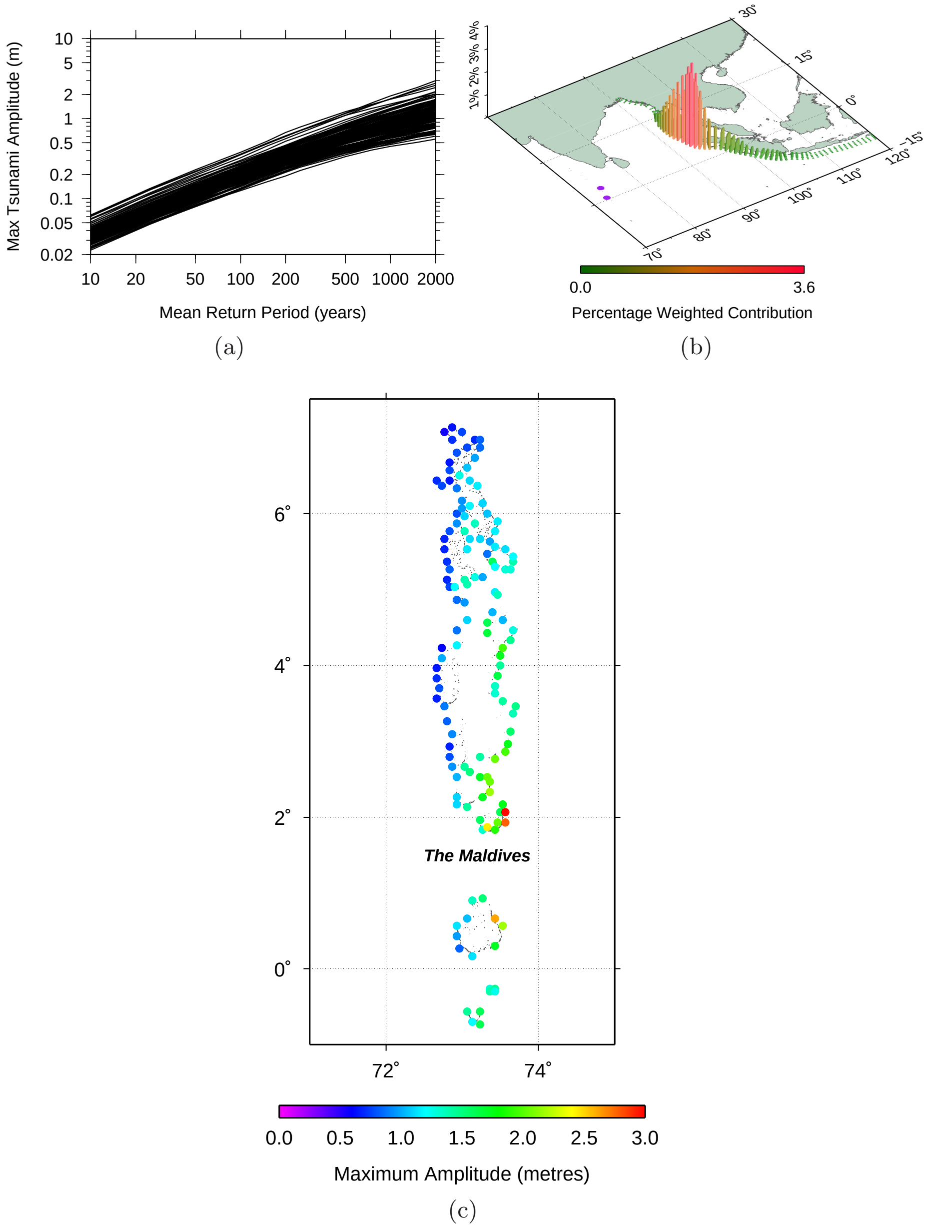

Figure 35: Maldives:- (a) Hazard curves for all model output points. (b) National weighted deaggregated hazard. (c) Maximum amplitude at a 2000 year return period for all model output points.

5.21 Mauritius & Rodrigues (low hazard)

In the low hazard assessment the hazard offshore Rodrigues is significantly higher than that off Mauritius (Figure 36(c)). The hazard at the 2000 year return period mostly originates from Sumatra, but there is also a contribution from the Andaman zone (Figure 36(b)). At this return period the maximum amplitude varies from about 0.3m to 1.2m for the two islands (Figure 36(a))

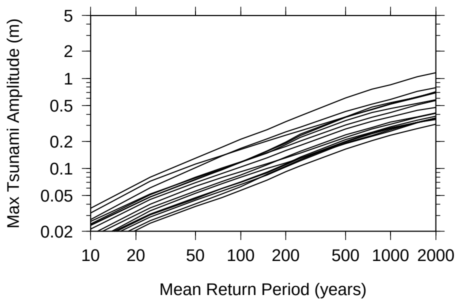

(a)

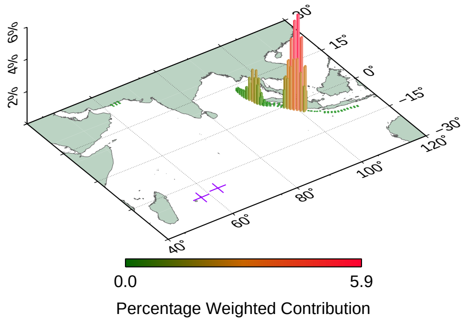

(b)

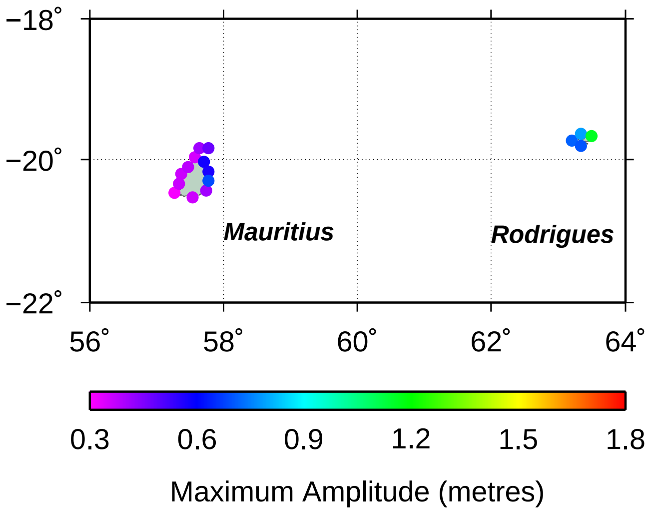

(c)

Figure 36: Mauritius:- (a) Hazard curves for all model output points. (b) National weighted deaggregated hazard. (c) Maximum amplitude at a 2000 year return period for all model output points.

5.22 Mauritius & Rodrigues (high hazard)

In the high hazard assessment, the hazard off the east coast of Mauritius is similar to that off most of Rodrigues except for one point (Figure 37(c)). At the 2000yr return period the amplitude ranges from 0.7m to 1.7m (Figure 37(a)) and comes from the entire stretch of the Sunda Arc from Sumba to Andaman with a peak off Sumatra (Figure 37(b))

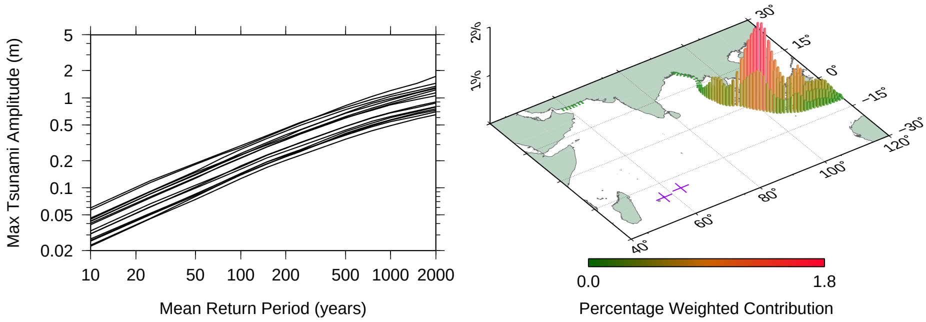

(a) (b)

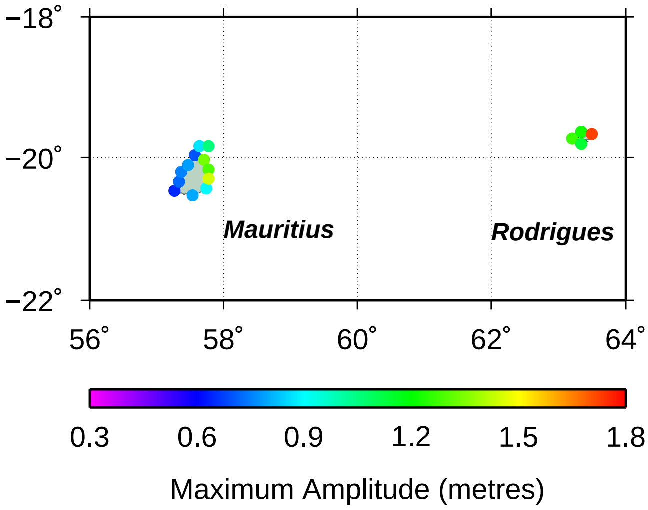

(c)

Figure 37: Mauritius:- (a) Hazard curves for all model output points. (b) National weighted deaggregated hazard. (c) Maximum amplitude at a 2000 year return period for all model output points.

5.23 Mayotte (low hazard)

As Figure 38(a) indicates, for a 2000 year return period the model output points off Mayotte have a maximum amplitude between 0.2 and 0.3 metres. The hazard at a return period of 2000 years is dominated by the Andamans, with a smaller contribution from Sumatra (Figure 38(b)). The hazard is slightly higher for points off the east coast of Mayotte (Figure 38(c)).

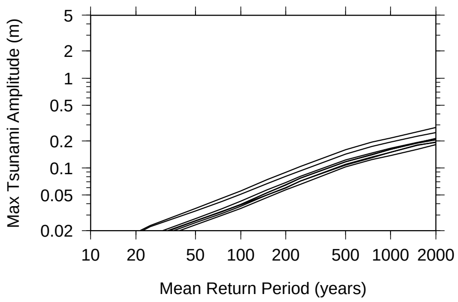

(a)

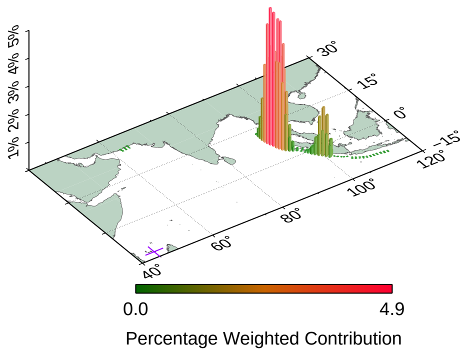

(b)

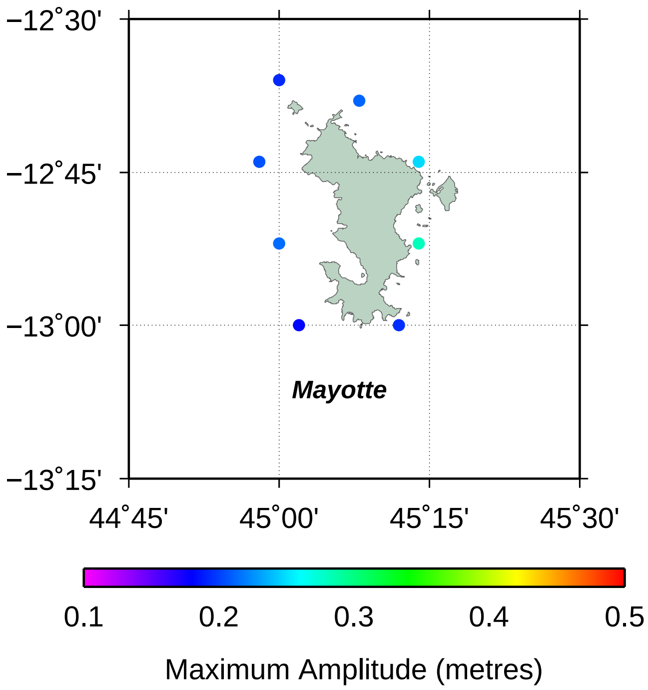

(c)

Figure 38: Mayotte:- (a) Hazard curves for all model output points. (b) National weighted deaggregated hazard. (c) Maximum amplitude at a 2000 year return period for all model output points.

5.24 Mayotte (high hazard)

Figure 39(a) shows that the maximum amplitudes at a 2000 year return period in the high hazard assessment vary from 0.3 to 0.4 metres. The hazard is again higher on the east coast of Mayotte than the west (Figure 39(c)). The deaggregated hazard map at this return period comes entirely from the Sunda Arc with a peak off the the Andaman section and a smaller peak off the Sumatra section (Figure 39(b)).

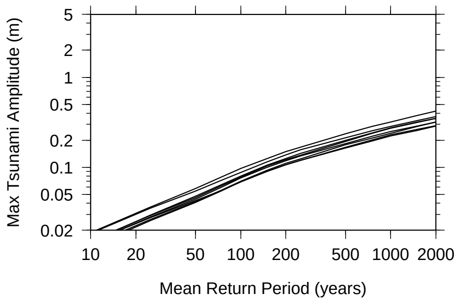

(a)

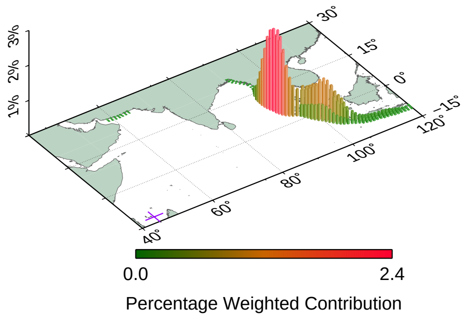

(b)

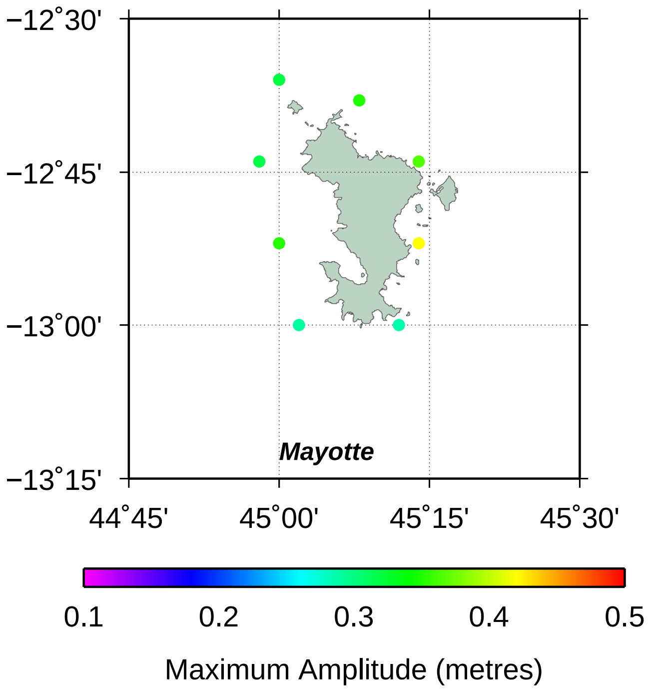

(c)

Figure 39: Mayotte:- (a) Hazard curves for all model output points. (b) National weighted deaggregated hazard. (c) Maximum amplitude at a 2000 year return period for all model output points.

5.25 Mozambique (low hazard)

The hazard off Mozambique has a great deal of variabilty (Figure 40(c)). The hazard is much higher in extreme northern and southern ends of the country which are not protected by Madagascar. Values at the 2000 year return period vary from 0.1 to 0.5m (Figure 40(a)). The hazard comes from the Andaman and central Sumatra segments of the Sunda Arc (Figure 40(b)).

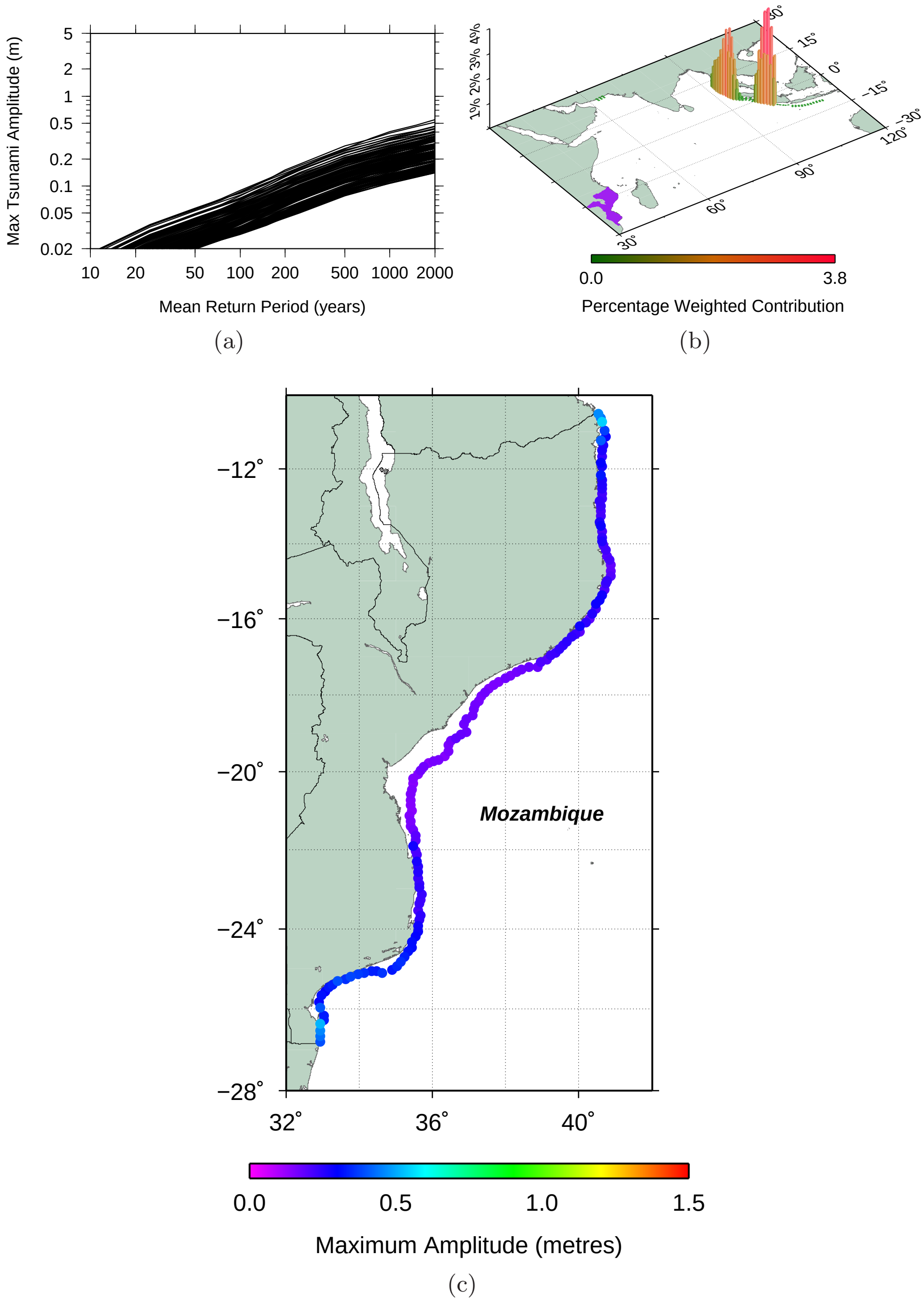

Figure 40: Mozambique:- (a) Hazard curves for all model output points. (b) National weighted deaggregated hazard. (c) Maximum amplitude at a 2000 year return period for all model output points.

5.26 Mozambique (high hazard)

The distribution of the maximum amplitude at the 2000 year return period in the high hazard assessment is similar to that in the low hazard one. Hazard is much higher at the extreme north and south of the country than in the centre and is higher in the south than in the north (Figure 41(c)). This is primarily due to the addition of the South Sandwich zone to the high hazard assessment. The contribution from the Sunda Arc is actually predicted to be smaller than that from the South Sandwich zone at the 2000 year return period for Mozambique (Figure 41(b)). Hazard values range from 0.3m to 1.4m at the 2000 year return period (Figure 41(a)).

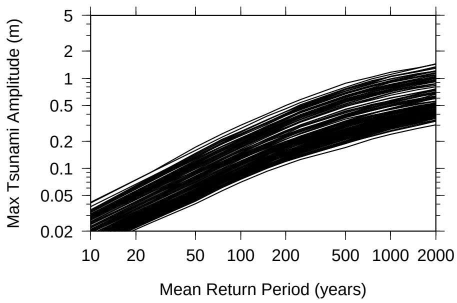

(a)

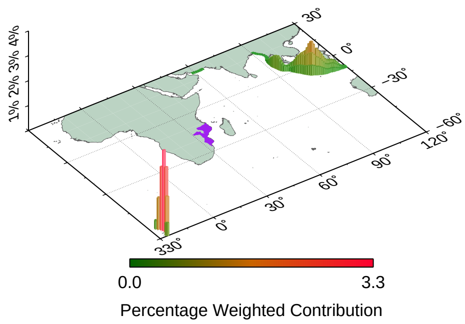

(b)

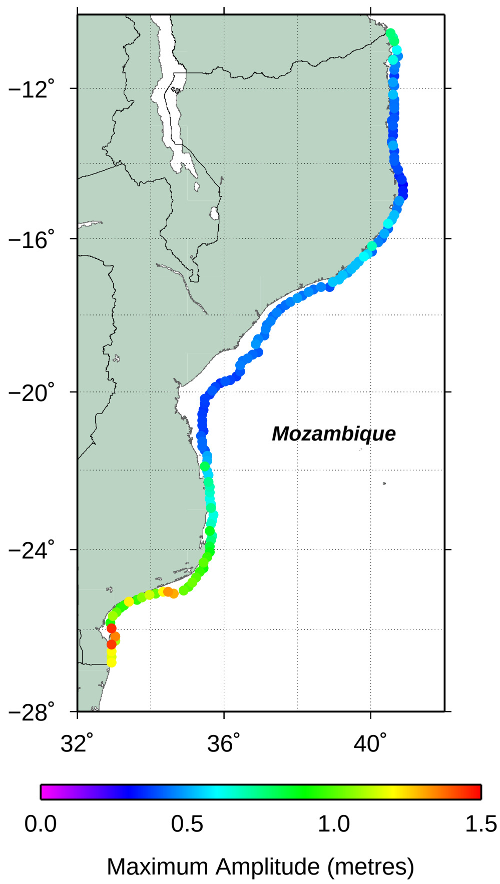

(c)

Figure 41: Mozambique:- (a) Hazard curves for all model output points. (b) National weighted deaggregated hazard. (c) Maximum amplitude at a 2000 year return period for all model output points.

5.27 Oman (low hazard)

Figure 42(a) shows that the maximum amplitudes increase from south to north across the points offshore Oman. Values range from about 0.1m in the north to 0.6m in the south at the 2000 year return period (Figure 42(a)). Tha main source of the hazard to Oman is the Makran and Andaman zones with some contributions from central Sumatra (Figure 42(b)) for this return period.

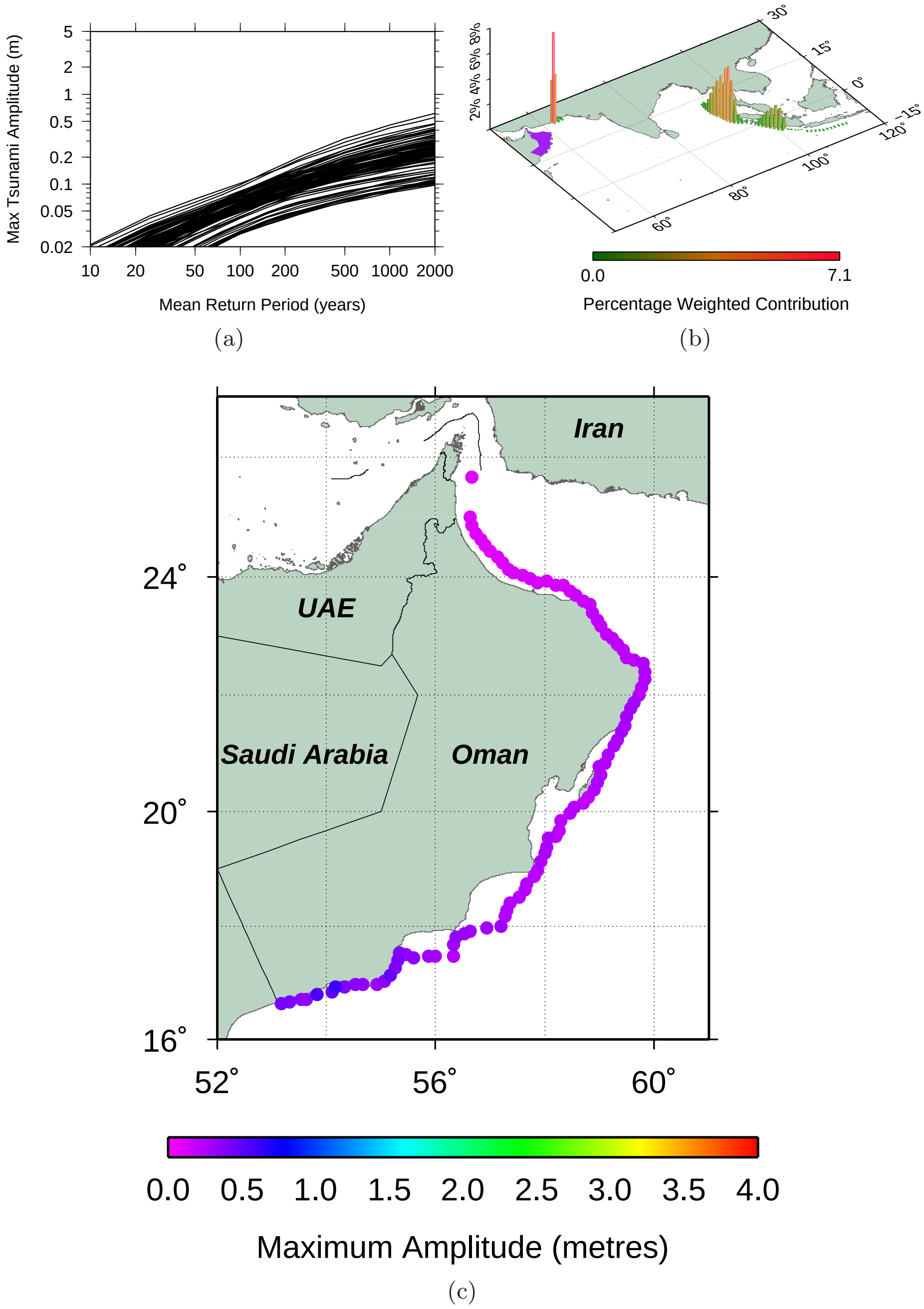

Figure 42: Oman:- (a) Hazard curves for all model output points. (b) National weighted deaggregated hazard. (c) Maximum amplitude at a 2000 year return period for all model output points.

5.28 Oman (high hazard)

In the high hazard assessment the hazard off northeast Oman which directly faces the western Makran is significantly larger than any other section of the Omani coast (Figure 43(c)). One isolated point has a maximum exceedence amplitude at 2000 years of 5m, however since that point is isolated it should be treated with caution (Figure 43(c)). The hazard for the rest of the Omani coast ranges from 0.5m to 3.8m (Figure 43(a)). In this high hazard assessment the hazard at the 2000 year return period is dominated by the Western Makran, with a relatively small contribution from Sumatra (Figure 43(b)).

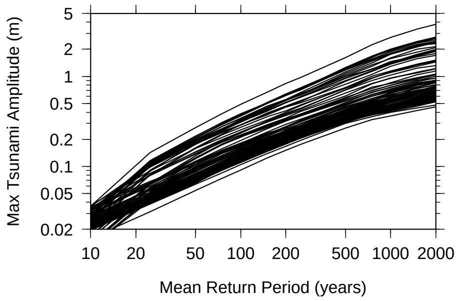

(a)

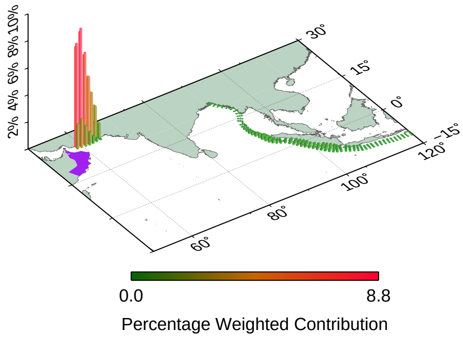

(b)

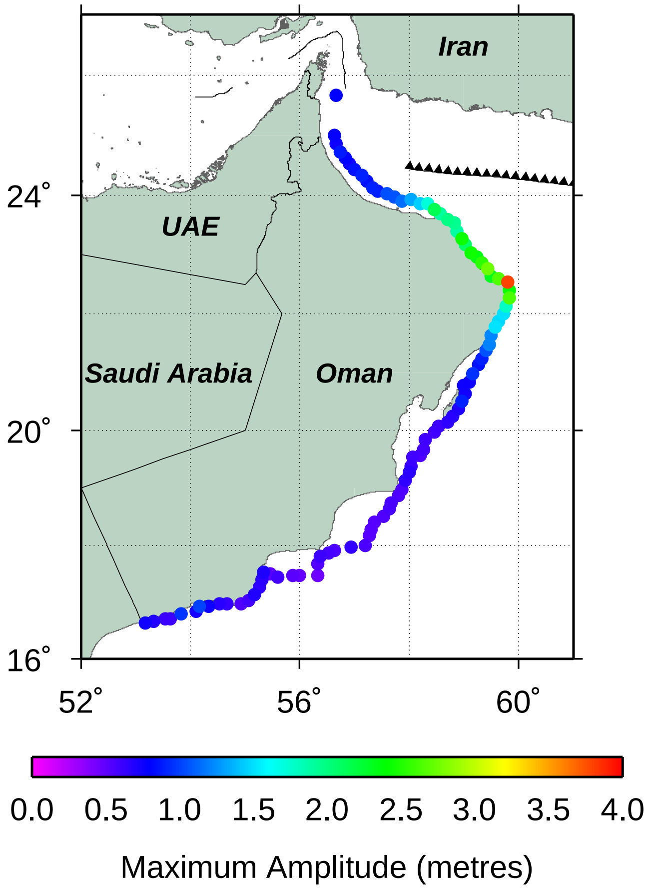

(c)

Figure 43: Oman:- (a) Hazard curves for all model output points. (b) National weighted deaggregated hazard. (c) Maximum amplitude at a 2000 year return period for all model output points.

5.29 Pakistan (low hazard)

The hazard offshore Pakistan has a great deal of variability in the low hazard map. The section of the coast offshore the eastern Markan has maximum exceedence amplitudes at the 2000 year return period of between 0.1 and 0.9m, while that for the rest of the coast ranges to as low as 0.2m (Figure 44(a and c)). The hazard is dominated by that from the eastern Markan (Figure 44(b)).

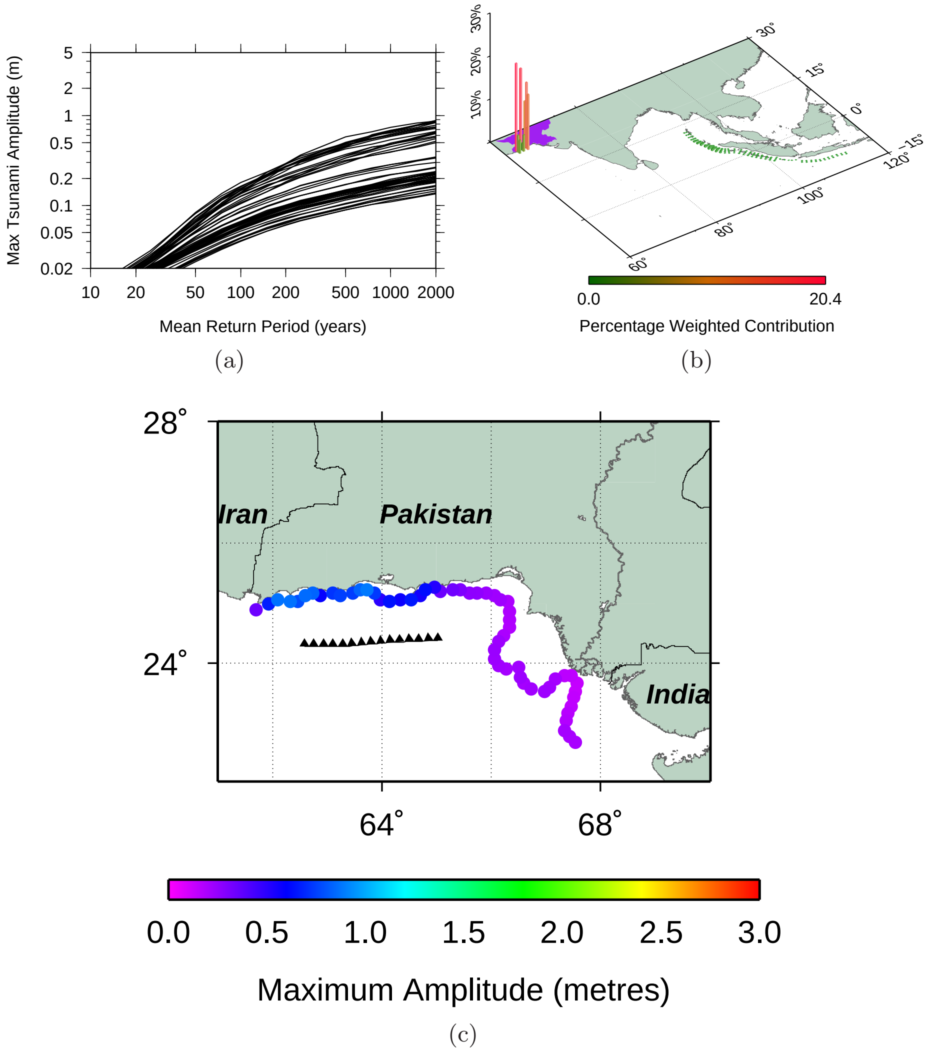

Figure 44: Pakistan:- (a) Hazard curves for all model output points. (b) National weighted deaggregated hazard. (c) Maximum amplitude at a 2000 year return period for all model output points.

5.30 Pakistan (high hazard)

As with the low hazard assessment, the maximum exceedence amplitude for western Pakistan offshore the Makran zone is much higher than that for eastern Pakistan (Figure 45(c)). Amplitudes range from 0.4m in the east to 2.8m in the west (Figure 45(a)). The hazard at this return period is again dominated by the Makran (Figure 45(b)).

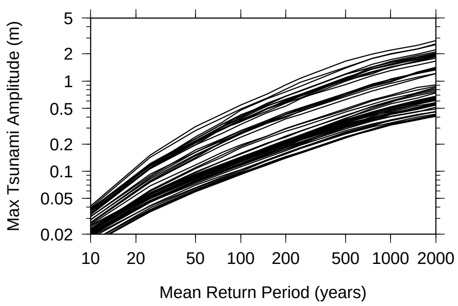

(a)

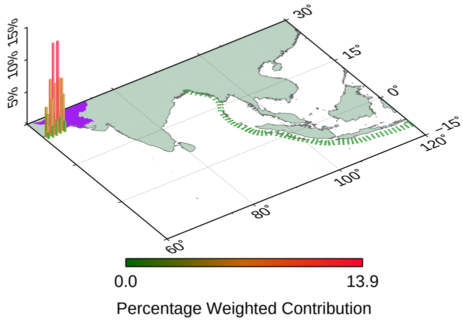

(b)

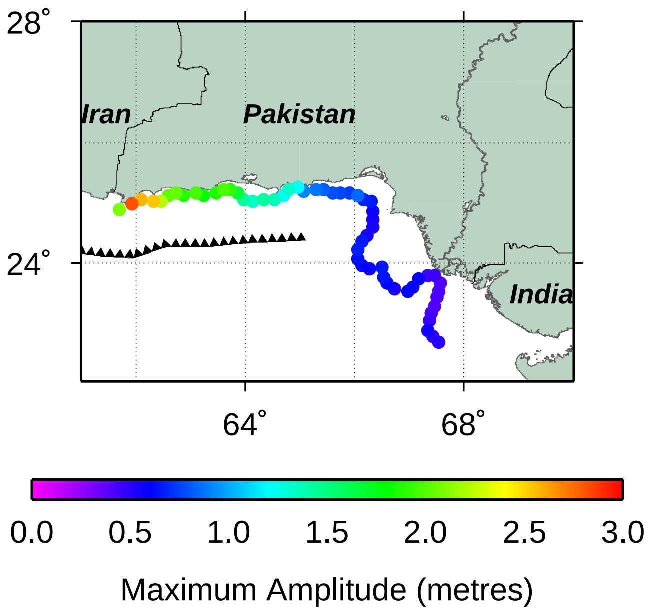

(c)

Figure 45: Pakistan:- (a) Hazard curves for all model output points. (b) National weighted deaggregated hazard. (c) Maximum amplitude at a 2000 year return period for all model output points.

5.31 Reunion (low hazard)

Maximum amplitudes for a 2000 year return period vary from 0.3 to 0.7 metres (Figure 46(a)), with the highest values off the eastern and southeastern coasts (Figure 46(c)). Figure 46(b) indicates that the greatest contribution to the hazard in this region is made by the central Sumatra segment of the Sunda Arc with a smaller contribution from the Andaman segment.

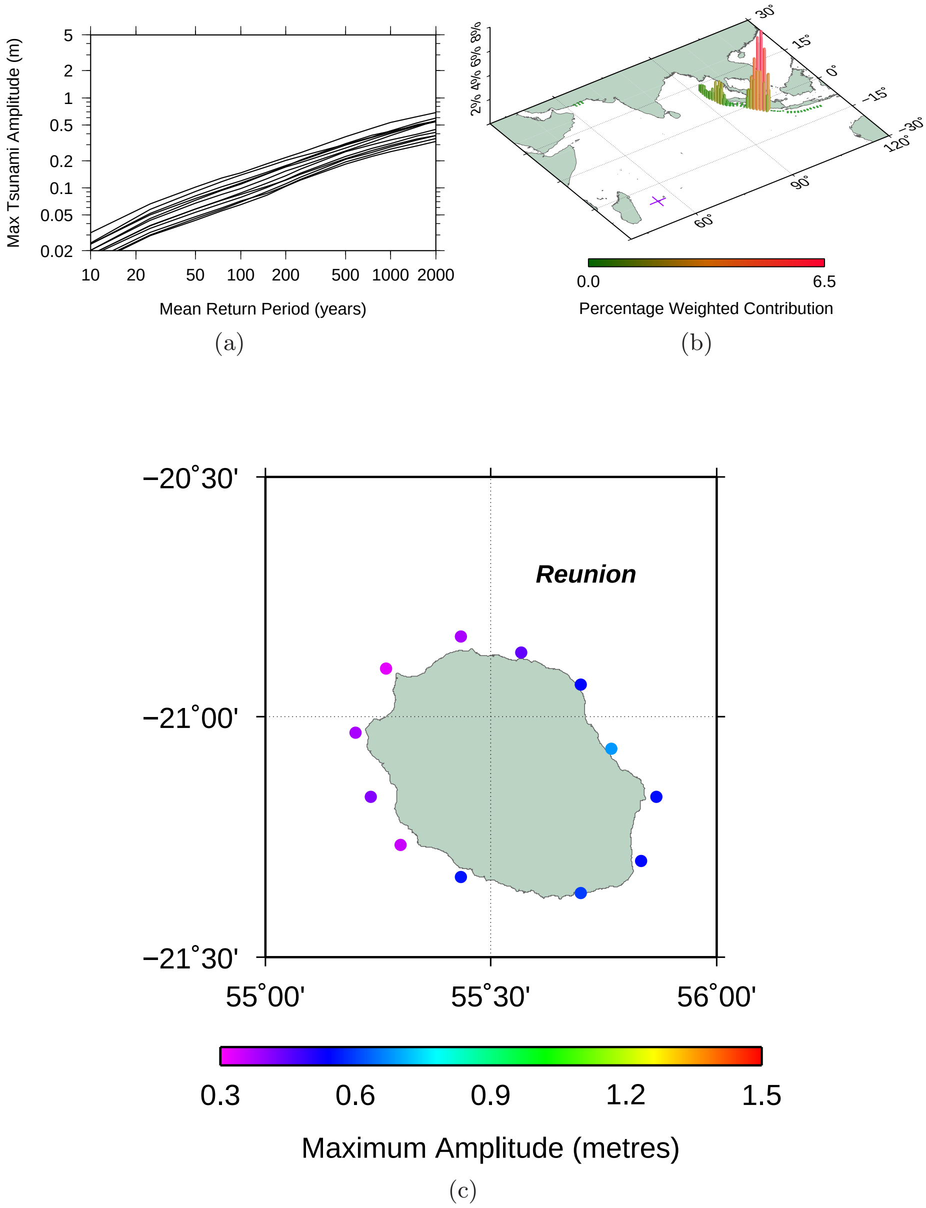

Figure 46: Reunion:- (a) Hazard curves for all model output points. (b) National weighted deaggregated hazard. (c) Maximum amplitude at a 2000 year return period for all model output points.

5.32 Reunion (high hazard)

Maximum amplitudes for a 2000 year return period vary from 0.7 to 1.4 metres in the high hazard assessment for Reunion at the 2000 year return period (Figure 47(a)). The highest values again being off the northeast and southern coasts (Figure 47(c)). Most of the hazard at this return period comes from the Sunda Arc and peaks off Sumatra (Figure 47(b)). Some of the hazard also comes from the South Sandwich zone as well.

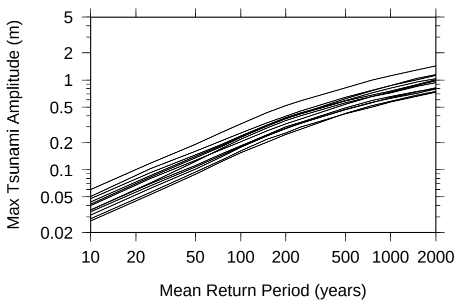

(a)

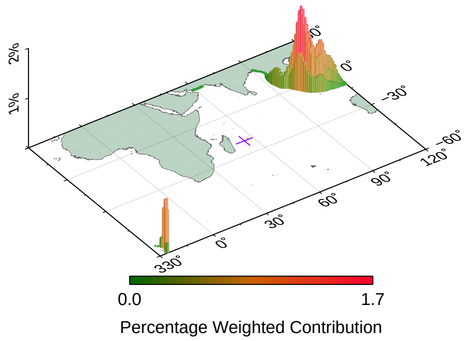

(b)

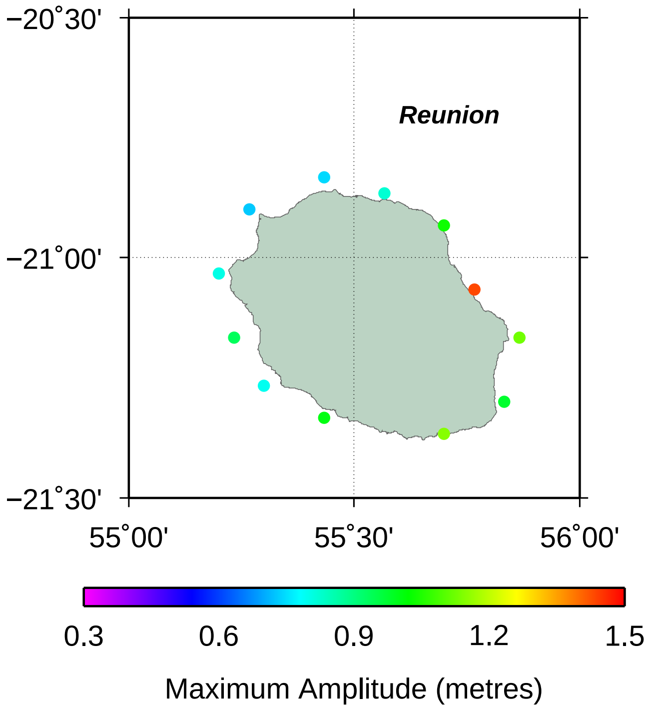

(c)

Figure 47: Reunion:- (a) Hazard curves for all model output points. (b) National weighted deaggregated hazard. (c) Maximum amplitude at a 2000 year return period for all model output points.

5.33 Seychelles (low hazard)

Hazard in the Seycelles at the 2000 year return period is at a maximum for the islands in the northeast part of the archipelgio (Figure 48(c)). Values range from about 0.1m to 0.8m depending on location (Figure 48(a)). The most important subduction zone for the Seycelles from this assessment is the Andaman section of the Sunda Arc, with a smaller contribution from Sumatra (Figure 48(b))

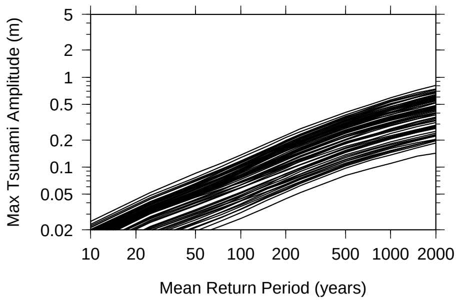

(a)

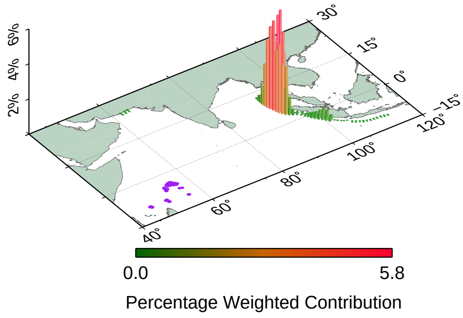

(b)

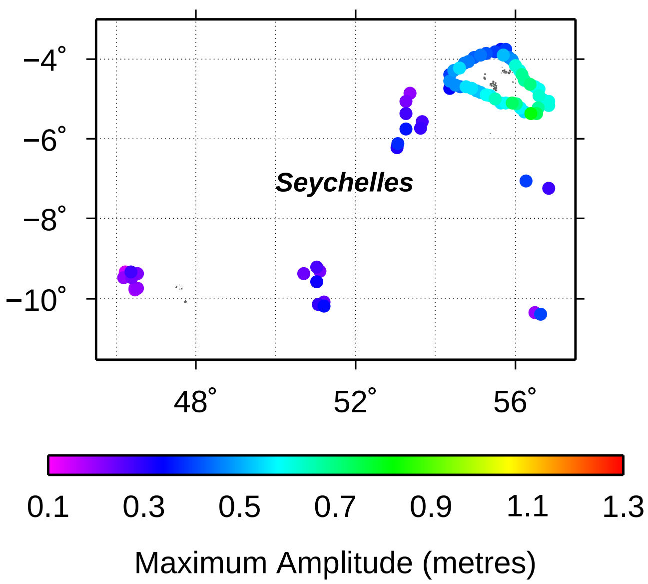

(c)

Figure 48: Seychelles:- (a) Hazard curves for all model output points. (b) National weighted deaggregated hazard. (c) Maximum amplitude at a 2000 year return period for all model output points.

5.34 Seychelles (high hazard)

As with the low hazard assessment, the hazard offshore islands in the northeast of the Seychelles is much higher than it is for the rest of islands (Figure 49(c)). Values range from 0.2m to 1.2m at the 2000 year return period (Figure 49(a)). Most of this hazard again comes from Andaman, but there is also a strong contribution from Sumatra (Figure 49(c)).

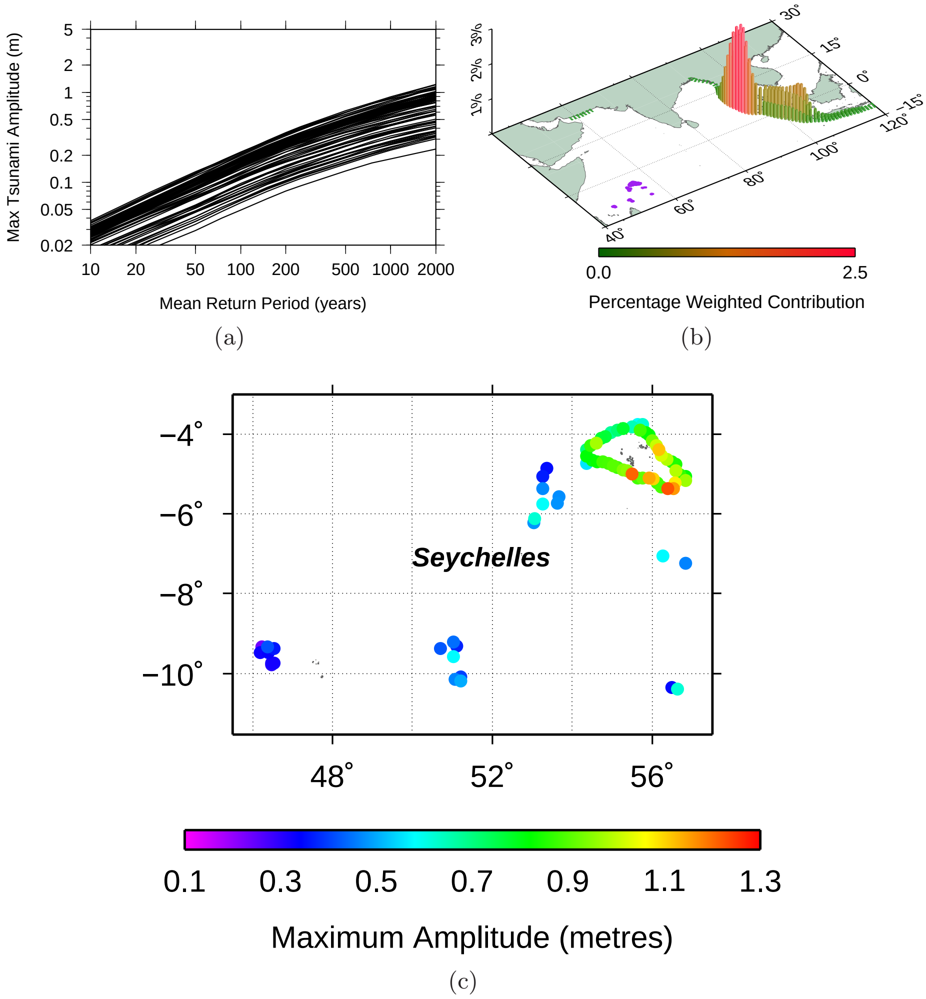

Figure 49: Seychelles:- (a) Hazard curves for all model output points. (b) National weighted deaggregated hazard. (c) Maximum amplitude at a 2000 year return period for all model output points.

5.35 Somalia (low hazard)

The hazard for Somalia originates predominantly from the Andman segment, with a small contribution from central Sumatra (Figure 50(b)). The hazard is much higher on the eastern coast facing the Indian Ocean than on the northern coast facing Yemen (Figure 50(c)). There are two distinct hazard curves for each coast (Figure 50(a)). The northern coast varies from 0.1m to 0.25m, while the northern coast varies from under 0.4m to about 0.7m at the 2000 year return period.

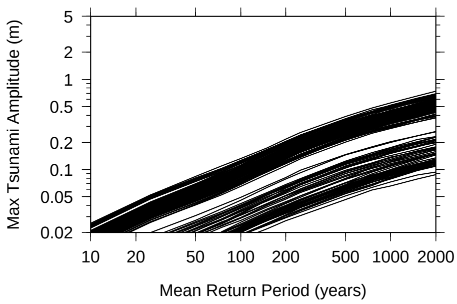

(a)

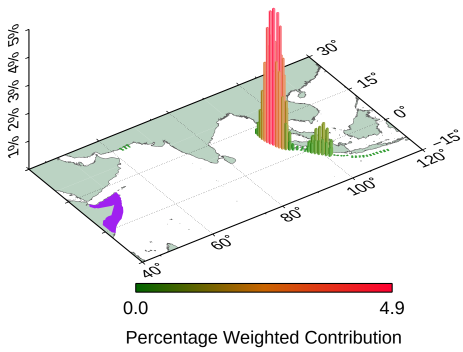

(b)

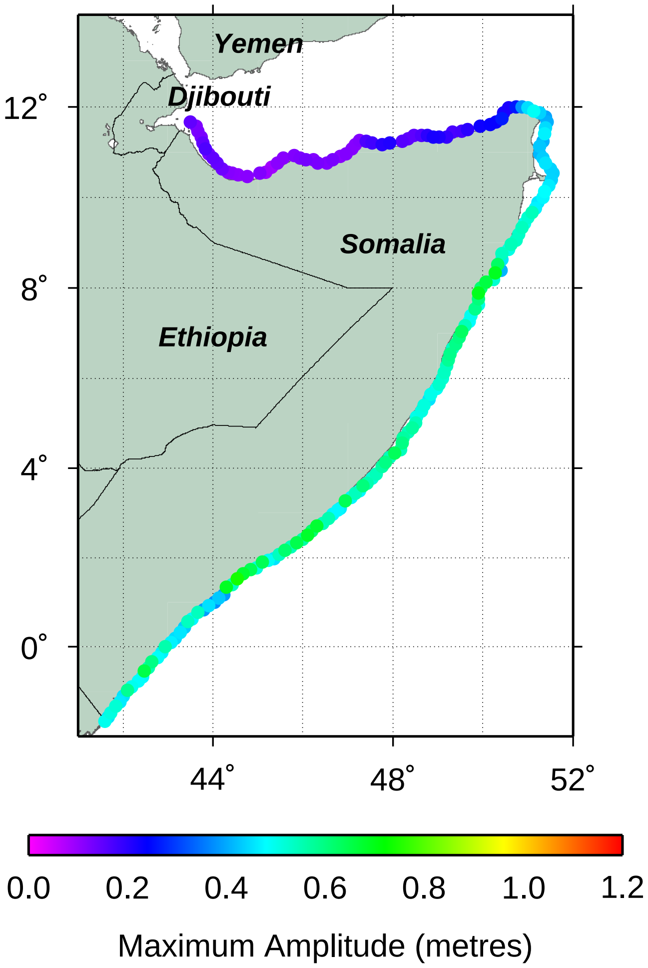

(c)

Figure 50: Somalia:- (a) Hazard curves for all model output points. (b) National weighted deaggregated hazard. (c) Maximum amplitude at a 2000 year return period for all model output points.

5.36 Somalia (high hazard)

The hazard for Somalia is again quite different for the northern and eastern coasts of Somalia (Figure 51(c)). Hazard values range from 0.2m to 1.1m with the highest values all along the eastern coast (Figure 51(a)). The hazard at the return period again mostly comes from the Andmana zone but Sumatra also contributes (Figure 51(b)).

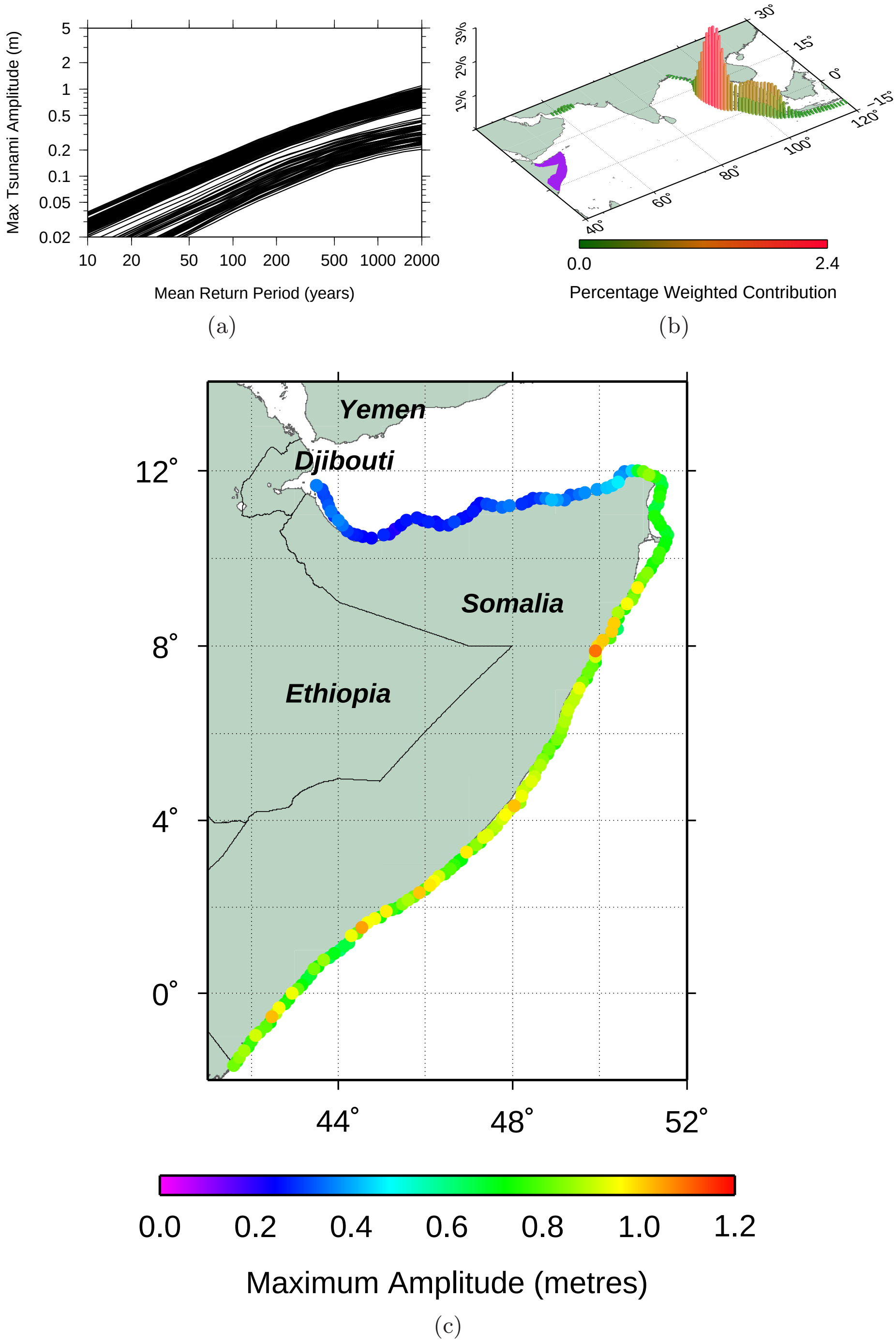

Figure 51: Somalia:- (a) Hazard curves for all model output points. (b) National weighted deaggregated hazard. (c) Maximum amplitude at a 2000 year return period for all model output points.

5.37 South Africa (low hazard)

The maximum amplitudes for a 2000 year return period increase from 0.6m offshore northern South Africa and decreases to 0.2m offshore southern South Africa (Figure 52(a and c)). The main source of the hazard at this return period is central Sumatra, but the Andaman also contributes (Figure 52(c)).

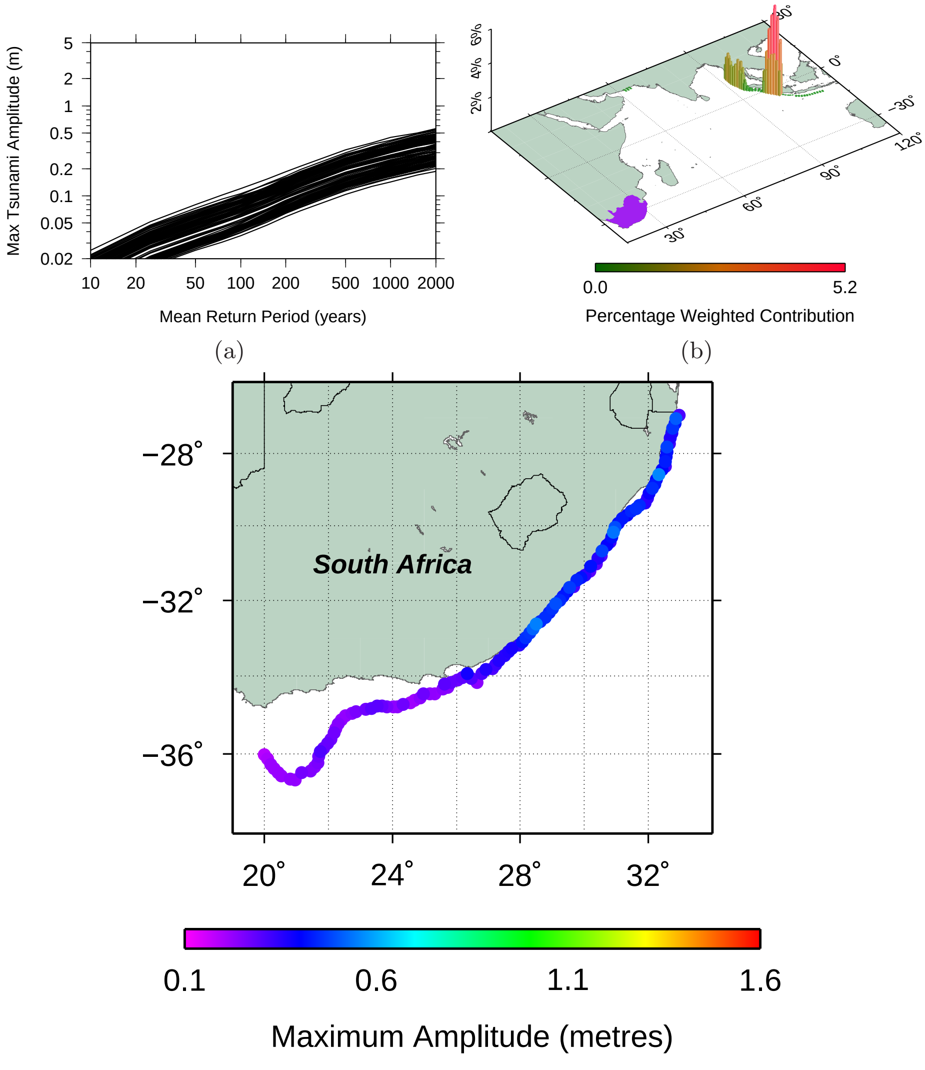

(a) (b) (c)

Figure 52: South Africa:- (a) Hazard curves for all model output points. (b) National weighted deaggregated hazard. (c) Maximum amplitude at a 2000 year return period for all model output points.

5.38 South Africa (high hazard)

In the high hazard assessment the hazard is less evenly distributed and peaks offshore eastern South Africa (Figure 53(c)). Values range from 0.6m to 1.6m at the 2000 year return period (Figure 53(a)) . The main source of the hazard to South Africa in the high hazard assessment is the South Sandwich Islands zone (Figure 53(b)). However, the Sumatra section of the Sunda Arc still makes a significant contribution.

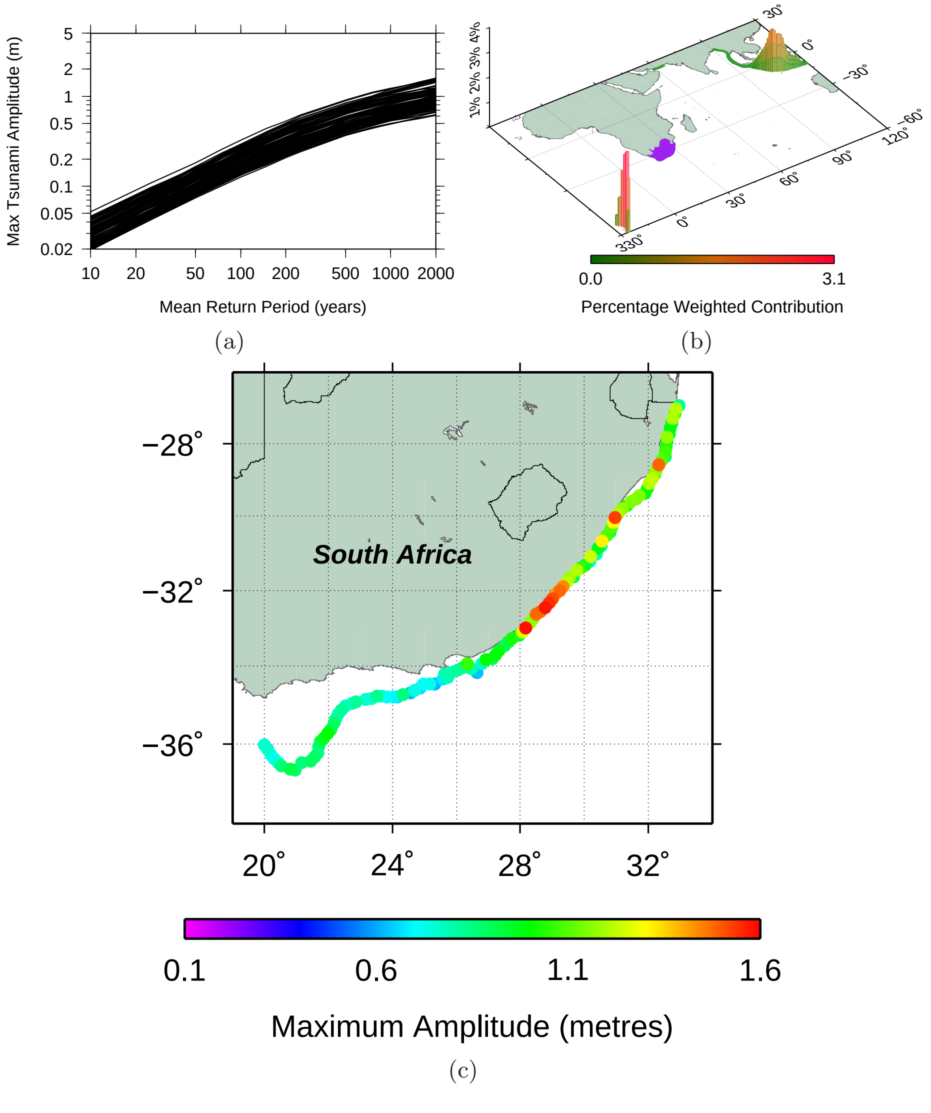

Figure 53: South Africa:- (a) Hazard curves for all model output points. (b) National weighted deaggregated hazard. (c) Maximum amplitude at a 2000 year return period for all model output points.

5.39 Sri Lanka (low hazard)

The hazard offshore the eastern coasts of Sri Lanka at a 2000 year return period is much higher than offshore the western coasts of Sri Lanka which face India (Figure 54(c)). Values range from 0.4m to 3m, depending on the choice of coast (Figure 54(a)). The hazard here is naturally dominated by the Andaman zone Figure 54(b)).

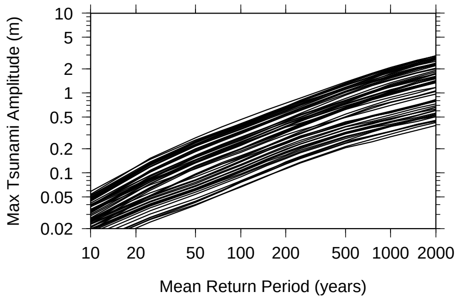

(a)

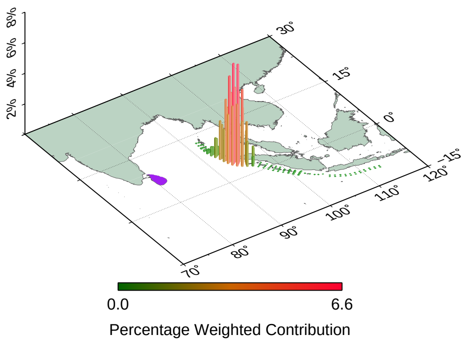

(b)

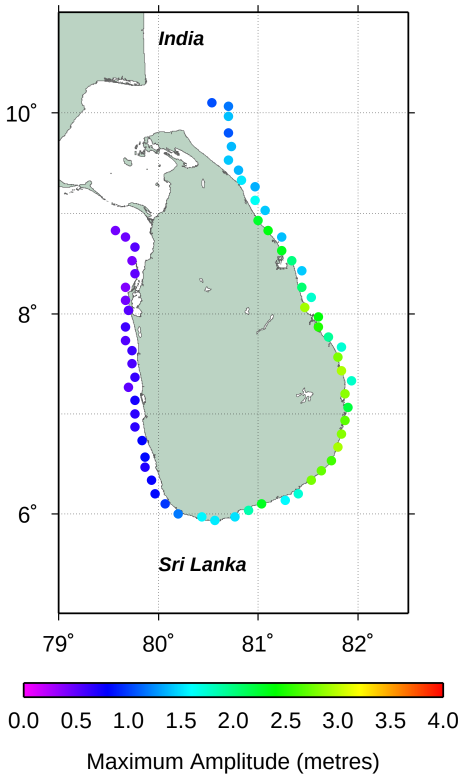

(c)

Figure 54: Sri Lanka:- (a) Hazard curves for all model output points. (b) National weighted deaggregated hazard. (c) Maximum amplitude at a 2000 year return period for all model output points.

5.40 Sri Lanka (high hazard)

The hazard offshore Sri Lanka is again much higher off the eastern, particularly the south-east coasts, at the 2000 year return than offshore the western and northern coasts (Figure 55(c)). Values range from 0.6m to nearly 3.7m Figure 55(a)). Again, the main source of this hazard is the Andaman zone Figure 55(b)).

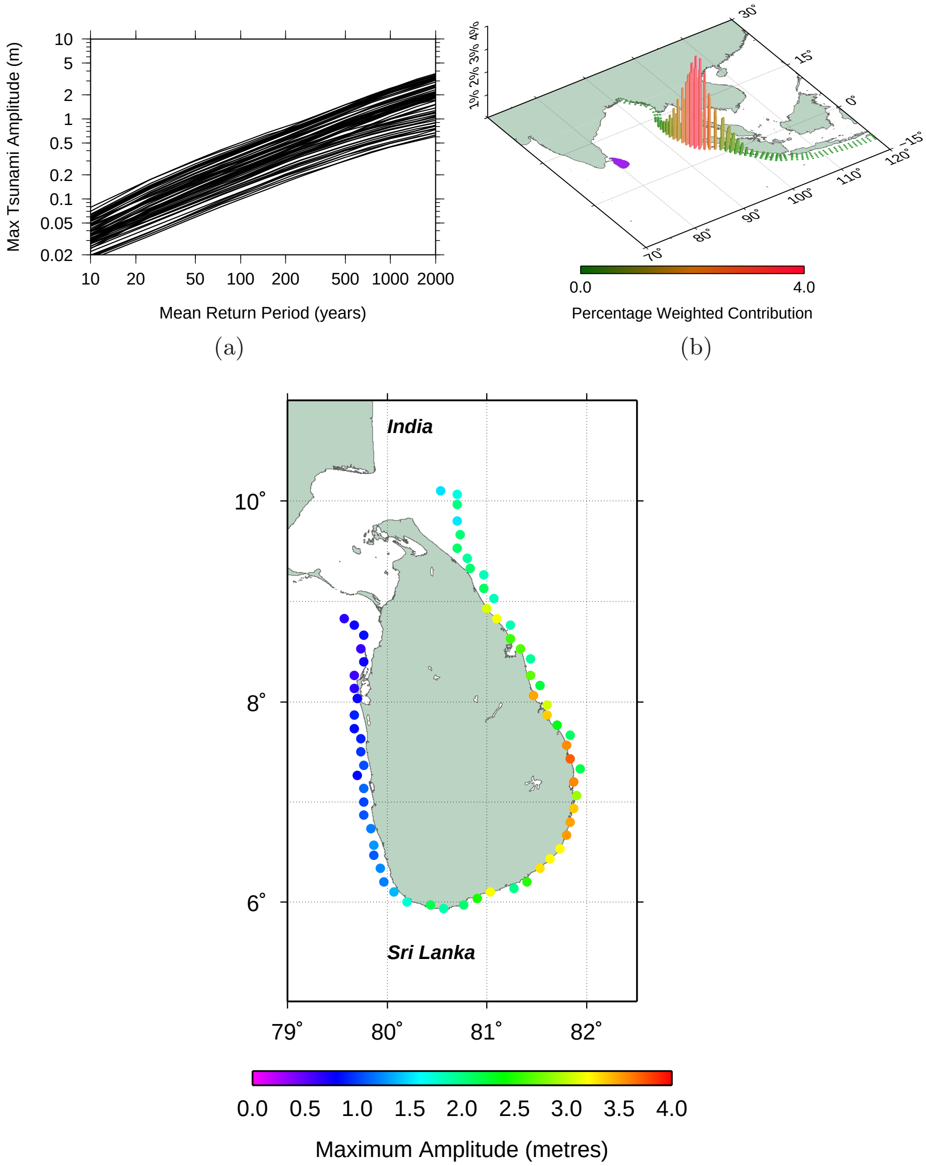

(a) (b)

(c)

Figure 55: Sri Lanka:- (a) Hazard curves for all model output points. (b) National weighted deaggregated hazard. (c) Maximum amplitude at a 2000 year return period for all model output points.

5.41 Tanzania (low hazard)

Referring to Figure 56(c), the hazard offshore of Tanzania is fairly even with the exception of points on the western side of islands which are protected by the islands themselves. The maximum tsunami amplitude at the 2000 year return period ranges from 0.2m to 0.5m Figure 56(a)). The hazard at this return period mostly comes from the Andaman segment, with a small contribution from the central Sumatran segment as well Figure 56(b)).

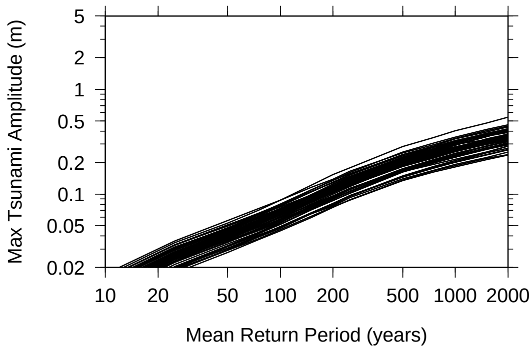

(a)

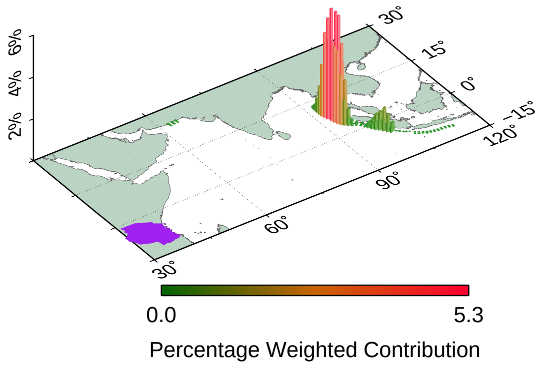

(b)

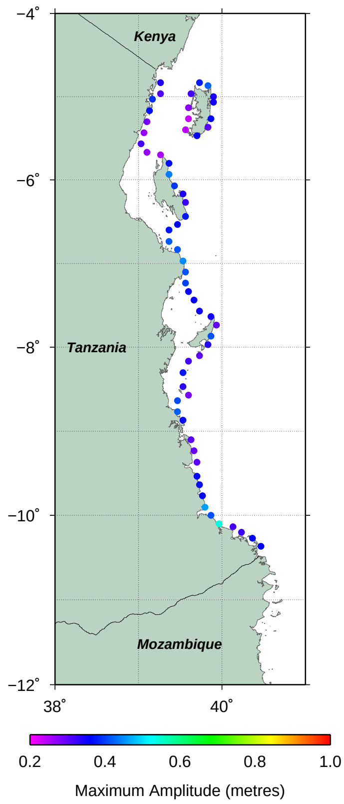

(c)

Figure 56: Tanzania:- (a) Hazard curves for all model output points. (b) National weighted deaggregated hazard. (c) Maximum amplitude at a 2000 year return period for all model output points.

5.42 Tanzania (high hazard)

As Figure 57(c) shows, the high hazard assessment also predicts a fairly uniform hazard distribution along the Tanzanian coast. One point has a noticeably higher hazard than the rest, but since this is an isolated point the result should be treated with caution. Hazard mostly comes the Andaman and, to a lesser extent, Sumatra segments of the Sunda Arc Figure 57(b)). Maximum tsunami amplitudes at the 2000 year return period range from 0.4m to over 0.9m Figure 57(a)).

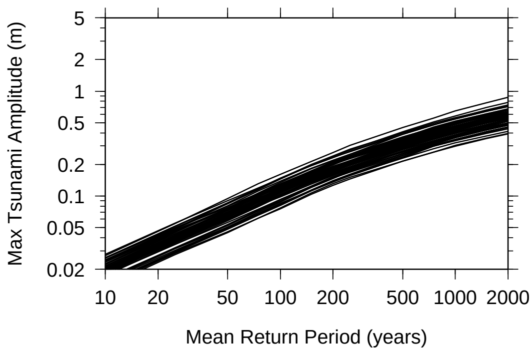

(a)

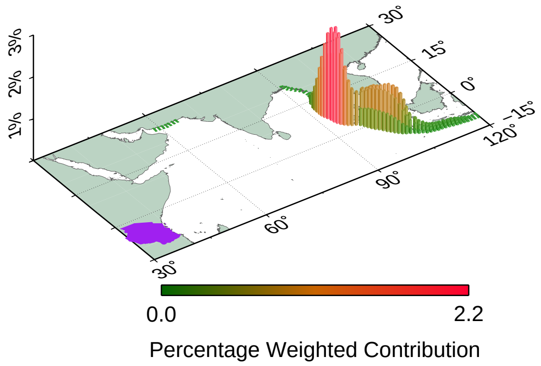

(b)

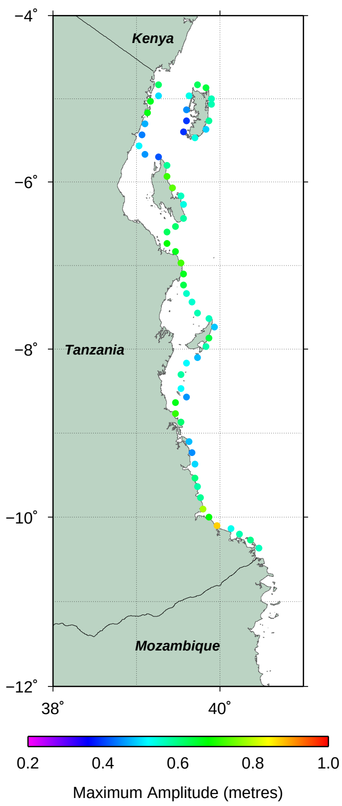

(c)

Figure 57: Tanzania:- (a) Hazard curves for all model output points. (b) National weighted deaggregated hazard. (c) Maximum amplitude at a 2000 year return period for all model output points.

5.43 Thailand (low hazard)

The hazard offshore Thailand in the low hazard assesment decreases from north to south Figure 58(c). Amplitudes at the 2000 year return period range from over 0.7m to 1.9m Figure 58(a). This hazard mostly originates from the southern Andaman zone Figure 58(b).

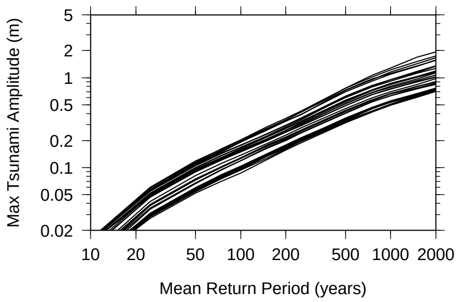

(a)

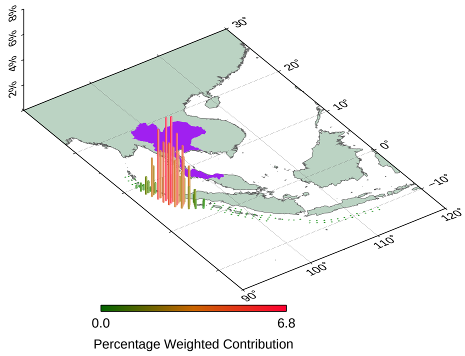

(b)

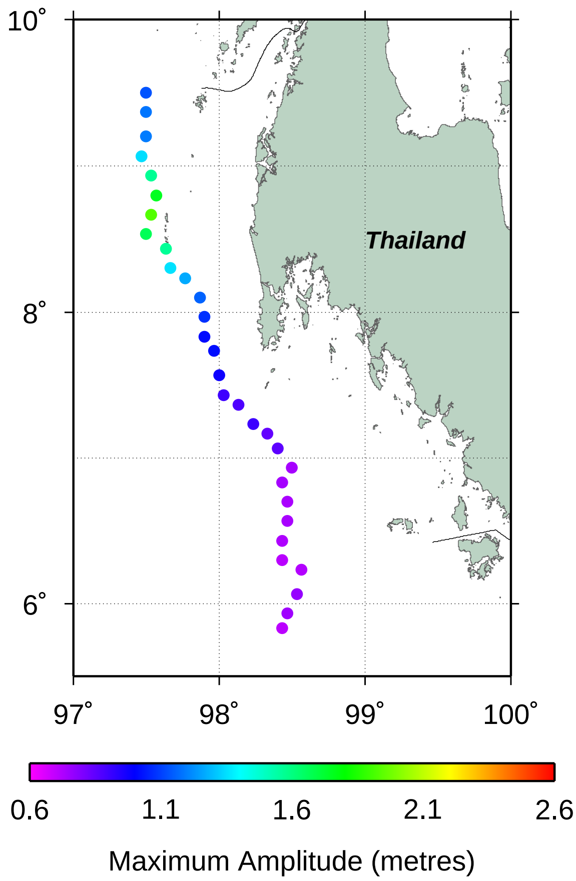

(c)

Figure 58: Thailand:- (a) Hazard curves for all model output points. (b) National weighted deaggregated hazard. (c) Maximum amplitude at a 2000 year return period for all model output points.

5.44 Thailand (high hazard)

The distubution of the hazard from the high hazard assessment is similar that from the low one, it is much higher in the north than the south (Figure 59(c)). However it should be pointed out, that the maximum tsunami amplitude is everywhere quite high (between 0.8m and 2.5m at the 2000 year return period, see Figure 59(a)). The Andaman is by far the most important subduction zone segment for Thailand (Figure 59(b)).

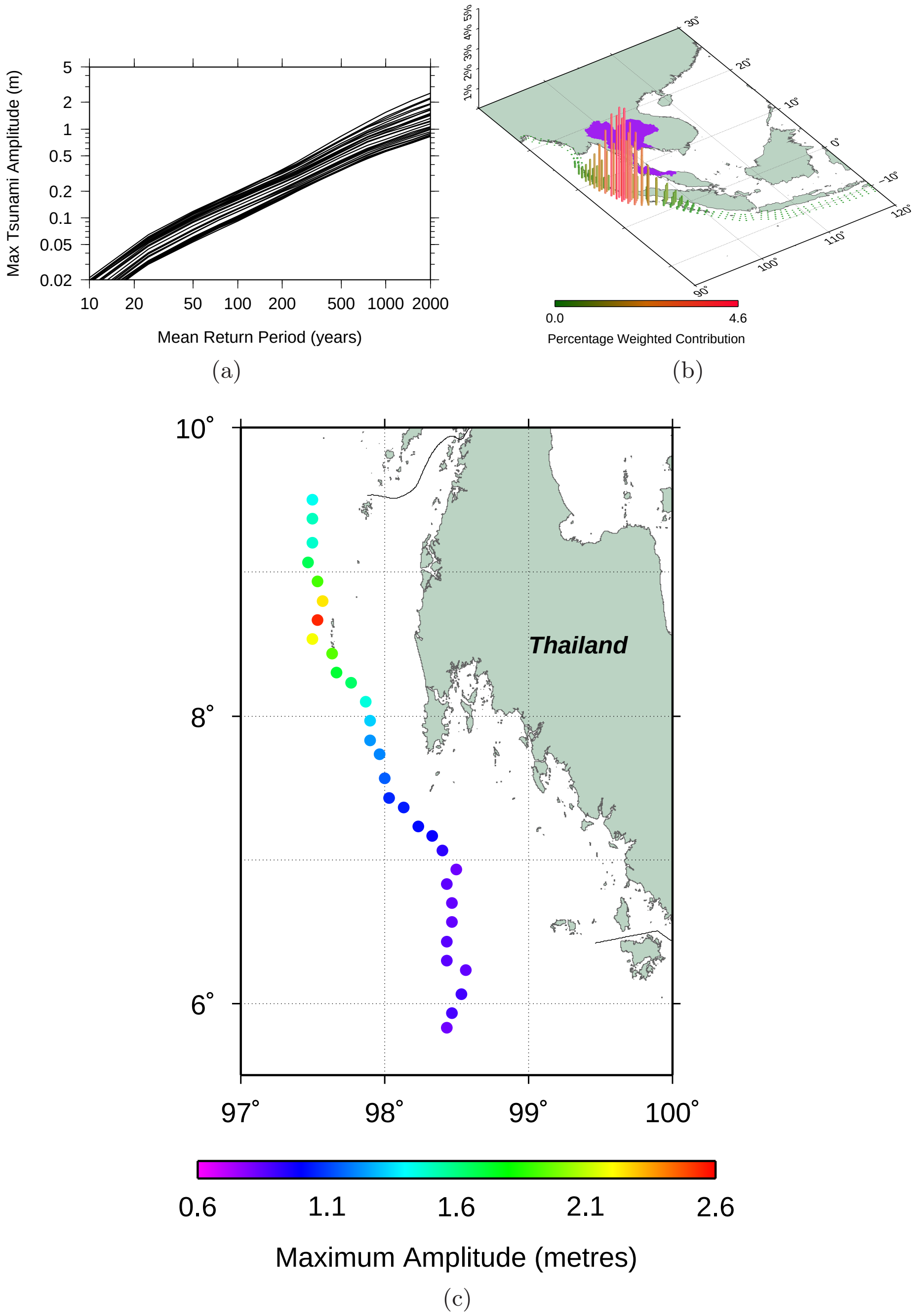

Figure 59: Thailand:- (a) Hazard curves for all model output points. (b) National weighted deaggregated hazard. (c) Maximum amplitude at a 2000 year return period for all model output points.

5.45 United Arab Emirates (low hazard)

The hazard for the short section of coast included in this assessment is everywhere quite low (at around 0.1m at the 2000 year return period, see Figure 60(a and c)). This hazard mostly comes from the Makran and to a lesser extent the Andaman and central Sumatra segments (Figure 60(c)). The tsunami hazard within the Persian Gulf was not considered in this assessment.

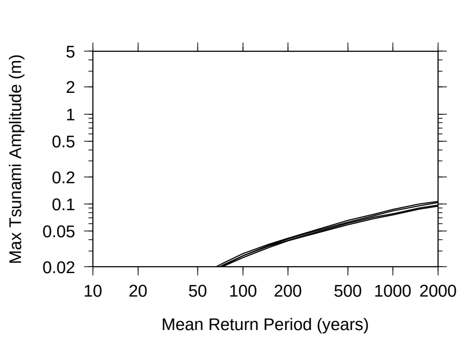

(a)

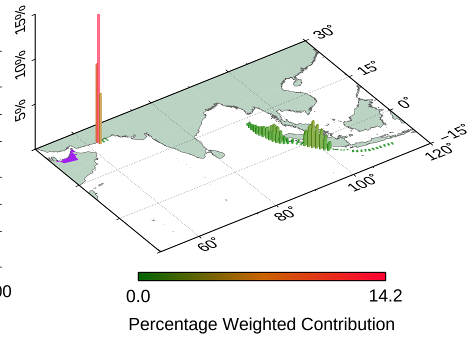

(b)

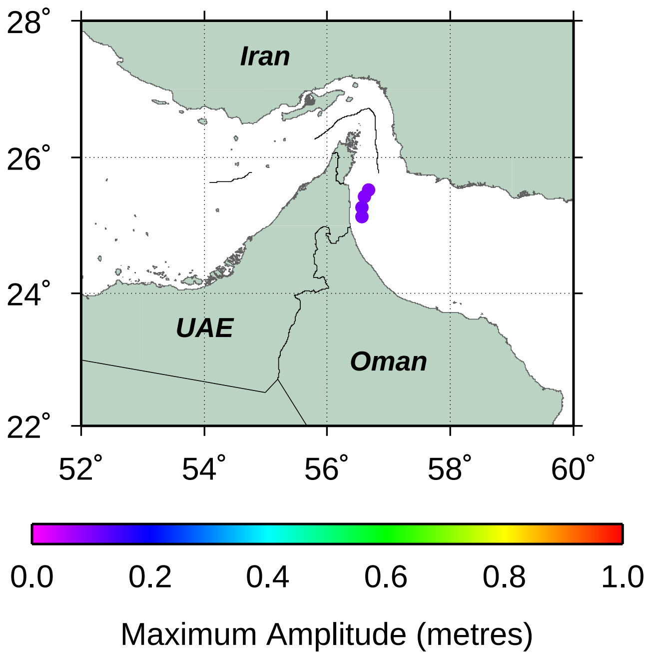

(c)

Figure 60: United Arab Emirates:- (a) Hazard curves for all model output points. (b) National weighted deaggregated hazard. (c) Maximum amplitude at a 2000 year return period for all model output points.

5.46 United Arab Emirates (high hazard)

The hazard offshore the UAE from the high hazard assessment was noticably higher, about 0.8m at the 2000 year return period Figure 61(a and c). The hazard is dominated by the western Makran Figure 61(b).

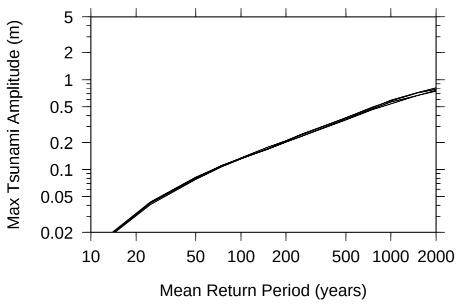

(a)

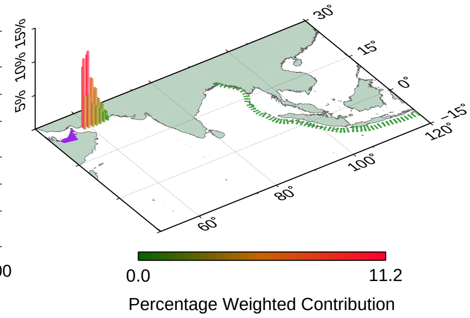

(b)

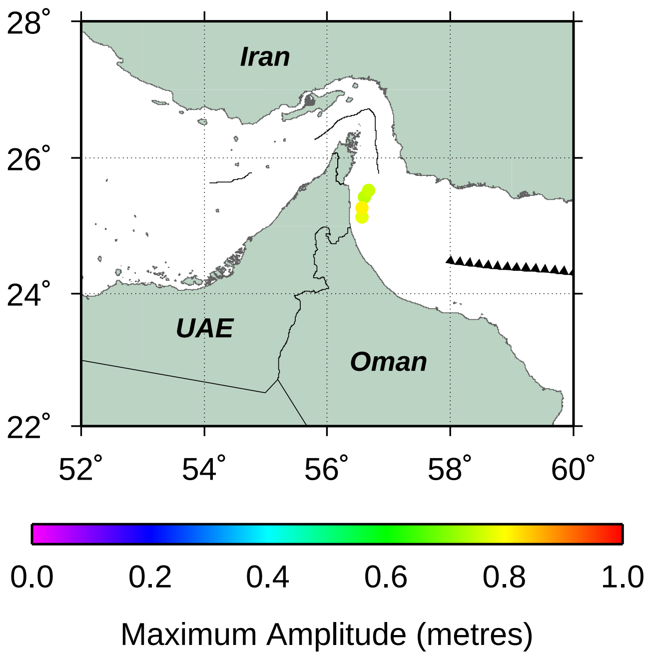

(c)

Figure 61: United Arab Emirates:- (a) Hazard curves for all model output points. (b) National weighted deaggregated hazard. (c) Maximum amplitude at a 2000 year return period for all model output points.

5.47 Yemen (low hazard)

The hazard offshore Yemen varies considerably; it is much higher off eastern Yeman and Socotra than offshore west Yemen Figure 62(c). Points along the Red Sea coasts were not included in this assessment. The maximum tsunami amplitude at the 2000 year return period ranges from 0.09m to just under 0.8m Figure 62(a). This hazard mostly comes from the Andaman and central Sumatra segments Figure 62(c).

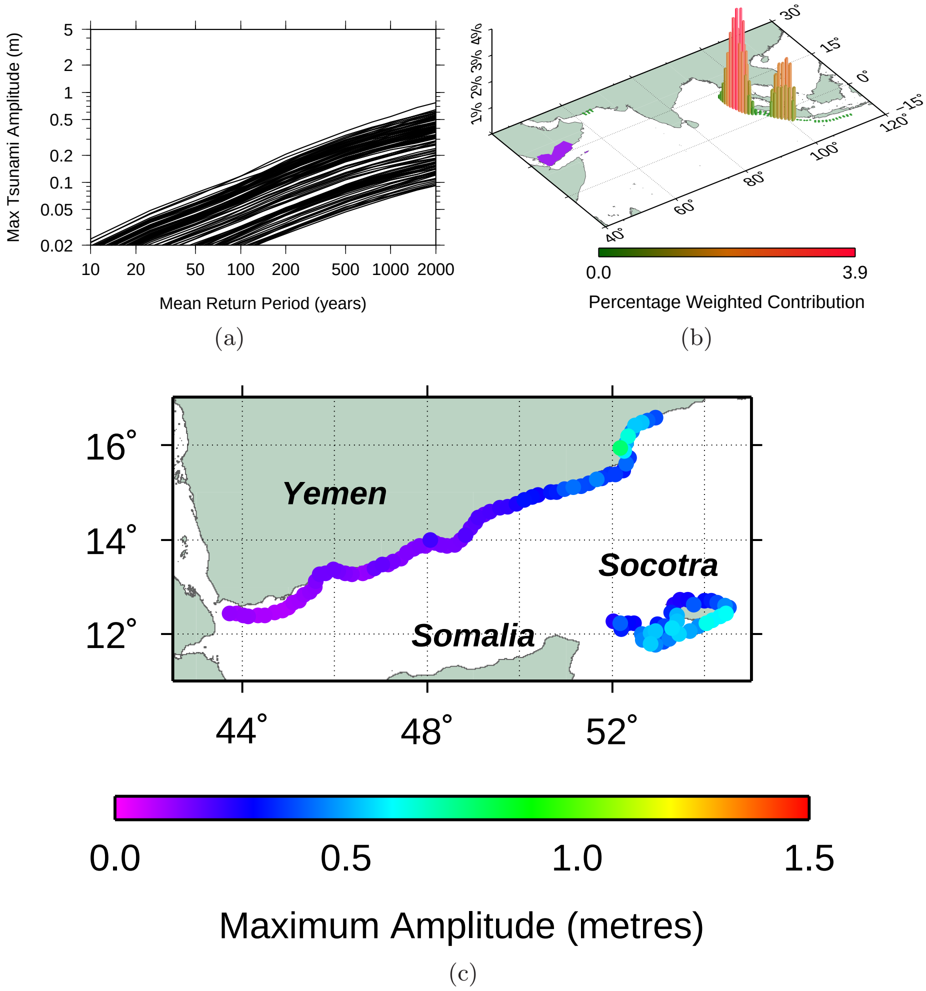

Figure 62: Yemen- (a) Hazard curves for all model output points. (b) National weighted deaggregated hazard. (c) Maximum amplitude at a 2000 year return period for all model output points.

5.48 Yemen (high hazard)

In the high hazard map, the tsunami hazard to Yemen also originates mostly from Andaman and Sumatra at the 2000 year return period Figure 63(b). However, the eastern Makran is close enough to also contribute a small amount to the hazard at this return period. Tsunami amplitudes at the 2000 year return period range from 0.2m to 1.3m Figure 63(a) and is again much higher for eastern Yemen and Socotra than for the rest of Yemen Figure 63(c).

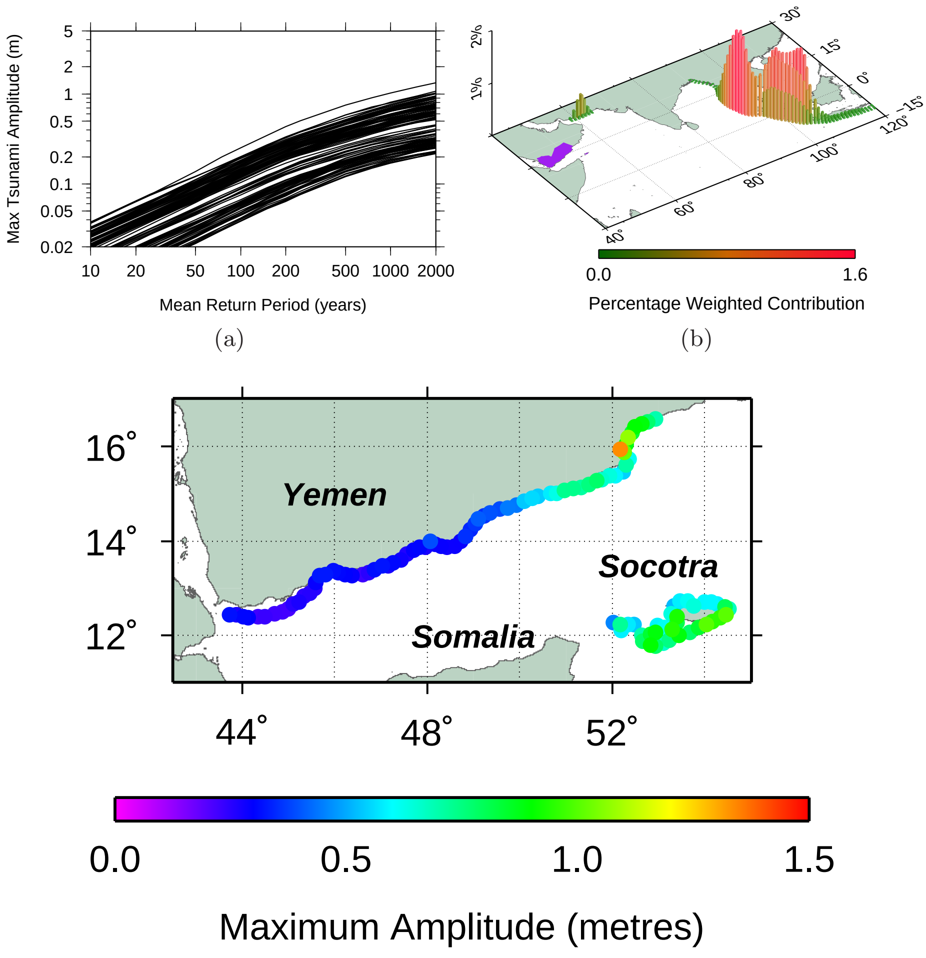

(a) (b) (c)

Figure 63: Yemen- (a) Hazard curves for all model output points. (b) National weighted deaggregated hazard. (c) Maximum amplitude at a 2000 year return period for all model output points.

6 Conclusion

In summary, by considering earthquake sources in the Indian Ocean, South Sandwich and Puysegur subduction zones, we have modelled nearly 25,000 tsunami to offshore of all the Indian Ocean nations. The probability of each tsunami was determined by estimating what fraction of the global subduction zone seismicity would be expected on each zone and partitioning the global seismicity accordingly. For each subduction zone a range of different maximum magnitudes and earthquake source geometry models were included in the final hazard assessment presented here.

This assessment was designed to allow Indian Ocean nations to prioritise which coastlines have the highest tsunami hazard and should be considered for future, more detailed, study. The nations with the highest hazard at the 1 in 2000 year return period level are listed in Table 1 in the Introduction.

Several major conclusions can be drawn from the report:

- Several nations, particularly those in the northeast of the Indian Ocean, have a very high tsunami hazard, particularly Indonesia. These nations are usually close to the Sunda Arc subduction zone or are perpendicular to it (eg Indonesia, India and Sri Lanka). These were also the nations most affected by the 2004 Indian Ocean tsunami. The tsunami from the Andaman, Arakan and Sumatran zones dominate the hazard at the 2000 year return period. The hazard for Indonesia east of the Sunda Strait is controlled mostly by the activity on the Java-Sumba section of the Sunda Arc subduction zone. Unfortunately the maximum magnitude for this section of the Sunda Arc is quite uncertain. This means that the tsunami hazard for this area is consequently also very uncertain at the long (ie 2000 yr) return periods (see Figure 3).
- The nations located northwest of the Indian Ocean (eg Iran, Pakistan and UAE) have a more moderate hazard than Indonesia. The hazard here is controlled by the activity of the Makran subduction zone, which also has an uncertain maximum magnitude.
- For the islands in the central to western Indian Ocean potentially dangerous tsunami can come from either the Makran or the western Sunda Arc zone. The offshore hazard is somewhat lower for these islands because they are significant further from the tsunami source.
- For nations in the southwest Indian Ocean (eg eastern South Africa, Madagascar, Mozambique and Reunion) some of the 2000 year hazard also comes from the South Sandwich zone in the southern Atlantic as well as from the Sunda Arc. The hazard for these nations is otherwise moderate.

For more details on specific nations, please see the relevant section in Section 5, the KML files on the accompaning DVD or contact Geoscience Australia directly.

While we believe the overall results of this study are reliable and useful, we do recommend that more detailed studies be undertaken, particularly of the nations with the highest hazard. In particular, future studies should use a higher resolution and more accurate bathymetry. The resolution of the bathymetry used here is not high enough to determine precisely the offshore heights with great confidence, particularly for islands. However, we believe the relative levels of hazard are reliable and have been consistently assessed for all nations in this study.

The other major source of uncertainty in this assessment is with our estimate of the likelihood of a major (Mw8+) events for many of the source zones. This is one of the most important but at the same time most poorly constrained parameters in the analysis.

Nations for which this is a particular problem have a large difference between the high and low hazard maps (see Figure 3). In this assessment, we estimated this likelihood by extrapolating from the frequency of smaller earthquakes. However, we cannot be sure that any given zone can, or ever has, produced an earthquake larger than has been observed for the zone. The only way to reduce this uncertainity is by studies into the palaeo-record of specific nations for evidence of pre-historic large inundations from tsunami.

It is also important to note that low offshore wave heights do not always correspond to low impact. For coastlines with high concentrations of population near sea level, even a moderate to low tsunami may have the potential to cause significant damage. Therefore we recommend more detailed inundation studies of the potentially at risk communties be undertaken in order to more confidently quantify the potential impact to the Indian Ocean nations of a major tsunami reaching their shores.

7 Future Work

The Indian Ocean Probabilistic Tsunami Hazard Assessment presented here is a first-pass assessment whose full potential will be achieved only if it is followed up by further work to reduce the uncertainties and to better tailor the results so that they can be optimally utilized by the disaster management community. Much of the future work that would be needed to improve tsunami hazard assessment in the Indian Ocean was already evident at the time of the ICG/IOTWS Workshop on Indian Ocean Tsunami Hazard Assessment held in Bandung, Indonesia, 17-18 July, 2007. This report has therefore adopted the following recommendations from the Bandung workshop regarding future work, with appropriate modification to reflect the results presented here:

1. **Continue to assess Indian Ocean tsunami hazards**. Tsunami hazard assessments are indispensable for the guidance and support of tsunami mitigation measures, including the effective deployment of instrumental warning systems. To play these roles however, they must include the following:

   (a) **Communicate uncertainty**. Little is known about maximum earthquake magnitudes and rupture modes, and the recurrence times of tsunami events in the Indian Ocean. The uncertainties in a tsunami hazard assessment should reflect this lack of knowledge, and these uncertainties should be clearly expressed in the hazard assessment. Here, this uncertainty has been expressed through the development of low-hazard and high-hazard assessments, but this may create potential for confusion in applying the results to mitigation efforts. Alternative means for expressing uncertainty should be considered in future assessments.

   (b) **Follow up with validation and inundation mapping**. The hazard assessment presented here expresses hazard as offshore tsunami height, but to understand potential impact this must be followed up with inundation modelling, which can be guided by the deaggregated hazard produced as part of this assessment. Inundation modelling should be validated where possible against data from historic and prehistoric (i.e., from paleotsunami studies) events.

   (c) **Update periodically**. The hazard maps, being based on information that is incomplete, will need regularly scheduled updating, at intervals of five years or less, to reflect new insights from future earthquakes and tsunami, present-day geodetic deformation, and past earthquakes and tsunami identified in geologic and written records. Also, information on non-earthquake sources, such as volcanic eruptions and submarine landslides, should be included in future revisions.

   (d) **Guide usage**. Contributors to the hazard assessments should work with emergency managers and planners for mutual benefit in tailoring the assessments to practical needs and ensuring that the assessments are put to good use. In particular, expert advice will be needed to determine the relative weight with which the low-hazard and high-hazard maps should be considered in any particular application.

2. **Support these assessments with geology, geodesy, and written history**. The high uncertainties indicated in the assessment presented here can be reduced only through some combination of the following:

   (a) **Provide geologic hindsight**. Earthquake and tsunami history needs to span thousands of years to cover the range of tsunami sizes and recurrence intervals for each tsunami source in the probabilistic hazard assessment. Accordingly, paleotsunami studies on the coastlines of the Indian Ocean should be accelerated, and their use in combination with other paleoseismic techniques should be extended to all subduction-zone regions of the Indian Ocean.

(b) **Monitor subduction-zone deformation**. Such measurements are needed to constrain convergence rate and strain accumulation as indicators of expectable earthquake size and frequency. While current efforts are providing some of this information for Sumatra, much-expanded coverage is needed for the other Indian Ocean subduction zones Andaman-Nicobar, Arakan, Java and Makran. Needed also is better regional coordination to optimize use of observational capacity.

(c) **Discover additional written records of past tsunami**. Such records form the usual basis for estimating tsunami size, frequency, and potential impact. For the Indian Ocean, with its long history of writings by native people and outsiders, it is important to go beyond existing compilations of historical materials, and it is also important to evaluate and provide supporting documentation for every historical tsunami that influences the probabilistic hazard assessment.

8 Acknowledgements

We are grateful for the support of the many scientists who contributed both directly and indirectly to the work that went into this report. In particular we are grateful to Prof. Sam Hettiarachchi and Dr. John Schneider, who shepherded the project as part of the work program of ICG/IOTWS Working Group 3. We are also grateful to the participants in the UNESCO-IOC Workshop on Methodologies for Indian Ocean Hazard Assessment, who helped frame the discussion of earthquake sources to be considered, and in particular to Dr. Brian Atwater who best articulated some of the concerns about the expression of uncertainty and the need for further work in tsunami geology. Finally, we thank AusAID for the patience and financial support needed to see the work through to completion. The views expressed in this publication are those of the authors and not necessarily those of the Australian Agency for International Development (AusAID).

9 References

Abercrombie, R.E., Antolik, M.A., and G. Ekstrom, 2003. The June 2000 Mw 7.9 earthquakes south of Sumatra: Deformation in the India-Australia Plate, J. Geophys. Res., 108(B1), 2018, doi:10.1029/2001JB000674.

Abercrombie R.E., Antolik, M.A., Felzer, K.R., and G. Ekstrom, 2001. The 1994 Java earthquake: slip over a subducting seamount. J Geophys Res 106:6595-6607.

Allport, J.K. and R.J. Blong, 1995. *The Australian Tsunami Database (ATDB)*, Sydney: School of Earth Sciences, Macquarie University.

Ambraseys N.N., and C.P. Melville, 1982. A history of Persian earthquakes. Cambridge University Press, pp 219.

Ammon, C.J., Kanamori, H., Lay, T., and A.A. Velasco, 2006. The 17 July 2006 Java tsunami earthquake, *Geophy. Res. Lett.*, 33, doi:10.1029/2006GL028005.

Barrientos, S.E. and S.N. Ward, 1990. The 1960 Chile earthquake: inversion for slip distribution from surface deformation. *Geophys. J. Int.* **103**, pp.589-598.

Bassin, C., Laske, G. and G. Masters, 2000. The current limits of resolution for surface wave tomography in North America, *EOS Trans AGU*, **81**, F897. http://mahi.ucsd.edu/Gabi/rem.html.

Bathgate, J., Volti T.. and Greenslade, D. J. M., 2008. The Joint Australian Tsunami Warning Centre: responding to a tsunamigenic earthquake - Puysegur Trench, 30 September 2007. *Preview*, 133, April 2008, pp. 40-44.

Bayer, R., Chery, J., Tatar, M., Vernant, Ph., Abbassi, M., and F. Masson, 2006. Active deformation in Zagros?Makran transition zone inferred from GPS measurements, *Geophys. J. Int.*, 165, 373-381 doi: 10.1111/j.1365-246X.2006.02879.

Beauregard, J. O., 2001. Explosive rhyodacitic volcanism: The evolution and frequency of pre-1883 eruptions at Krakatau volcano, Indonesia, Phd Thesis, University of Rhode Island, pp 358.

Bilham, R., Lodi, S., Hough, S., Bukhary, S., Murtaza Khan, A. and S.F.A. Rafeeqi, 2007. Seismic hazard in Karachi, Pakistan: Uncertain past, uncertain future. Seism. Res. Lett., 78, 601-613.

Bird, P., 2003. An updated digital model of plate boundaries. *Geochem. Geophys. Geosys.* **4**(3), 1027, doi:10.1029/2001GC000252.

Briggs, R.W., Sieh, K., Meltzner, A.J., Natawidjaja, D., Galetzka, J., Suwargadi, B., Hsu, Y., Simons, M., Hananto, N., Suprihanto, I., Prayudi, D., Avouac, J.-P., Prawirodirdjo, L., and Y. Bock, 2006. Deformation and slip along the Sunda megathrust during the great Nias-Simeulue earthquake of March 2005, Science, 311 (5769), 1897-1901. doi:10.1126/science.1122602.

Bryant, E., 2001. *Tsunami: the underrated hazard*, Cambridge University Press, Cambridge.

Burbidge, D., Cummins, P., 2007. Assessing the threat to Western Australia from tsunami generated by earthquakes along the Sunda Arc, Natural Hazards, 43, 319-331.

Burbidge, D., Cummins, P. and Mleczko R., and H.K. Thio, 2008. A Probabilistic Tsunami Hazard Assessment for Western Australia, Pure and Applied Geophysics, 165, 2059-2088.

Byrne D.E., Sykes L.R., and D.M. Davis, 1992. Great thrust earthquakes and aseismic slip along the plate boundary of the Makran subduction zone. J Geophys Res 97:449-478

Chamot-Rooke, N., Jestin, F., de Voogd, B. and Phedre Working Group, 1993. Intraplate shortening in the central Indian Ocean determined from a 2100-km-long north-south deep seismic reflection profile, Geology, 21, 1043-1046.

Chlieh, M., Avouac, J.P., Sieh, K., Natawidjaja, D.H., and J. Galetzka, 2008. Heterogeneous coupling on the Sumatra megathrust constrained from geodetic and paleogeodetic measurements, J. Geophys. Res, 113, 5305, doi:10.1029/2007JB004981.

Cummins, P.R., 2007. The potential for giant tsunamigenic earthquakes in the northern Bay of Bengal. Nature 449, 75?78. doi:10.1038/nature06088.

Gudmundsson , O. and M. Sambridge, 1998. A regionalized upper mantle (RUM) seismic model, *J. Geophys. Res.* **B4**, pp.7121-7136.

ICMMG - *see* Institute of Computational Mathematics and Mathematical Geophysics.

Jankaew, K., Atwater, B.F., Sawai, Y., Choowong, M., Charoentitirat, T., Martin, M.E., and A. Prendergast, 2008. Medieval forewarning of the 2004 Indian Ocean tsunami in Thailand, Nature 455, 1228-1231.

Johnson, R. W., 1987. Large-scale volcanic cone collapse: the 1888 slope failure of Ritter volcano, and other examples from Papua New Guinea. *Bull. Volcanol.* **49**, pp.669-679.

Keys, J.G., 1963. The tsunami of 22 May 1960 in the Samoa and Cook Islands. *Bull. Seism. Soc. Am.* **53**(6), pp.1211-1227.

Kopp, H. and N. Kukowski, 2003. Backstop geometry and accretionary mechanics of the Sunda margin, *Tectonics*, **22**, 6, 1072, doi:10.1029/2002TC001420. Lynnes, C.S., and T. Lay, 1988. Source process of the great 1977 Sumba earthquake, 93, 13,407-13,420.

Mader, C.L., 2002. Modeling the 1958 Lituya Bay mega-tsunami, II. *Sci. of Tsun. Haz.* **20**(5), pp.241-250.

Mei, C., Stiassnie, M. and D. Yue, 2005. *Theory and Applications of Ocean Surface Waves.* Singapore: World Scientific.

Monecke, K., Finger, M., Klarer, D., Kongko, W, McAdoo, B.G., Moore, A.L. and Sudrajat, S.U., A 1,000 year sedimetn record of tsunami recurrence in northern Sumatra, 2008. *Nature*, **455**, 1232-1234.

Mokhtari, M. , Abdollahie Fard, I., and Hessami, K., 2008. Structural elements of the Makran region, Oman sea and their potential relevance to tsunamigenisis, Natural Hazards, v47, pp. 185-199.

Musson, R.M.W., 2009. Subduction in the Western Makran: The Historian's contribution, J. Geol. Soc., 166, 387-391.

Myles, D., 1986. *The Great Waves.* London: Robert Hale.

Narayan, J. P., Sharma, M. L. and B.K. Maheshwari, 2005. Effects of Medu and coastal topography on the damage pattern during the recent Indian Ocean tsunami along the coast of Tamilnadu. *Sci. Tsunami Haz.* **23**(2), pp.9-18.

Natawidjaja, D. H., Sieh, K., Chlieh, M., Galetzka, J., Suwargadi, B. W., Cheng, H., Edwards, R. L., Avouac, J.-P. and Ward, S. N., 2006. Source parameters of the great Sumatran megathrust earthquakes of 1797 and 1833 inferred from coral microatolls, J. Geophys. Res., 111, doi:10.1029/2005JB004025. 2 National

Geophysical Data Centre, 2007. *Global Tsunami Database*, National Oceanic and Atmospheric Administration, Washington, viewed 23 May 2007, <http://ngdc.noaa.gov/seg/hazard/tsu_db.shtml>.

NGDC - *see* National Geophysical Data Centre.

Okal, E.A. and C.J. Hartnday, 2008. South Sandwich: The forgotten subduction zone and tsunami hazard in the south Atlantic. *Eos Trans. AGU*, 89(53), Fall Meet. Suppl., Abstract OS51E-08.

Okal, E.A., Borrero, J. and C.E. Synolakis, 2004. The earthquake and tsunami of 1865 November 17: evidence for far-field tsunami hazard from Tonga. *Geophys. J. Int.* **157**, pp.154-174.

Ortiz, M., Bilham, R. 2003. Source area and rupture parameters of the 31 December 1881 $M_w = 7.9$ Car Nicobar earthquake estimated from tsunamis recorded in the Bay of Bengal, *J.* Geophys. Res. **108**(B4), doi:10.1029/2002JB001941.

Parsons, T. and E. L. Geist, 2008. Tsunami probability in the Caribbean region, Pure and Applied Geophysics, 165, 2089-2116.

Page, W. D., Alt, J. N., Cluff, L. S., and G. Plafker, 1979., Evidence for the recurrence of large-magnitude earthquakes along the Makran coast of Iran and Pakistan, Tectonophysics, 52, 533-547.

Pendse, C. G., 1948. A short note on the Mekran earthquake of the 28th November 1945, Jour. Scient. Indust. Res., 5, 106-108.

Rajendran, C. P., Rajendran, K., Anu, R., Earnest, A., Machado, T., Mohan, P. M. and J. Freymueller, 2007. Crustal deformation and seismic history associated with the 2004 Indian Ocean earthquake: a perspective from the Andaman-Nicobar Islands, Bull. Seism. Soc. Am. 97, no. 1A, S174-S191.

Rajendran, C.P., Ramanamurthy, M.V., Reddy, N. T. and Rajendran, K., 2008a. Hazard implications of the late arrival of the 1945 Makran tsunami, *Current Science* **45**(12), 1739-1743.

Rajendran, C.P., Sha-hosseini, M., Beni, A. N. and Ranjendran, K., 2008b. The hazard implications of the 1945 Makran tsunami source: Interpretations based on the recent investigations, AOGS abstract, SE58-A002.

Sieh, K., Natawidjaja, D., Meltzner, A.J., Shen, C.-C., Cheng, H., Li, K.-S., Suwargadi, B.W., Galetzkam J., Philibosian, B. and Edwards, R.L., 2008. Earthquake supercycles inferred from sea-level changes recorded in the corals of west Sumatra, **322**, 1674-1677.

Song, Y.T., Ji, C., Fu, L.-L., Zlotnicki, V., Shum, C.K., Yi, Y. and V. Hjorleifsdottir, 2005. The 26 December 2004 tsunami source estimated from satellite radar altimetry and seismic waves. *Geophys. Res. Lett.* **32**, L20601, doi:10.1029/2005GL023683.

Stein, S., and Okal, E., Ultralong Period Seismic Study of the December 2004 Indian Ocean Earthquake and Implications for Regional Tectonics and the Subduction Process, Bull. Seism. Soc. Am.., 97, S279-S295, 2007.

Taylor, F.W., Edwards, R.L., Wasserburg, G.J. and C. Frohlich, 1990. Seismic recurrence intervals and timing of aseismic subduction inferred from emerged corals and reefs of the Central Vanuatu (New Hebrides) Frontal Arc. *J. Geophys. Res.* **95**(B1), pp.393-408.

Thomas, C., Burbidge, D., and P. Cummins, 2007. *A Preliminary Study into the Tsunami Risk faced by Southwest Pacific Nations*, Geoscience Australia.

Wang, R., Martin, F.L., and F. Roth, 2006. Computation of deformation induced by earthquakes in a multi-layered crust – FORTRAN programs EDGRN EDCMP. *Comp. and Geosc.* **29**, pp.195-207 (inc. erratum).

Ward, S. N., and Asphaug, E., 2000. Asteroid impact tsunami: A probabilistic hazard assessment, Icarus,145, 64-78.

Ward, S. N. and S. Day, Cumbre Vieja volcano: potential collapse and tsunami at La Palma, Canary Islands, 2001. Geophys. Res. Lett., 28, 3397-3400.

Webster, M. A. and P. Petkovic, 2005. *A*ustralian Bathymetry and Topography Grid, June 2005, Geoscience Australia, Record 2005/12.

Wells, D. L. and K. J. Coppersmith, 1994. New empirical relationships among magnitude, rupture length, rupture width, rupture area and surface displacement, *BSSA*, **84**(4), 974-1002.

Wessel, P. and W. H. F. Smith, 1991. Free software helps map and display data, *EOS Trans*, AGU, **72**, 441.

Appendix A PTHA Method

A.1 Summary

The probabilistic tsunami hazard assessment undertaken in this study seeks to assess the probabilities of certain waveheights being exceeded due to the arrival of a tsunami at the locations under investigation. These probabilities are expressed in terms of expected *return periods*. This method has been used previously (for example in Burbidge *et al*, 2007, 2008) and is based on a well established method of probabilistic seismic hazard assessments. Broadly, it involves producing and analysing a very large catalogue of synthetic tsunami which is produced by combining, in various ways, a much smaller number of synthetic tsunami. The steps involved are:

1. Determine the locations at which the assessment of hazard will be made (the *model output points*, see Figure 2).
2. Create a model of the faults to be considered (that is, the location and geometry of the subduction zones under consideration, Figure 5).
3. Divide these faults into smaller fixed size subfaults. In this study, subfaults consisting of 100 × 50 kilometre rectangular segments were used (Figure 64).
4. Model the deformation of the sea floor produced by an earthquake involving one metre of slip on each subfault, and model the propagation of the resulting tsunami to each of the model output points.
5. Create a catalogue of synthetic earthquakes along the faults, containing values for their location, area, magnitude, and the probability that each event might occur.
6. Determine which subfaults fall within the rupture area of each synthetic earthquake, and to what extent each such subfault contributes to the synthetic event (that is, what slip should be attributed to the subfault). In this assessment the slip was assumed to be evenly distributed across all sub-faults withing the rupture area.
7. Combine the modelled tsunami produced by each contributing subfault (from Step 4) to estimate the tsunami produced by the synthetic event.
8. Aggregate over the resulting catalogue of synthetic tsunami to determine relationships between maximum tsunami amplitudes and their probabilities.

In this study the tsunami from a total of 121 subfaults in the low hazard assessment and 267 in the high hazard assesment. These were combined in different ways to produce a catalogue of 5,948 (low hazard assessment) or 15,973 (high hazard assessment) synthetic tsunamis conresponding to the number of branches on the two logic trees.

More detailed information on the method used is presented below.

A.2 Bathymetry

The bathymetry was based on a combination of the US Naval Research Laboratory's two minute Digital Bathymetric Database (DBDB2) and Geoscience Australia's 250 metre dataset (Webster & Petkovic, 2005), which was resampled to a regular grid of locations spaced two arc minutes apart. This is a 'generic' bathymetry dataset and, while there are higher resolution data available for some parts of the study region, because of the very large study area it was not possible to perform the computations at a higher resolution with the computational resources available. Two arc minutes (≈ 3.7 kilometres) is considered to be an adequate resolution for modelling the propagation of tsunami in the open ocean in deep water, and since the model output points were chosen to lie in water at least 100 metres deep (see Section A.3), for the most part the resolution will be adequate for modelling the tsunami amplitudes at those points. However there are several effects of the resolution that should be noted:

- In many nations the bathymetry is very steep so that neighbouring bathymetric grid points may fall on dry land and in water as deep as several thousand metres.
- Some very small islands may not be represented in the bathymetry at all, that is, there may be no 'dry' grid point that represents the island. In such a case the semi-automatic procedure adopted for selection of model output points (Section A.3) may not place a model output point near that island, and consequently there may be some very small inhabited islands within the nations included in this study that are not represented by model output points.
- Regions of very complex and rapidly varying bathymetry may not be adequately represented by the bathymetric dataset, and in these regions the modelling of the tsunami amplitudes must be interpreted with caution. Anywhere were the water depth changes rapidly (such as offshore islands) is particularly sensitive to this. Thus in the global bathymetric dataset used here, islands may be poorly represented.

A.3 Model Output Points

The model output points were produced by determining the bathymetric grid points that are as close as possible to each of the Indian Ocean nations, but at least 100 metres deep. The resulting set of grid points was thinned to reduce data volume, and edited manually to ensure that populated islands (according to the LandScan$^{\mathrm{TM}}$ 2004 dataset) were adequately represented. The locations of the 3,329 model output points used in the study are shown in Figure 2. While the water depth at each model output point is at least 100 metres, in many cases it may be much deeper, because of the steeply varying bathymetry in the region of some of the nations in the study, and the resolution of the bathymetry data used. In order to be able to compare results from output points at different depths, Green's Law in absence of focusing (see for example Mei *et al*, 2005) has been used to normalise all results to a nominal depth of 100 metres. Thus if z_{actual} is the modelled waveheight at an output point of depth d, then the normalised waveheight at that output point,

$$z = z_{\text{actual}} \left(\frac{d}{100} \right)^{\frac{1}{4}}$$

may be considered to be the equivalent waveheight at a depth of 100 metres if there is no focussing or de-focussing of the wave between the two points. All results in this study were expressed in terms of these normalised waveheights.

A.4 Fault Model

This was based on the plate model of Bird (2003). The dip was estimated from the Regional Upper Mantle (RUM) model of Gudmundsson and Sambridge (1998) or from papers based on seismic surveys of specific subduction zones. A map of the subfaults used in the high hazard assessment is shown in Figure 64. The subfaults in this figure are coloured according to depth.

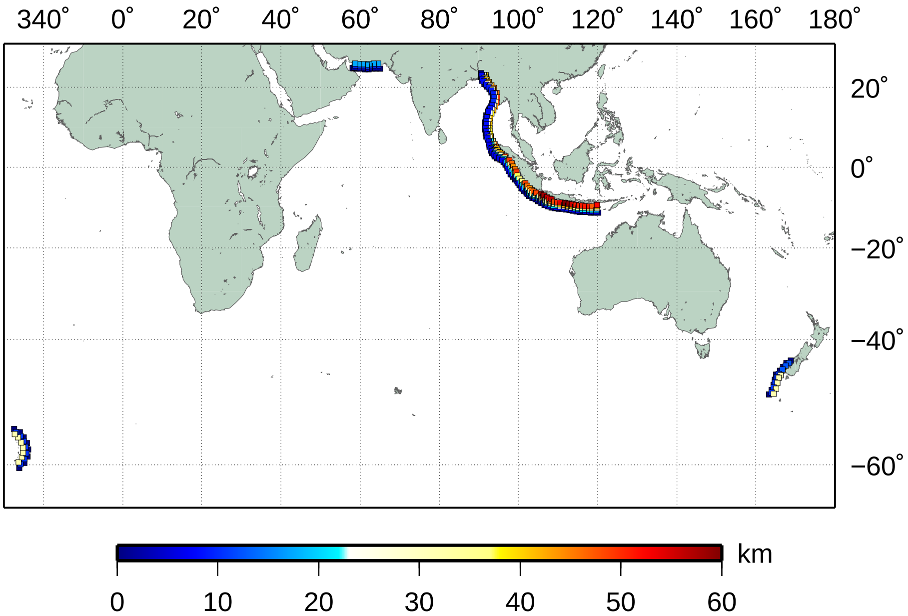

Figure 64: Location of the subfaults used in the high hazard assessment study, showing the depth of the centroid of each subfault.

A.5 Numerical Modelling

The sea floor deformation was calculated by representing the fault as a dislocation in a layered elastic medium. The elastic properties of the crust were based on CRUST2.0 (Bassin *et al*, 2000) and Kopp and Kukowski (2003). The general method used to calculate the sea floor deformation is described in more detail in Wang *et al* (2006).

The tsunami propagation was modelled using a staggered grid finite difference scheme to numerically solve the linear shallow water wave equations.

A.6 Catalogue of Synthetic Earthquakes

The earthquake catalogue was developed using a logic tree approach. Each branch of the tree represents some characteristic of an earthquake, for example magnitude, area or depth, and has an associated probability. The tips of the outermost branches represent the synthetic earthquakes, and the probability of each earthquake is the product of the probabilities of those branches of the tree leading to that earthquake.

Activity rates were estimated as the fraction of the global subduction zone seismicity that would be expected on each zone based on plate motion rates and the length and geometry of each subduction zone. The method used is similar to the one described in Burbidge *et al* (2008) and has subsequently been used for PTHA for Australia and the SW Pacific. Major differences include allowing the dip to vary and rescaling for the new segmentation models of the Sunda Arc in the low and high hazard assessments. The recurrence was assumed to obey the tapered Gutenberg-Richter relation up until a maximum magnitude cut-off value that differed for each zone (see Table 2). Every magnitude between 7.0 and the maximum was modelled at increments of 0.1 magnitude units. Figure 65 shows the earthquake recurrences curves for the low and high hazard assessments.

The curves were checked against the history of large earthquakes on each segment to ensure that values are reasonable. Earthquake catalogs used for this were assembled from some of the literature referred to in the Introduction, and are presented in Tables 3 and 4 for the low- and high-hazard end member assessments, respectively. It should be noted that some gross assumptions were made in order to combine results from instrumental, historical, and geological studies. For example, completeness periods were taken to roughly correspond to the period in which historical accounts are available, except in the case of the Andaman and central Sumatra sections (segments B and D, respectively) of the Sunca Arc, where paelotsunami and paleogeodetic studies were deemed to be adequate to define a longer completeness interval for very large earthquakes. Magnitudes for some historical earthquakes were assigned based on their rupture lengths and/or tusnami excitation inferred from historical accounts, and for some prehistoric earthqaukes were assumed to be commensurate with more modern events that left similar geologic signatures. Also, it seems possible that the catalogue data for the Sunda Arc may be biased towards lower return periods because of the series of large earthquakes experienced there sine the 2004 Sumatra-Andaman earthquake. In any case, the comparison with actual earthquake acivity plotted in Fig. 65 suggests that the synthetic catalogues used for the low- and high-hazard assessments are reasonable end members for the range of earthquake activity consistent with the available data.

For all modelled magnitudes, three different possible rupture areas were included in the synthethic catalogue. The Wells and Coppersmith (1994) relations were used to determine the area and resulting length as a function of magnitude. In total, over 20,000 earthquakes were included in this assessment (high and low).

A.7 Deaggregating the Hazard

Deaggregation of the hazard allows the source of the hazard at a particular location, or over a country as a whole, to be identified. There are a number of ways of deaggregating hazard and this section is devoted to an explanation of the methods adopted in this study.

A.7.1 Deaggregated Hazard Maps

A deaggregated hazard map allows the main sources of the hazard to be identified for a *single offshore location* for a *single return period*:

1. Choose the return period and the offshore location (model output point) at which the deaggregation is to be performed.
2. Find all events in the synthetic catalogue of tsunami that produce a wave that exceeds a given amplitude at the given model output (call these the *exceedance events*), along with their probabilities.
3. For each exceedance event, find the subfaults that constitute that event and apportion the probability of the event equally among those subfaults.
4. Sum these probabilities over all the exceedance events, to calculate a probability for each of the subfaults included in that particular assessment.

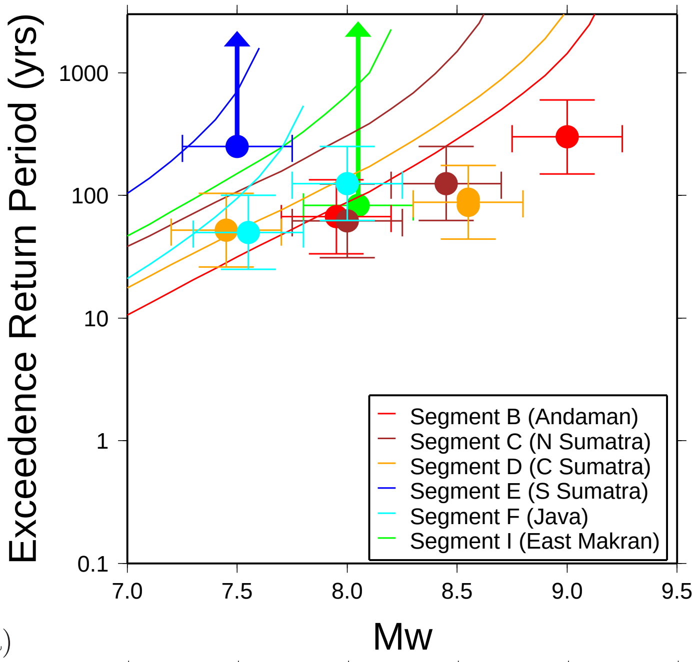

(a)

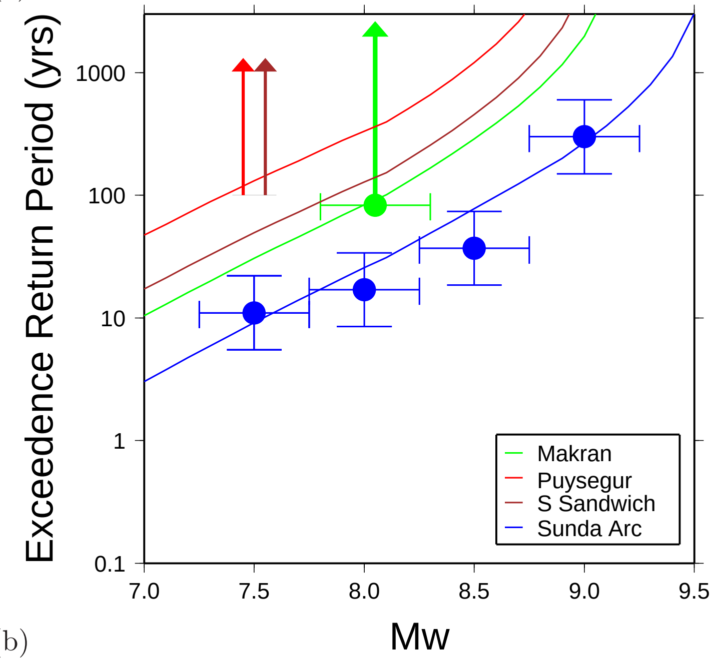

(b)

Figure 65: Earthquake recurrence models for the (a) low and (b) high hazard assessments. This shows the average return period between earthquakes exceeding the magnitude shown on the x-axis. Observed recurrence rates from Tables 3 and 4 are plotted, with error bars indicated the width of the half-unit magnitude bins, and an assumed uncertainty in return period ranging from one-half to double the estimated period. Note that since no large (Mw≥7.5) megathrust earthquakes are known to have occured in the Puysegur Trench or South Sandwich Arc, they are assumed in (b) to have return periods longer than the instrumental period (since 1900).

Segment	Magnitude	Completeness Interval (years)	No. Earthquakes	Recurrence Interval	Historical Events	References
B	8.0	200	3	67	1881[1],1941[1],2004[1]	Ortiz and Bilham (2003)
	9.0	600	3	300	1400[2],2004[1]	Moneke *et al.* (2009), Jankaew *et al.* (2009)
C	8.0	250	4	62	1843[3],1861[3],1907[3],2005[1]	Newcomb & McCann (1987), Briggs *et al* (2005)
	8.5	250	2	125	1861,2005	
D	7.5	250	6	42	1770[3],1797[4],1818[3],1833[4], 2007a[1],2007b[1]	Newcomb & McCann (1987), Natawidjaja *et al* (2006)
	8.5	250	3	83	1797[4],1833[4],2007a[1]	
	8.5	650	7	93	1350[2],1380[2],1606[2],1685[2] 1797[4],1833[4],2007a[1]	Sieh *et al.* (2008)
E	7.5	250	1	>250	2000[1]	Abercrombie *et al.* (2003)
F	7.5	250	6	42	1840[3],1859[3],1921[3], 1994[1],2006[1]	Newcomb & McCann (1987), Abercrombie *et al* (2001), Ammon *et al* (2007)
	8.0	250	2	125	1994[1],2006[1]	
I	8.0	250	≤ 3	≥ 83	1765[3],1851[3],1945[1]	Byrne *et al.* (1992)

Table 3: Summary of megathrust earthquake catalog used to verify the earthquake activiy rates plotted in Fig. 65a, for the low-hazard assessment. Segments refer to those indicated in Fig 5. Events are binned in half-magnitude increments, and completeness intervals are guessed at based on the availability of historical accounts or paleotsunami/paleogeodetic data. The method for inferring magnitude is indicated by the superscript following each event year, which refer to: [1] instrumentally measured ; [2] inferred from paleotsunami or paleogeodetic data to be commensurate with more modern events having similar signatures; [3] inferred from rupture lengths and/or tsunami excitation based on historical accounts; [4] estimated from paleogeodetic mapping of coseismic uplift/subsidence.

Subduction Zone	Magnitude	Completeness Interval (years)	No. Earthquakes	Recurrence Interval	Historical Events
Sunda	7.5	200	18	11	1797,1818,1833,1840,1843,1859,1861, 1881,1907,1921,1941,1994,2000,2004, 2005,2006,2007a,2007b
	8.0	200	13	15	1797,1833,1843,1861,1881,1907,1941, 1994,2004,2005,2006,2007a,2007b
	8.5	200	13	15	1797,1833,1861,2004,2005,2007a
	9.0	600	2	300	1400,2004
Makran	8.0	250	$\leq$3	$\geq$83	1765,1851,1945
Puysegur	7.5	100	0	$\geq$100	
S. Sandwich	7.5	100	0	$\geq$100	

Table 4: Summary of megathrust earthquake catalog used to verify the earthquake activiy rates plotted in 65, for the high hazard assessment. Completeness intervals correspond to the miniumum of those from Table 3 for the Sunda Arc, are the same for the Makran, and are assumed to correspond to the instrument period (since 1900) for magnitude 7.5 earthquakes in the Puysegur Trench and South Sandiwch Arc. Methods for inferring magnitude are as indicated in Table 3 for the corresponding earthquakes.

5. Express the results as a percentage contribution from each subfault.

6. Map these contributions.

A.8 National Weighted Deaggregated Hazard Maps

Each deaggregated hazard map is peculiar to the model output point for which it is produced, and indicates the source of the hazard at that particular model output point only. Thus it is possible for a deaggregated hazard map for a point on one side of an island to indicate that the main source of the hazard at that point is the Sunda Arc, for example, while such a map for a point on the other side of the island might indicate that the major source of hazard for that point is the Makran subdcution zone. A national weighted deaggregated hazard map gives some indication of the source of hazard to the country as a whole:

1. Choose the return period.

2. Deaggregate the hazard as described above *for all the model output points offshore the country*, to obtain the relative contributions of each of the subfaults, for every model output point.

3. Weight the contributions of each subfault at each model output point by the maximum tsunami amplitude for the chosen return period at that model output point.

4. Sum the results over all the model output points, and express as a percentage of the total contribution.